11. SITE 757[1]

Shipboard Scientific Party[2]

HOLE 757A

Date occupied: 1 June 1988

Date departed: 1 June 1988

Time on hole: 7 hr, 40 min

Position: 17°01.458′S, 88°10.899′E

Bottom felt (rig floor; m; drill-pipe measurement): 1661.1

Distance between rig floor and sea level (m): 10.87

Water depth (drill-pipe measurement; corrected m): 1650.2

Total depth (rig floor; corrected m): 1670.5

Penetration (m): 9.4

Number of cores: 1

Total length of cored section (m): 9.4

Total core recovered (m): 9.40

Core recovery (%): 100

Oldest sediment cored:
Depth sub-bottom (m): 9.4
Nature: foraminifer nannofossil ooze
Earliest age: Pleistocene
Measured velocity (km/s): 1.5

HOLE 757B

Date occupied: 1 June 1988

Date departed: 4 June 1988

Time on hole: 2 days, 20 hr, 20 min

Position: 17°01.458′S, 88°10.899′E

Bottom felt (rig floor; m; drill-pipe measurement): 1663.0

Distance between rig floor and sea level (m): 10.87

Water depth (drill-pipe measurement; corrected m): 1652.1

Total depth (rig floor; corrected m): 2037.8

Penetration (m): 374.8

Number of cores: 43

Total length of cored section (m): 374.8

Total core recovered (m): 271.94

Core recovery (%): 72

Oldest sediment cored:
Depth sub-bottom (m): 369.2
Nature: tuff
Earliest age: late Paleocene
Measured velocity (km/s): 2.2–2.4

Basement:
Depth sub-bottom (m): 369.2
Nature: plagioclase phyric basalt
Measured velocity (km/s): 4.6–5.3

HOLE 757C

Date occupied: 4 June 1988

Date departed: 5 June 1988

Time on hole: 1 day, 12 hr

Position: 17°01.389′S, 88°10.812′E

Bottom felt (rig floor; m; drill-pipe measurement): 1654.5

Distance between rig floor and sea level (m): 10.87

Water depth (drill-pipe measurement; corrected m): 1643.6

Total depth (rig floor; corrected m): 2075.2

Penetration (m): 420.7

Number of cores: 12

Total length of cored section (m): 106.1

Total core recovered (m): 67.78

Core recovery (%): 63

Oldest sediment cored:
Depth sub-bottom (m): 372.8
Nature: tuff
Earliest age: late Paleocene
Measured velocity (km/s): 2.8

Basement:
Depth sub-bottom (m): 372.8
Nature: porphyritic basalt
Measured velocity (km/s): 4.5–5.3

Principal results: Site 757 (proposed Site NER-2C) is near the crest of Ninetyeast Ridge, about 230 km southeast of Osborne Knoll. Together, the three drilling locations of Leg 121 on the Ninetyeast Ridge were designed to sample the basement through time and the sedimentary section through both time and latitude. Site 757 is the midpoint of that transect, and it is roughly halfway between Deep Sea Drilling Project (DSDP) Sites 253 and 214.

A specific objective at Site 757 was to sample basalt at a location midway between DSDP sites to study the evolution of the Kerguelen/Ninetyeast hot spot as well as vertical changes in geochemistry in the volcanic section. Samples from this location would yield a detailed northward-motion curve for the Indian plate from paleomagnetic studies, with particular emphasis on the Eocene-Oligocene section and basement. Borehole televiewer (BHTV) logging in basement was planned to look for breakouts as an indicator of *in-situ* stress. This site also forms the central point in the south-north paleoceanographic/climatic transect of Leg 121.

The proposed site location was picked at shotpoint 2660 on the seismic-reflection survey conducting during *Robert D. Conrad* Cruise 2707. The approach survey was somewhat longer than usual in order to resolve uncertainties regarding the structural grain in the area of the site. The final site location is about 2800 m northwest of, but in the same tectonic position as, the proposed site. Site 757 is on the eastern edge of the summit horst on this part of Ninetyeast Ridge, but downdip to the southeast from the structural crest.

---

[1] Peirce, J., Weissel, J., et al., 1989. *Proc. ODP, Init. Repts.*, 121: College Station, TX (Ocean Drilling Program).

[2] Shipboard Scientific Party is as given in the list of Participants preceding the contents.

Hole 757A missed the mud line. Hole 757B was cored with the advanced hydraulic piston corer (APC) and extended core barrel (XCB) systems 1 m into basement. The Navidrill (NCB) was then deployed, for the third time on Leg 121, to cut two cores. Hole 757C was spot cored and washed to 363 m below seafloor (mbsf) and then cored with the rotary core barrel (RCB) to 421 mbsf. Actual basement penetration was 48 m below the depth where the driller first felt hard rock. A medical emergency terminated drilling, precluding chances to extend an excellent basement hole and eliminating all hope of logging.

The following lithologic units are recognized:

Unit I (0–212 mbsf): Pleistocene (Zone CN15) to lower Eocene (Zone CP10/P8) nannofossil ooze, which is divided into two subunits:

Subunit IA (0–169 mbsf): Pleistocene to middle Eocene (Zone CP13b) bioturbated nannofossil ooze, with foraminifers in the upper 40 m.

Subunit IB (169–212 mbsf): middle to lower Eocene calcareous ooze with nannofossils in the upper part and ash in the lowermost part. Lithification generally increases downcore, and the ooze grades to chalk at the bottom of the subunit.

Unit II (212–369 mbsf): upper Paleocene volcaniclastics that can be subdivided into two subunits:

Subunit IIA (212–250 mbsf): upper Paleocene volcanic ash with glauconite and foraminifers at the top of the subunit, lapilli (2–5 mm in diameter), shell fragments, and basalt pebbles.

Subunit IIB (250–369 mbsf): undated volcanic tuff, half of which contains coarse lapilli (2–5 mm diameter) and the other half is massive and homogeneous. Rounded basalt pebbles, shell fragments, pebbles of flint, and sedimentary structures such as millimeter-scale laminae and sharp contacts also occur in the subunit. The tuff immediately overlying the basalts is red-brown in color and contains shelly material.

Unit III (369–421 mbsf): basaltic flows with minimal evidence of intercalated ash material. A total of 20 flow units were recovered, one from Hole 757B and 19 from Hole 757C. The majority of the flows are less than 1 m in thickness, including several for which the entire unit was recovered. The maximum flow thickness is 5.5 m. The flows are all plagioclase phyric; several contain more than 20% phenocrysts. The degree of alteration varies from slight to high, with pervasive replacement of the groundmass by smectite. The majority of the flows are vesicular. Vesicles and veins are infilled with a variety of minerals, including calcite, limonite, chlorite, smectites, and, particularly in the lower units, zeolites.

In geochemical analyses, the basalts at Site 757 are less enriched in incompatible elements, and are thus somewhat closer to mid-ocean ridge basalt (MORB) composition, than those at Site 756 or elsewhere on Ninetyeast Ridge. The differences downhole are also significant in that the two lowermost flow units (5.87-m recovery) are geochemically distinct (relatively enriched in incompatible elements) and must have a different magmatic parent than the lavas higher in the section.

These flows were erupted subaerially, and the ashes above the flows are the product of phreatic volcanism near the wave base. The phreatic phase of volcanism must have continued for a considerable period of time, as there is at least one normal and parts of two reversed polarity intervals within the ash section. The sediments of late Paleocene age immediately above the basalt indicate a very shallow environment that quickly deepened to bathyal depths by early Eocene time. Thus, it appears that Site 757 was subsiding as volcanism waned, and subsidence to moderate depths occurred quickly after ash production ended. The late Paleocene age of the oldest datable sediments is the same as the age predicted using a hot-spot model.

Recovering the paleomagnetic record in the Eocene-Oligocene section was a key objective because it should define the manner in which the Indian plate slowed down as it collided with Asia. Unfortunately, paleolatitudes may not be recoverable from this section because the magnetization is very soft and unstable, with large changes in both declination and inclination observed after storage in the laboratory for a few hours. There is a small chance that a stable signal may yet be resolvable with shorebased studies done in a magnetically clean environment.

The fossil assemblages at Site 757 were expected to have more tropical affinities than those of the previous sites because the site is 1200 km north of Site 756. The paleontological assemblages in the Paleocene and Eocene sediments at Site 757 are temperate to subtropical, and the assemblages are identical to those seen at Broken Ridge in the same age range. Indications of tropical to subtropical assemblages occur in the middle Oligocene to Holocene, and few of the higher latitude species seen at Broken Ridge in this age range are present at Site 757.

The NCB was deployed for the third time on Leg 121 at Site 757. All indications are that the first core was cut properly, but only 65 cm of basalt was recovered, apparently because the core catcher failed. The NCB failed to make headway on the next core, and only 11 cm of basalt was recovered. We feel that the pieces of rock that fell out of the previous core created a rubble pile that prevented the high-speed bit from establishing a clean cut.

BACKGROUND AND OBJECTIVES

This section includes a brief synopsis of overall drilling objectives on Ninetyeast Ridge and discusses in detail the goals for Site 757, the central site drilled on the ridge during Leg 121. A more complete discussion of the overall objectives and their implications may be found in the "Leg 121 Background and Objectives" chapter (this volume).

Central Site 757

Site 757 lies midway between DSDP Sites 253 and 214 (Fig. 1). The site is positioned to sample basement near to, but south of, Osborne Knoll. Basement age at this location is predicted to be 58 Ma, according to the hot-spot models of Duncan (1978) and Duncan et al. (in press). Figure 2 shows the paleogeography of the site at its predicted basement age.

Site 757 is at 17°01.42′S, 88°10.85′E, in a water depth of 1644 m on the eastern edge of the summit horst, downdip to the southeast from the structural crest (see Fig. 43). Three holes on a northwest-southeast line were drilled at Site 757 (see "Operations" section, this chapter). The deepest hole reached a total depth of 421 mbsf after penetrating 212 m of pelagic ooze and 209 m of volcanics, of which the lower 42 m consists of intercalated flows and volcaniclastics. Coring operations were terminated prematurely by a medical emergency.

Objectives

In general terms, the objectives for drilling on Ninetyeast Ridge fall into three broad categories: petrology, northward motion of the Indian plate, and paleoceanography/paleoclimatology.

A basic premise of the petrologic objectives on Leg 121 was to sample the volcanism of the Kerguelen/Ninetyeast hot spot through time by sampling along the length of Ninetyeast Ridge to study variations on a long time scale and also by sampling vertically to study variations within individual volcanic sections on a short time scale. With the unexpected discovery at Broken Ridge of an extensive ash sequence, which was produced presumably by the Kerguelen/Ninetyeast hot spot, sampling proximal ashes and basement rocks produced by the same volcanic source through the same time period (Late Cretaceous to middle Eocene) became more important.

In particular, Site 757 provided an opportunity to sample volcanic ash and basement of the same age (late Paleocene) as the ashes sampled on Broken Ridge at Site 752. Furthermore, the seismic interpretation at the proposed location suggested the presence of a thick section of volcaniclastics, thus permitting a direct comparison to the ashes found at Broken Ridge. The drilling results confirmed these expectations.

The primary objective of the paleomagnetic studies of the Ninetyeast Ridge sites was to precisely define the slowing of the northward motion of the Indian plate during and after its collision with Asia. We know that it slowed by a factor of three from the rate before collision (~15 cm/yr, 70 to ~50 Ma) to the rate

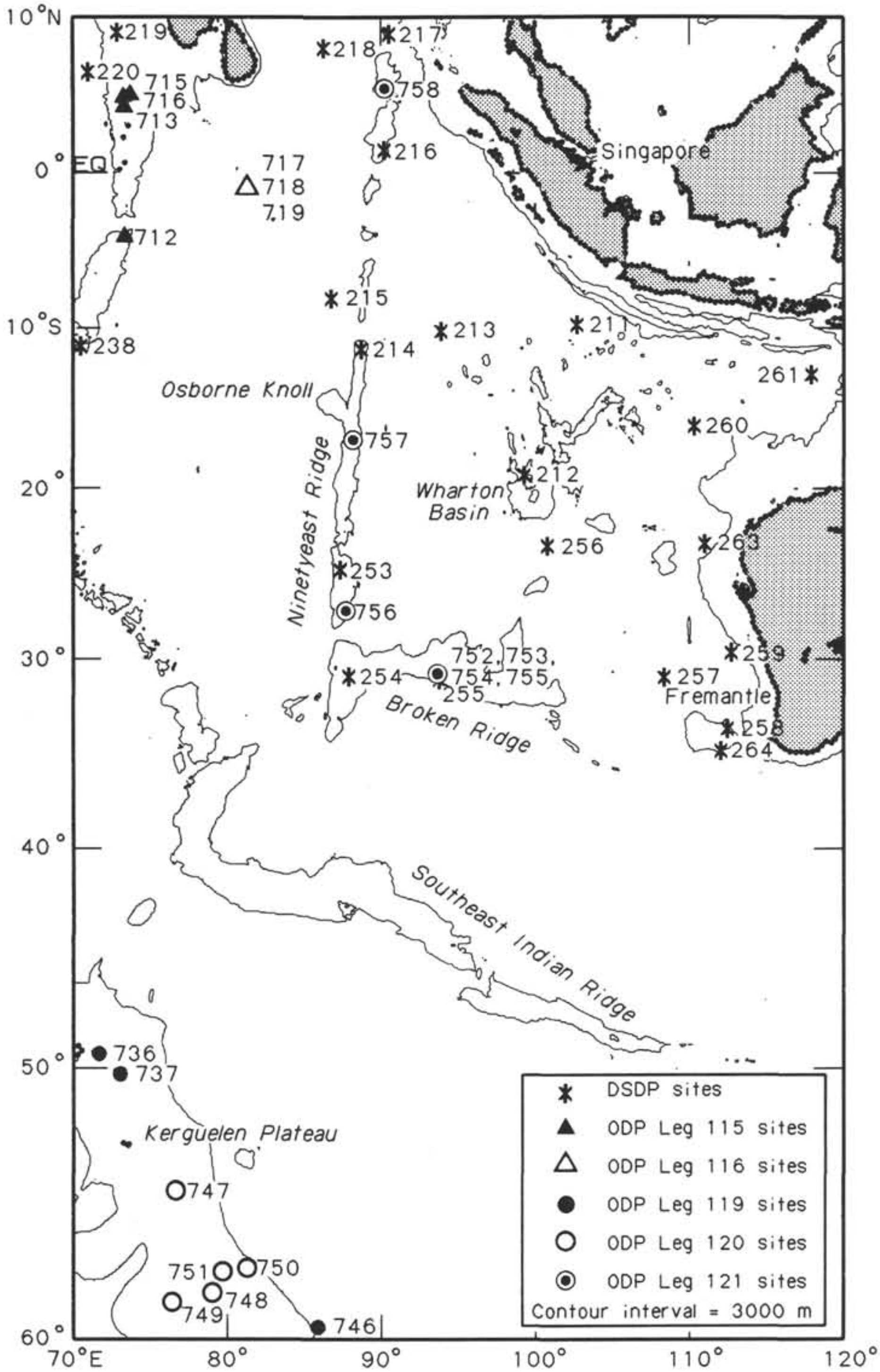

Figure 1. Site 757 location in the central part of Ninetyeast Ridge.

after collision (~ 5 cm/yr, after 40 Ma; Molnar and Tapponnier, 1975; Peirce, 1978; Patriat and Achache, 1984), but the details of its deceleration are unknown. The manner in which the Indian plate slowed during the middle and late Eocene may provide clues about the tectonic style of the deformation that developed between India and Asia during the early stages of collision. The volcaniclastics and flows at Site 757 should provide excellent paleolatitude data for the Indian plate for the time just prior to its deceleration. As the volcaniclastics appear to have been deposited over a significant length of time (see "Paleomagnetics" section, this chapter), more than one paleolatitude determination may be possible. Although an Eocene-Oligocene section was recovered at this site, initial shipboard indications are that the carbonate-rich oozes of that age are not likely to carry a stable paleolatitude signal.

A particular goal for a north-south paleoceanographic transect in the eastern Indian Ocean was to recover fossil records containing a mixture of species from two different climatic zones

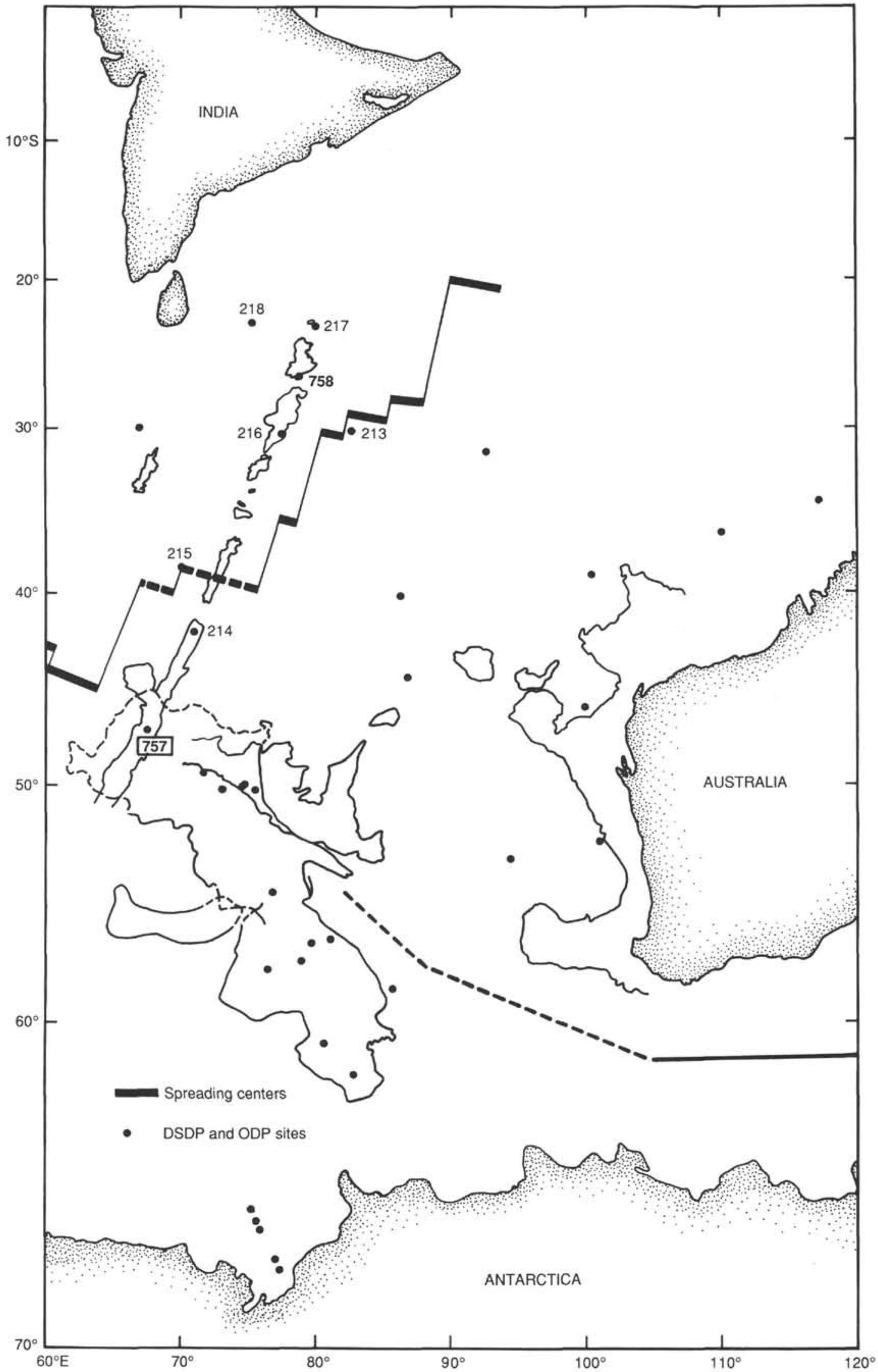

Figure 2. Reconstruction for 58 Ma, showing the position of Site 757 and adjacent features at the same time as its basement age, as predicted by Duncan et al. (in press). The northern Kerguelen Plateau is fixed at its present-day coordinates (model by Royer et al., in press).

(e.g., temperate and subtropical). Because many of the biostratigraphic time scales are based on the fossil record from one climatic zone (usually subtropical), it is often difficult to relate the fossils from one climatic assemblage to those of another with an accurate determination of relative stratigraphic ages. This confusion is further complicated by the time-transgressive nature of many critical biostratigraphic datums toward the ecological limits of any particular form. Sites with mixed zonal assemblages allow biostratigraphers to construct interzonal relationships and thus build more robust time scales with wider applicability.

Site 757 is expected to provide a mixed assemblage fossil record that changes upsection as the site moved northward. The lower section should be similar to that at Broken Ridge, with an increasing subtropical influence appearing in the Eocene. These mixed assemblages will allow bridging correlations to be made between the austral temperate assemblages common in the Southern Hemisphere, as found at Broken Ridge, and the low-latitude, subtropical assemblages that are widely used in several biostratigraphic zonation schemes (e.g., Banner and Blow, 1965; Blow, 1969; Berggren et al., 1985; Bolli et al., 1985). Farther up in the section, near the base of the Neogene, we should begin to observe significant tropical influxes, allowing us to correlate between subtropical and tropical assemblages. Initial analysis of the cores indicates that such expectations are justified.

Eolian dust recovered from pelagic sediments provides a quantitative record of both the intensity of zonal winds and the aridity of the eolian source areas (Rea et al., 1985). One important paleoclimatological goal of Leg 121 was to recover continuous stratigraphic sections of Cenozoic age in order to analyze the eolian record. Ninetyeast Ridge is ideally located for this study because it lies between the great deserts of Africa and Australia and therefore should receive an adequate supply of dust. Furthermore, locations on top of the ridge are protected from abyssal reworking, and there should be fewer unrecognized contributions from hemipelagic input. The backtrack history of the three sites on Ninetyeast Ridge (see Fig. 16 of the "Leg 121 Background and Objectives" chapter) will provide a paleoclimatic record that spans nearly 50° of latitude.

Site 757 was intended to provide a section in southern subtropical to temperate latitudes which has a reasonably complete stratigraphic record and, therefore, a useful paleoclimatic record. In contrast, because the Neogene section recovered at Broken Ridge is winnowed and may contain some minor disconformities, it probably does not contain a good paleoclimatic record.

Other objectives planned for Site 757 included an operational deployment of the Navidrill mud-motor coring system in basalts and an expanded logging program, including a logging run of the BHTV to measure breakouts as an indicator of *in-situ* stress. The results of the third deployment of the NCB during Leg 121 are reported in the "Operations" section. The logging program was precluded by the medical emergency that terminated Hole 757C.

OPERATIONS

Transit to Site 757

With the pipe on deck at 1020 hr, 29 May, the vessel was secured for sea, departed Site 756, and proceeded north to the central of the three Ninetyeast Ridge drilling locales. We chose a route east of the direct course between sites so that a magnetometer survey of uncharted seafloor-spreading anomalies could be completed east of, and parallel to, the ridge. At 1700 hr on 31 May the seismic gear was streamed as the vessel slowed to 7 kt to commence the site survey, which lasted about 10 hr. On the second pass over the site a Datasonics beacon was dropped, officially beginning Hole 757A at 0210 hr, 1 June. Site operation plans included two probable holes: one for APC/XCB coring the sediment section, with continued coring into basement with the NCB, followed by a second hole to gain 50 m or more penetration into basement. In an effort to maximize the results of coring two holes, their positions were selected to be offset 100 m to either side from the beacon (Fig. 3). The final site location is approximately 2800 m northwest of proposed Site 757.

Site 757

Hole 757A

Holes 757A and 757B were positioned 100 m southeast of the actual beacon position. The hole plan called for APC/XCB operations to XCB refusal, followed by either NCB or RCB coring to achieve adequate basement penetration and recovery. Accordingly, the conventional APC/XCB bottom-hole assembly (BHA) was made up, but with two modifications. Because we wanted oriented piston cores at this low-latitude site (17°01′S), the nonmagnetic drill collar was included. In addition, a stand of 8¼-in. drill collars was added to allow for more weight on bit during the Navidrill coring operations, which would make penetration of the 11⁷/₁₆-in. bit through basalt a little easier.

The drill pipe was run to the chosen depth for the mud-line APC shot, and the first piston corer was activated. The recovered core barrel contained a full core and thus had missed the mud line despite a very conservative estimate of water depth obtained from the precision depth recorder.

Hole 757B

The pipe was pulled clear of the seafloor and backed up an additional 3 m before we attempted to take another mud-line core. Despite a normal shoot-off sequence, the overshot shear pin failed while the core barrel was being recovered. This allowed the core barrel to fall back to the bottom of the pipe, where it probably punched another hole in the mud and ingested more core material. This core would have been discarded because it would have been useless for defining the mud line, but the point was moot because the core barrel was found to be empty when recovered. A third attempt was made to get a

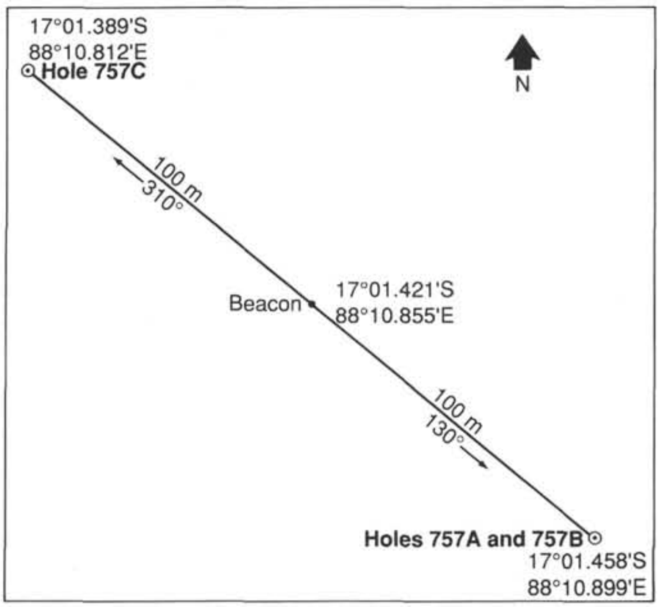

Figure 3. Location of Site 757 drill holes relative to beacon position.

proper mud-line core, and in spite of a shattered core liner, the seafloor was established at a working water depth of 1663.0 m below the rig floor. This depth contradicts the apparent results of Hole 757A, which had recovered a full core liner with the bit poised at a depth of 1661 m. Rather than spend more time in search of an unambiguous mud-line depth, the results of the Hole 757B mud-line core were accepted and coring continued in Hole 757B.

Nineteen piston cores were then taken in gradually indurating calcareous ooze (Table 1). Cores 121-757B-3H to 121-757B-19H were oriented magnetically using the Multishot camera. The multishot results were very consistent and showed the hole to have an initial drift of 2°, which decreased with depth to 1.2° at Core 121-757B-19H. Drift direction was 325° ± 5°. APC refusal was defined by 110,000-lb overpull while extracting Core 121-757B-19H, although no previous core had experienced more than 15,000-lb overpull. Core recovery during the piston core sequence was nearly perfect.

The Leg 121 XCB coring system was deployed next, and we took Cores 121-757B-20X through 121-757B-41X. Recovery was generally good, although some cores suffered reduced recovery owing to packing off in the cutting shoe. Because we found a few random chunks of basaltic clasts and chert in the cores starting with Core 121-757B-25X (222 mbsf), we replaced the long-sawtooth steel shoe on the XCB with short-sawtooth impregnated cutting shoes in coring from 222 to 370.3 mbsf. Core 121-757B-40X took 55 min to penetrate just 3 m, but the recovered core contained only hard, packed clay. A fresh XCB was pumped down for Core 121-757B-41X, and 1 m of penetration in basalt was achieved in 45 min. The recovered core barrel contained 1.26 m of basalt.

The Navidrill coring system was subsequently deployed in the hope of reaching the scientific objective of penetrating 50 or more meters into basement without having to trip the pipe for the RCB system. The first NCB coring run apparently penetrated 4.0 m, but lost almost all of the core that was cut. Only 0.65 m of basalt was in the core barrel. A core-catcher failure was declared the best explanation for the missing core. The kerf of the assumed 4-m-deep NCB hole was then drilled, and it felt very much like hard basalt the whole way. The NCB was pumped down for the second, and final, time. The second NCB core attempt was a poor run, with evidence of both improper seating by the core barrel in the BHA and probable stallout of the mud motor. Only three basalt chunks were recovered. With such scant results, we abandoned our attempt of reaching more than 50 m into basement in reasonable time with the NCB. The NCB equipment was rigged down, and the pipe was tripped out of the hole, with the bit reaching the rig floor at 0615 hr, 4 June. Basement recovery in Hole 757B was 37%, for a total time on hole of 2.85 days.

Hole 757C

The ship was offset 200 m northwest, 100 northwest of the beacon (Fig. 3), and a conventional RCB BHA with a new 9⅞-in. RBI C-4 bit was made up and run to the seafloor. A mud-line punch core established the drilling depth as 1654.5 m below the rig floor. The hole was then drilled to 121.5 mbsf without coring. Cores 121-757C-2R to 121-757C-5R were taken in soft ooze to acquire spot core samples for geochemical and paleomagnetic comparison with Hole 757B. The bit was then washed to a depth of 362.9 mbsf, where routine coring began just above basement to overlap the stratigraphy of Hole 757B. Cores 121-757C-8R to 121-757C-12R were taken in basalt to a depth of 420.7 mbsf, representing 47.88 m of penetration into basement with a recovery of 51% (Table 1).

Coring operations were abruptly terminated in order to proceed to the Cocos Islands for the medical evacuation of a Catermar employee suffering from a life-threatening blockage of his intestinal tract. The pipe was pulled and, as soon as the bit was on deck, the vessel made preparations to get under way. Departure for the Cocos Islands was at 1845 hr, 5 June.

Table 1. Coring summary, Site 757.

Core no.	Date (June 1988)	Time (local)	Depth top (mbsf)	Depth bottom (mbsf)	Length cored (m)	Length recovered (m)	Recovery (%)
121-757A-							
1H	1	1040	0.0	9.4	9.4	9.40	100.0
					9.4	9.40	100.0
121-757B-							
1H	1	1250	0.0	4.5	4.5	3.91	86.9
2H	1	1330	4.5	14.0	9.5	9.63	101.0
3H	1	1405	14.0	23.6	9.6	9.79	102.0
4H	1	1445	23.6	33.2	9.6	8.12	84.6
5H	1	1525	33.2	42.8	9.6	8.47	88.2
6H	1	1605	42.8	52.5	9.7	9.26	95.4
7H	1	1640	52.5	62.2	9.7	8.38	86.4
8H	1	1730	62.2	71.8	9.6	9.37	97.6
9H	1	1810	71.8	81.5	9.7	9.43	97.2
10H	1	1850	81.5	91.2	9.7	8.45	87.1
11H	1	1925	91.2	100.8	9.6	9.49	98.8
12H	1	2010	100.8	110.5	9.7	9.36	96.5
13H	1	2045	110.5	120.1	9.6	9.42	98.1
14H	1	2125	120.1	129.8	9.7	9.56	98.5
15H	1	2200	129.8	139.5	9.7	9.28	95.7
16H	1	2240	139.5	149.1	9.6	8.13	84.7
17H	1	2310	149.1	158.8	9.7	9.66	99.6
18H	2	0025	158.8	168.5	9.7	9.86	101.0
19H	2	0115	168.5	174.7	6.2	6.19	99.8
20X	2	0245	174.7	182.7	8.0	9.39	117.0
21X	2	0345	182.7	192.4	9.7	9.63	99.3
22X	2	0445	192.4	202.0	9.6	6.75	70.3
23X	2	0525	202.0	211.7	9.7	6.69	68.9
24X	2	0650	211.7	221.4	9.7	7.46	76.9
25X	2	0755	221.4	231.0	9.6	7.12	74.1
26X	2	1010	231.0	240.7	9.7	3.16	32.6
27X	2	1205	240.7	250.4	9.7	9.75	100.0
28X	2	1340	250.4	260.0	9.6	6.87	71.5
29X	2	1530	260.0	269.7	9.7	5.77	59.5
30X	2	1810	269.7	279.4	9.7	4.58	47.2
31X	2	2005	279.4	289.0	9.6	1.99	20.7
32X	2	2230	289.0	298.6	9.6	3.83	39.9
33X	3	0005	298.6	308.3	9.7	0.47	4.8
34X	3	0350	308.3	317.9	9.6	3.07	32.0
35X	3	0530	317.9	327.6	9.7	4.69	48.3
36X	3	0715	327.6	337.3	9.7	3.97	40.9
37X	3	1205	337.3	346.9	9.6	4.06	42.3
38X	3	1305	346.9	356.6	9.7	1.38	14.2
39X	3	1420	356.6	366.3	9.7	2.56	26.4
40X	3	1610	366.3	369.3	3.0	0.97	32.3
41X	3	1755	369.3	370.3	1.0	1.26	126.0
42N	3	2025	370.3	374.3	4.0	0.65	16.2
43N	4	0030	374.3	374.8	0.5	0.11	22.0
					374.8	271.94	72.6
121-757C-							
1R	4	1220	0.0	9.7	9.7	9.65	99.5
2R	4	1500	121.5	131.1	9.6	9.71	101.0
3R	4	1530	131.1	140.8	9.7	2.86	29.5
4R	4	1600	140.8	150.5	9.7	9.71	100.0
5R	4	1630	150.5	160.1	9.6	9.19	95.7
6W	5	0005	160.1	362.9	202.8	1.13	(wash core)
7R	5	0200	362.9	372.4	9.5	1.71	18.0
8R	5	0340	372.4	382.0	9.6	3.00	31.2
9R	5	0610	382.0	391.7	9.7	8.83	91.0
10R	5	0820	391.7	401.4	9.7	3.83	39.5
11R	5	1025	401.4	411.1	9.7	4.01	41.3
12R	5	1255	411.1	420.7	9.6	5.28	55.0
	(Coring)				106.1	67.78	63.9
	(Washing)				202.8	1.13	
					308.9	68.91	

Site 757 to Cocos Islands

The ship proceeded at full speed to the Cocos Islands atoll, where a rendezvous with the Australian flying doctor service out of Perth had been arranged. During the 57-hr transit to Cocos

Island, the 3 × 18 wire rope on the forward sand line winch was removed and replaced with new wire. At 0400 hr on 8 June, the ship stopped off South Keeling Island of the Cocos group to take a launch alongside with the Australian doctor and local customs officials. The group departed with Catermar cook Fernando Dos Santos at 0430 hr. The ship then resumed its transit for the final northern site on Ninetyeast Ridge.

LITHOSTRATIGRAPHY AND SEDIMENTOLOGY

Lithologic Units

Drilling at Site 757 penetrated a 369-m-thick sequence of ooze and tuff and underlying basalt (Fig. 4). Drilling was terminated by a medical emergency. The lithologic sequence is divided into three units: Unit I, 211.7 m of lower Eocene to Pleistocene carbonate ooze; Unit II, 155.3 m of upper Paleocene(?) to lower Eocene waterlain ash and tuff; and Unit III, 47.9 m of basalt.

Unit I, the carbonate ooze, can be divided into two subunits on the basis of lesser lithologic variations (Table 2). Subunit IA (0–168.5 mbsf) is dominantly nannofossil ooze, with foraminifers in the top four cores. The micrite component that becomes apparent in Core 121-757B-16H forms the dominant component in Subunit IB. The upper subunit ranges in color from stark white (whiter than Munsell color 10YR 8/1) and white (10YR 8/1 and 10YR 8/2) to very pale brown and pale brown (10YR 8/3, 10YR 7/3, and 10YR 6/3). The oozes of Subunit IA are completely bioturbated and display scattered oval to circular mottles.

Subunit IB (168.5–211.7 mbsf) is 43.2 m of calcareous ooze with nannofossils in the upper part and ash in Sections 121-757B-23X-5 and 121-757B-23X-CC. Lithification varies in this subunit, but increases gradually downcore, and the ooze grades to chalk in Sections 121-757B-23X-4 through 121-757B-23X-CC. The unit is very pale brown (10YR 7/3 and 10YR 8/3) to white and stark white (10YR 8/1). The oozes and chalk of Subunit IB are strongly bioturbated and mottled.

Grain-size analyses of bulk sediment from Unit I were conducted on three samples from every core. Results (Table 3 and Fig. 5) indicate coarser material in about the upper 30 m with an average size of 4.5ϕ (44 μm) that reflects the foraminifer content. The underlying ooze becomes finer grained with increasing depth, with grain size averaging approximately 6ϕ (16 μm) in diameter.

Unit II, the volcaniclastics, can be divided into two subunits on the basis of lithification (Table 2). Subunit IIA (211.7–250.4 mbsf) is 38.7 m of volcanic ash that contains a broad admixture of several components. Almost half of the uppermost Section 121-757B-24X-1 is composed of foraminifers. Glauconite is an important component of Section 2 through the core catcher of Core 121-757B-24X. Lapilli, 2 to 5 mm in diameter, are common, and some of the ash is characterized as lapilli ash or ash with lapilli. Shell fragments occur throughout and locally dominate the core (Fig. 6). A brachiopod shell was recovered from Section 121-757B-25X-2. Pebbles of basalt, usually rounded, are common (Fig. 6), and obsidian pebbles occur in the unit. Smear slides of the ash are dominated by the glass component and show glauconite, feldspar, and traces of quartz and fossil material. Pebbles in the ash are matrix-supported; sharp contacts are present (Fig. 7), along with faint horizontal layering both within the coarser lapilli areas and as laminae in the ash-dominated areas. One occurrence of cross bedding was observed in Unit II. The color of the ash ranges from grayish green (10G 4/2) to dusky green (5G 3/2) and very dark grayish green (5G 2.5/2).

Subunit IIB (250.4–369.0 mbsf) is 116.6 m of tuff. Half of the subunit is characterized by lapilli 2–5-mm in diameter, and the remainder is massive and homogeneous. The tuff contains rounded basalt pebbles, shell fragments and a shell hash (Section 3 and the core catcher of Core 121-757B-37X), and brown flint pebbles. The various sedimentary structures include millimeter-scale horizontal laminae and sharp contacts. The tuff has the same composition as the overlying ash: mostly volcanic glass, with minor feldspar, glauconite, and traces of quartz and fossils. Subunit IIB is dark in color, commonly dusky green (5G 3/2) and very dark grayish green (5G 2.5/2). In Section 121-757C-8R-1, the tuff directly overlying the basalt is dusky red (2.5YR 3/2) and contains shelly material.

Unit III consists of highly plagioclase phyric basalt; penetration was 7.8 m in Hole 757B and 47.9 m in Hole 757C (Table 2).

Discussion

The lithologic section at Site 757, at 17°S on the Ninetyeast Ridge, records a history of declining volcanism and continuing subsidence. The basalt flows, presumably the last expression of the constructional phase of this part of the ridge, are subaerial. Ash deposition onto the flows began in shallow water. The continued incorporation of rounded basalt pebbles and shelly layers into the ash and tuff units suggests a shallow-water setting, which is supported by the scoured contacts and cross lamination within the volcaniclastics. At the end of the time of ash deposition, the site was in slightly deeper water, as indicated by the abundance of foraminifers and the decline in the relative amounts of bivalve fragments and basalt clasts. The presence of matrix-supported grains and the general lack of size grading in the ashes imply very rapid deposition at rates high enough to overcome the natural tendency of marine processes to rearrange all sediment input into coherent size groupings.

Open-ocean pelagic sedimentation began on the small plateau near the ridge crest at the conclusion of the ash eruptive episode, during the earliest Eocene. Since then, sedimentation has been continuous. The rates, however, were slower in the Oligocene and early Miocene and more rapid in the Eocene and middle Miocene to Pleistocene. This rate pattern, with the Oligocene minima, typifies much of the eastern Indian Ocean.

BIOSTRATIGRAPHY

Summary

Three holes were drilled at Site 757. Hole 757B is of the most interest for paleontology because it was continuously cored to a total depth of 374.8 mbsf, and a thick upper Paleocene to Holocene sedimentary section was recovered. The hole was terminated when basaltic basement was penetrated. Sediments recovered at Site 757 consist of about 212 m of calcareous ooze (Cores 121-757B-1H to 121-757B-23X), overlying a 156-m-thick volcaniclastic unit.

The calcareous ooze contains abundant calcareous nannofossils and planktonic foraminifers and is dated as early Eocene to Holocene. A few benthic foraminifers occur in this unit. Throughout this unit, preservation of nannofossils is good to poor and preservation of foraminifers is good to moderate. Rare diatoms and other siliceous microfossils are found in the Pleistocene, but are absent below.

The top of the volcaniclastic unit (Core 121-757B-24X) contains coccoliths and foraminifers and is dated as late Paleocene. Most of the sediments below Core 121-757B-24X are barren of microfossils.

Stratigraphy

Calcareous nannofossils and planktonic foraminifers provide stratigraphic control of the section. A summary of the age-depth relationship using the calcareous nannofossil and fora-

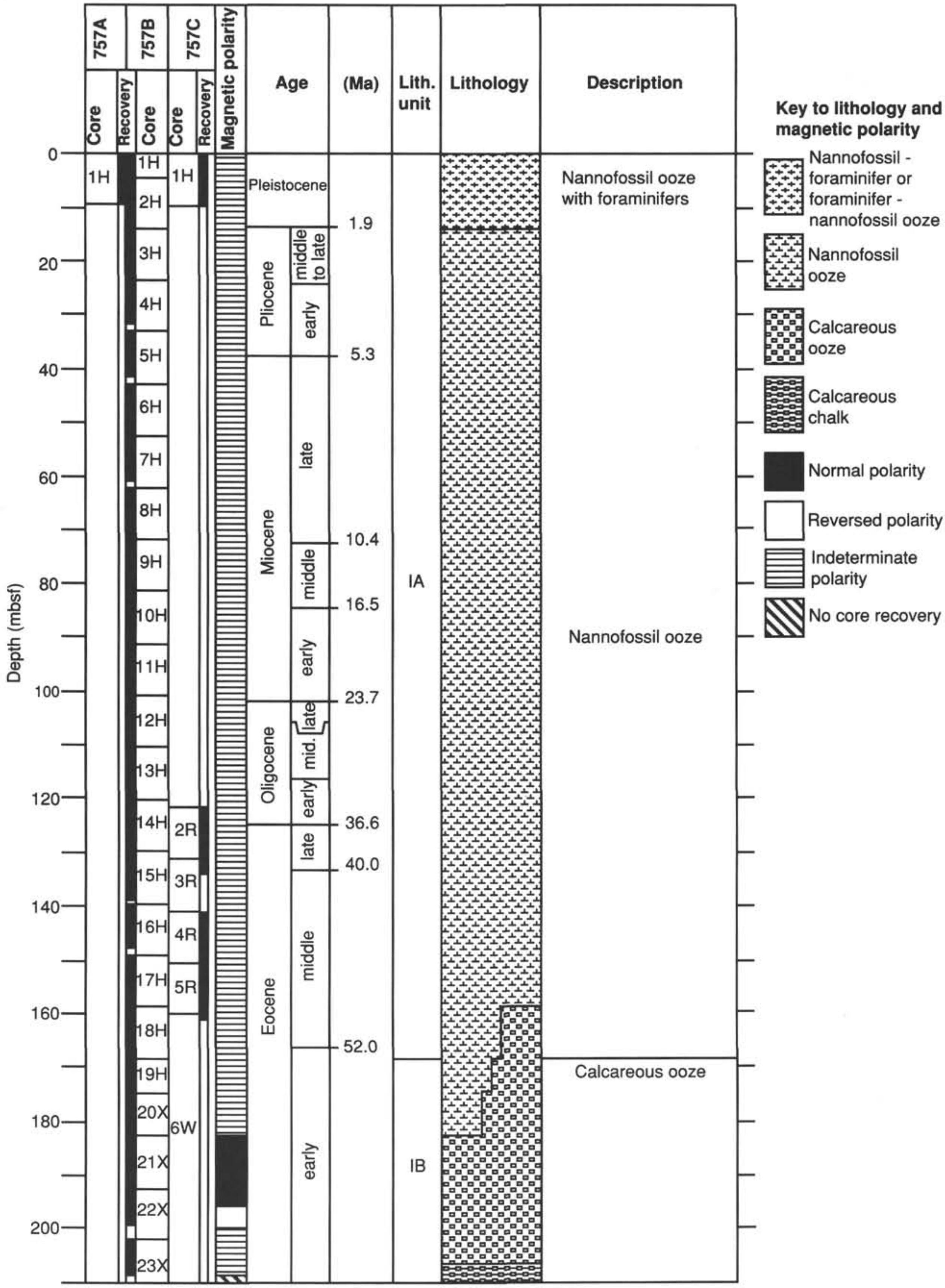

Figure 4. Site 757 summary diagram.

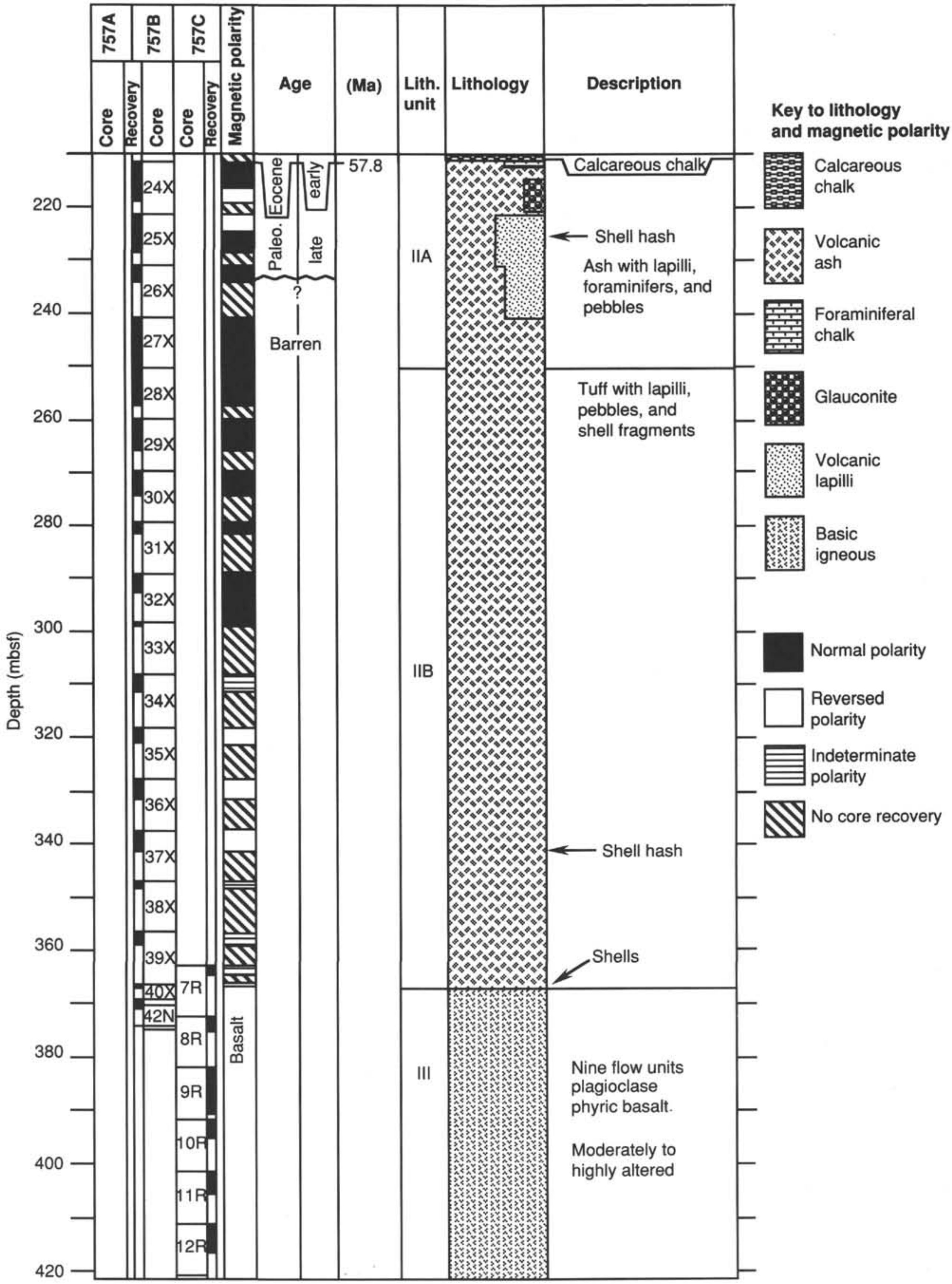

Figure 4 (continued).

Table 2. Lithologic units at Site 757.

Unit	Core interval	Depth (mbsf)	Lithology	Age
IA	757A-1H 757B-1H to -18H 757C-1R to -5R	0.0–168.5	Nannofossil ooze with foraminifers	Pleistocene–middle Eocene
IB	757B-19H to -23X	168.5–211.7	Calcareous ooze with chalk and ash	early Eocene
IIA	757B-24X to -27X	211.7–250.4	Ash with lapilli, foraminifers, and pebbles	early Eocene–late Paleocene
IIB	757B-28X to -40X 757C-7R	250.4–367.0	Tuff with lapilli, pebbles, and shells	late Paleocene(?)
III	757B-40X to -43N 757C-8R to -12R	369.0–374.8 372.8–420.7	Basalt with phenocrysts	late Paleocene(?)

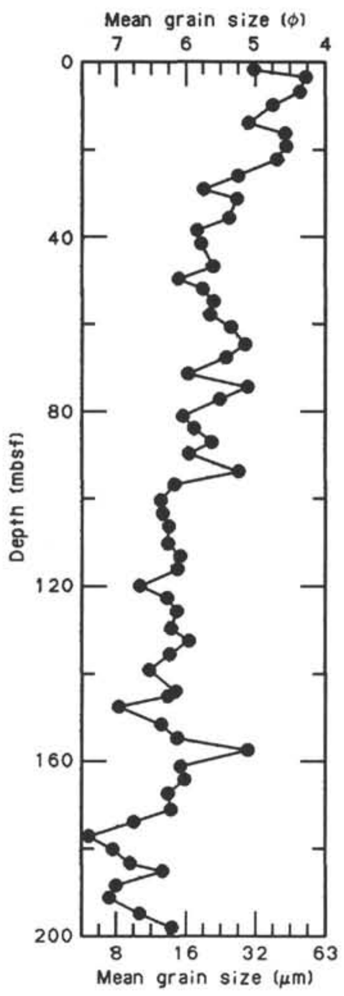

Figure 5. Bulk-sediment grain size of lithologic Unit I, Hole 757B.

Table 3. Grain-size analyses of bulk sediment from lithologic Unit I, Hole 757B.

Core, section, interval (cm)	Depth (mbsf)	Mean diameter (μm)	Mean diameter (ϕ)
1H-2, 70	2.03	30.60	5.03
1H-CC, 5	3.76	51.50	4.28
2H-2, 90	6.90	48.70	4.36
2H-4, 90	9.90	36.80	4.76
2H-7, 50	14.00	29.00	5.11
3H-2, 90	16.40	41.80	4.58
3H-4, 90	19.40	42.30	4.56
3H-6, 90	22.40	38.40	4.70
4H-2, 90	26.00	26.10	5.26
4H-4, 90	29.00	18.50	5.76
4H-6, 20	31.30	25.70	5.28
5H-2, 90	35.60	23.80	5.39
5H-4, 90	38.60	17.20	5.86
5H-CC, 10	41.60	17.90	5.80
6H-3, 95	46.75	20.40	5.62
6H-5, 95	49.75	14.40	6.12
6H-CC, 5	51.94	18.20	5.78
7H-2, 90	54.90	20.40	5.62
7H-4, 90	57.90	19.60	5.67
7H-CC, 1	60.72	24.30	5.36
8H-2, 90	64.60	28.00	5.16
8H-4, 92	67.62	23.20	5.43
8H-CC, 1	71.40	15.70	5.99
9H-2, 94	74.24	28.80	5.12
9H-4, 94	77.24	21.80	5.52
9H-CC, 1	81.06	15.00	6.06
10H-2, 92	83.92	16.70	5.90
10H-4, 92	86.92	20.00	5.64
10H-CC, 1	89.79	16.00	5.97
11H-2, 92	93.62	26.30	5.25
11H-4, 92	96.62	13.80	6.18
11H-CC, 1	100.53	11.90	6.39
12H-2, 92	103.22	12.20	6.36
12H-4, 92	106.22	13.00	6.27
12H-CC, 1	110.00	12.90	6.28
13H-2, 92	112.92	14.60	6.10
13H-4, 92	115.92	14.20	6.14
13H-CC, 1	119.76	9.70	6.69
14H-2, 92	122.52	12.80	6.29
14H-4, 92	125.52	14.10	6.15
14H-CC, 1	129.49	13.30	6.23
15H-2, 92	132.22	15.90	5.97
15H-4, 92	135.22	13.10	6.25
15H-CC, 1	138.91	10.70	6.55
16H-3, 135	143.85	13.90	6.17
16H-4, 92	144.92	12.90	6.28
16H-CC, 1	147.43	7.80	7.00
17H-2, 95	151.55	12.00	6.38
17H-4, 95	154.55	14.10	6.15
17H-6, 95	157.55	28.80	5.12
18H-2, 95	161.25	14.60	6.10
18H-4, 95	164.25	15.20	6.04
18H-6, 95	167.25	12.90	6.28
19H-2, 95	170.95	13.20	6.24
19H-4, 95	173.95	9.10	6.78
20X-2, 95	177.15	5.80	7.43
20X-4, 95	180.15	7.40	7.08
20X-6, 95	183.15	8.80	6.83
21X-2, 95	185.15	12.10	6.37
21X-4, 95	188.15	7.60	7.04
21X-6, 95	191.15	7.10	7.14
22X-2, 95	194.85	9.60	6.70
22X-4, 95	197.85	13.30	6.23

minifer datum levels (Table 4) is shown in Figure 8. A biostratigraphic zonation of Site 757 is shown in Figure 9.

The Pliocene/Pleistocene boundary is placed in Core 121-757B-2H, the Miocene/Pliocene boundary in Core 121-757B-5H, and the Miocene/Oligocene boundary in Core 121-757B-12H. The Eocene/Oligocene boundary is recorded in Core 121-757B-14H, and the boundary between Eocene and Paleocene is between Sections 1 and 2 of Core 121-757B-24X.

The sedimentary record seems to be fairly complete. However, the series is somewhat condensed in the middle Miocene and in the lowermost Eocene, as shown on the age-depth curve (Fig. 8), and hiatuses may exist.

Paleoenvironments

Sample 121-757B-25X-CC contains a benthic foraminifer assemblage that indicates an outer neritic environment (about

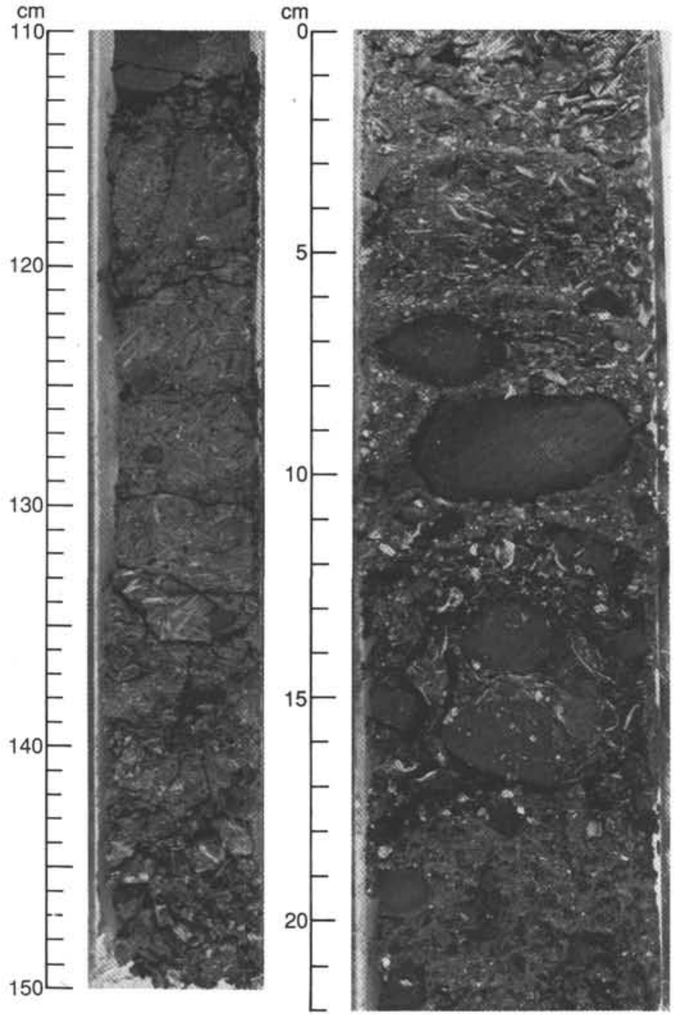

Figure 6. Shelly layer with rounded basalt pebbles in lithologic Subunit IIA (Sections 121-757B-25X-2, 110–150 cm, and 121-757B-25X-3, 0–22 cm).

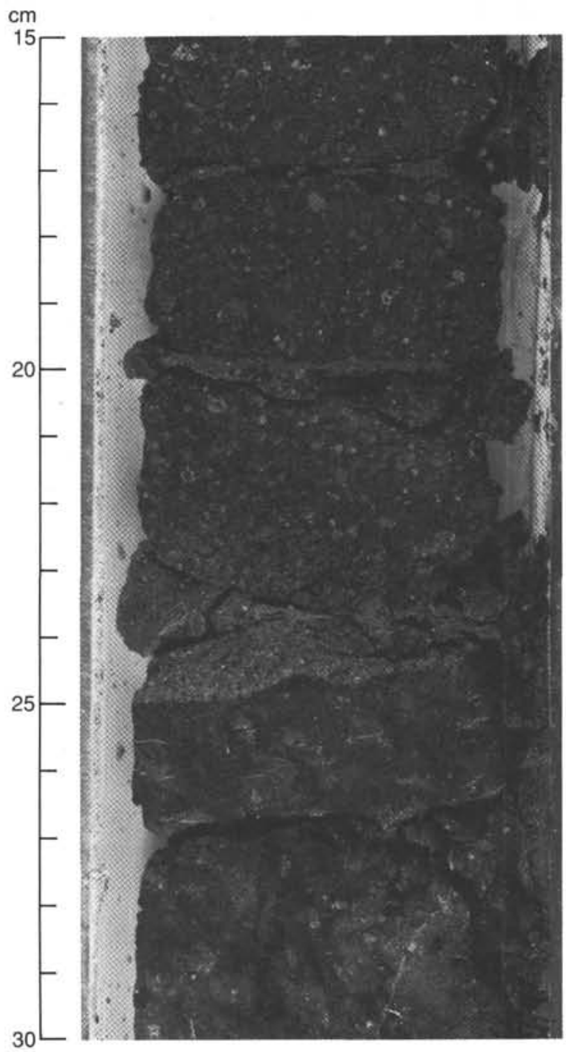

Figure 7. Sharp eroded contact with lapilli ash of lithologic Subunit IIA (Section 121-757B-25X-2, 15–30 cm).

100–200 m) existed during the Paleogene at Site 757. The water depth abruptly changed during the early Eocene, where the assemblage in Sample 121-757B-23X-CC indicates middle to upper bathyal depths (about 600 m). The faunas from Samples 121-757B-22X-CC to 121-757B-1H-CC indicate that deposition occurred at lower bathyal depths (about 1500 m) during the early Eocene to Holocene (Fig. 10).

Late Miocene through Holocene age calcareous nannofossil assemblages reflect subtropical to tropical conditions, whereas Paleocene through middle Miocene assemblages are of a more temperate nature. Similarly, planktonic foraminifers are typical subtropical to tropical faunas in the Neogene and upper Paleogene. More temperate assemblages were found in the lower Oligocene and Eocene.

This temporal variation presumably reflects the northward movement of Ninetyeast Ridge.

Calcareous Nannofossils

Upper Paleocene to Pleistocene sediments containing abundant calcareous nannofossils were recovered from Hole 757B. The hole was drilled to a total depth of 374.8 mbsf, and nannofossils are abundant down to Core 121-757B-24X (221.4 mbsf) where a transition from nannofossil chalk to volcaniclastics occurs. The chalks directly above this transition zone, in Core 121-757B-23X, are assigned to the lower Eocene *Tribrachiatus orthostylus* Zone (CP10). Sediments of the transition zone, in Samples 121-757B-23X-CC, and 121-757B-24X-1, 53–54 cm, are assigned to the *Discoaster binodosus* Subzone (CP9b). The remaining sections of Core 121-757B-24X are placed in the late Paleocene age *Discoaster multiradiatus* Zone (CP8). A hiatus may exist between these two zones, as the *Tribrachiatus contortus* Subzone (CP9a) was not identified. The volcaniclastic unit is barren of nannofossils, except for a few intervals that contain sparse, poorly preserved, non-age-diagnostic specimens.

Preservation in the nannofossil oozes is generally moderate to poor, except for good preservation in the upper Miocene to Pleistocene sediments. Preservation in the ash-rich upper Paleocene to lower Eocene units is also good.

Discoasters of the Eocene through middle Miocene are strongly overgrown with calcite while the coccoliths show signs of dissolution. For the most part, the delicate central area structure of each coccolith specimen has dissolved, leaving just the rims for identification. The calcite that dissolved from the coccoliths appears to have relocated on the larger crystal faces of the discoasters. The larger "seed" crystals easily act as sites of deposition for any spare calcite that may be present in the interstitial fluids of the sediment.

Table 4. Calcareous nannofossil and planktonic foraminifer datums, Hole 757B.

Species event[a]	Age (Ma)	Depth (mbsf)
Calcareous nannofossils		
LO *Pseudoemiliania lacunosa*	0.474	3.8–2.3
LO *Calcidiscus macintyrei*	1.45	10.5–9.0
LO *Discoaster brouweri*	1.9	13.5–12.0
LO *Discoaster tamalis*	2.6	17.0–15.5
LO *Reticulofenestra pseudoumbilica*	3.5	23.6–23.0
FO *Discoaster tamalis*	3.8	26.6–28.1
FO *Ceratolithus acutus*	5.0	38.2–39.7
LO *Discoaster quinqueramus*	5.6	44.3–42.8
FO *Amaurolithus primus*	6.5	52.5–54.0
FO *Discoaster quinqueramus*	8.2	62.2–63.6
LO *Discoaster hamatus*	8.85	71.8–71.2
LO *Coccolithus floridanus*	13.1	81.5–80.9
LO *Sphenolithus heteromorphus*	14.4	84.5–83.0
FO *Discoaster exilis*	15.4	89.0–90.5
FO *Sphenolithus heteromorphus*	17.1	95.7–97.2
FO *Sphenolithus belemnos*	21.5	98.7–100.2
FO *Discoaster druggii*	23.2	100.2–100.8
LO *Sphenolithus ciperoensis*	23.7	102.3–100.8
FO *Sphenolithus ciperoensis*	30.2	105.3–106.8
FO *Sphenolithus distentus*	34.2	110.5–112.0
LO *Reticulofenestra umbilica*	34.6	116.5–115.0
LO *Coccolithus formosus*	35.1	120.1–119.5
LO *Discoaster saipanensis*	36.7	124.6–123.1
FO *Isthmolithus recurvus*	37.8	129.1–129.8
LO *Chiasmolithus grandis*	40.0	133.3–131.8
LO *Nannotetrina fulgens*	45.4	155.1–153.6
LO *Chiasmolithus gigas*	47.0	159.9–158.4
FO *Chiasmolithus gigas*	48.8	166.0–167.5
FO *Nannotetrina fulgens*	49.8	174.7–175.3
FO *Discoaster sublodoensis*	52.6	185.7–187.2
LO *Tribrachiatus orthostylus*	53.7	203.5–202.0
FO *Discoaster lodoensis*	55.3	211.7–213.2
Planktonic foraminifers		
LO *Globigerinoides obliquus extremus*	1.6	0.0–4.5
LO *Globorotalia truncatulinoides*	1.9	4.5–14.0
LO *Globorotalia multicamerata*	2.9	4.5–14.0
FO *Globigerinoides fistulosus*	2.9	4.5–14.0
LO *Globoquadrina altispira*	2.9	14.0–23.6
LO *Sphaeroidinella seminulina*	3.0	23.6–33.2
FO *Globorotalia tosaensis*	3.1	23.6–33.2
LO *Globorotalia margaritae*	3.4	23.6–33.2
LO *Globigerina nepenthes*	3.9	23.6–33.2
FO *Sphaeroidinella dehiscens*	5.1	33.2–42.8
FO *Globorotalia tumida*	5.2	33.2–42.8
FO *Globigerinoides conglobatus*	5.3	33.2–42.8
LO *Globoquadrina dehiscens*	5.3	42.8–52.5
FO *Globorotalia plesiotumida*	7.7	52.5–62.2
LO *Globorotalia siakensis*	10.4	71.8–81.5
LO *Praeorbulina glomerosa curva*	14.9	81.5–91.2
LO *Globorotalia kugleri*	21.8	91.2–100.8
FO *Globoquadrina dehiscens*	23.2	91.2–100.8
LO *Pseudohastigerina*	34.0	110.5–120.1
LO *Globorotalia cocoaensis*	36.6	120.1–121.1
LO *Hantkenina*	36.6	120.1–121.1

[a] FO = first occurrence; LO = last occurrence.

Neogene

In Hole 757B, Pleistocene sediments are present down to Sample 121-757B-2H-4, 149–150 cm (13.5 mbsf), where the last occurrence of *Discoaster brouweri* is recorded. The Pleistocene nannofossil assemblage, which includes abundant *Ceratolithus cristatus*, reflects subtropical to tropical conditions.

The assemblages of the thick upper Miocene and Pliocene sections are also indicative of subtropical to tropical conditions. The fully developed assemblages include abundant amauroliths, ceratoliths, and scyphospheres. Also present are *Discoaster quinqueramus, Discoaster tamalis*, and *Ceratolithus acutus*. The first occurrence of *C. acutus* is recorded in Sample 121-757B-5H-4, 45–46 cm (38.2 mbsf), and is used to mark the Miocene/Pliocene boundary.

The Miocene section may not be complete, as the middle and lower Miocene sections are quite condensed in comparison to the upper Miocene and Pliocene sequences, and a hiatus is noted by the planktonic foraminiferal paleontologists within the interval containing the sediments placed in Zone CN5. Additional work on this interval is necessary to determine whether both Subzones CN5a and CN5b are present. The nannofossil assemblages of the lower and middle Miocene intervals lack abundant tropical forms and are of a more temperate nature. Forms such as *Discoaster neohamatus* and *Discoaster hamatus* were recognized, but other subtropical to tropical forms such as *Discoaster bollii* and species of the genus *Catinaster* have not yet been found.

Lower Miocene sediments contain abundant *Cyclicargolithus floridanus* and species of the genus *Sphenolithus*. All of the species used to zone lower Miocene sediments are present, with the exception of *Helicosphaera ampliaperta*. The taxa present include *Sphenolithus heteromorphus, Sphenolithus belemnos, Discoaster druggii*, and *Triquetrorhabdulus carinatus*. The last occurrence of *Sphenolithus ciperoensis* in Sample 121-757B-12H-1, 149–150 cm (102.3 mbsf), is used to denote the Oligocene/Miocene boundary.

Paleogene

Oligocene sediments are present from 102.3 to 124.6 mbsf. Middle and upper Oligocene sediments contain abundant *C. floridanus, Zyghrablithus bijugatus*, and *Reticulofenestra bisecta*. The zonal markers *Sphenolithus predistentus, S. distentus*, and *S. ciperoensis* are all present. Lower Oligocene assemblages include *Reticulofenestra umbilica, Coccolithus formosus, Isthmolithus recurvus*, and *Sphenolithus pseudoradians*. The Eocene/Oligocene boundary is based on the last occurrence of *Discoaster barbadiensis* and *Discoaster saipanensis*, which is recorded in Sample 121-757B-14H-3, 149–150 cm.

Upper Eocene sediments are confined to the interval from 124.6 to 133.3 mbsf. *D. barbadiensis, D. saipanensis, R. umbilica*, and *C. formosus* are abundant, and *I. recurvus, S. pseudoradians*, and *Bramletteius serraculoides* are common in this unit. Compared to the upper Eocene sections, the middle Eocene units present in the interval from 133.3 to approximately 174.7 mbsf are more expanded. The uppermost middle Eocene (CP14) contains abundant *B. serraculoides, Chiasmolithus grandis*, and *Pseudotriquetrorhabdulus inversus* (*Wiseorhabdus* of some authors). Sediments assigned to Zone CP13 contain the zonal marker *Nannotetrina fulgens* and the elusive but strikingly distinctive *Chiasmolithus gigas*, the entire range of which defines Subzone CP13b. Lower Eocene (Zones CP10 to CP12) sediments occur from 174.7 to 211.7 mbsf. The interval contains common to abundant but heavily overgrown *Discoaster sublodoensis, Tribrachiatus orthostylus*, and *Discoaster lodoensis*. Sediments in the interval from Section 121-757B-24X-1 to Sample 121-757B-24X-1, 53–54 cm, are assigned to Subzone CP9b, based on the presence of *T. orthostylus* and the absence of *D. lodoensis, Tribrachiatus bramlettei*, and *Tribrachiatus contortus*. The index fossils representative of Subzone CP9a were not found, which possibly indicates a hiatus between the lower Eocene sediments and the underlying Paleocene sections.

The remaining sections of Core 121-757B-24X are assigned to Zone CP8 based on the presence of common *Discoaster multiradiatus* and the lack of early Eocene markers. Other Paleocene species that were noted include *Zygodiscus sigmoides, Toweius eminens, Discoaster lenticularis, Discoaster nobilis*, and *Discoaster mohleri*. Sediments of this core also contain few *Braarudasphaera* sp. and *Micrantholithus* sp. which may be indicative of a shallow-water or restricted environment of deposition.

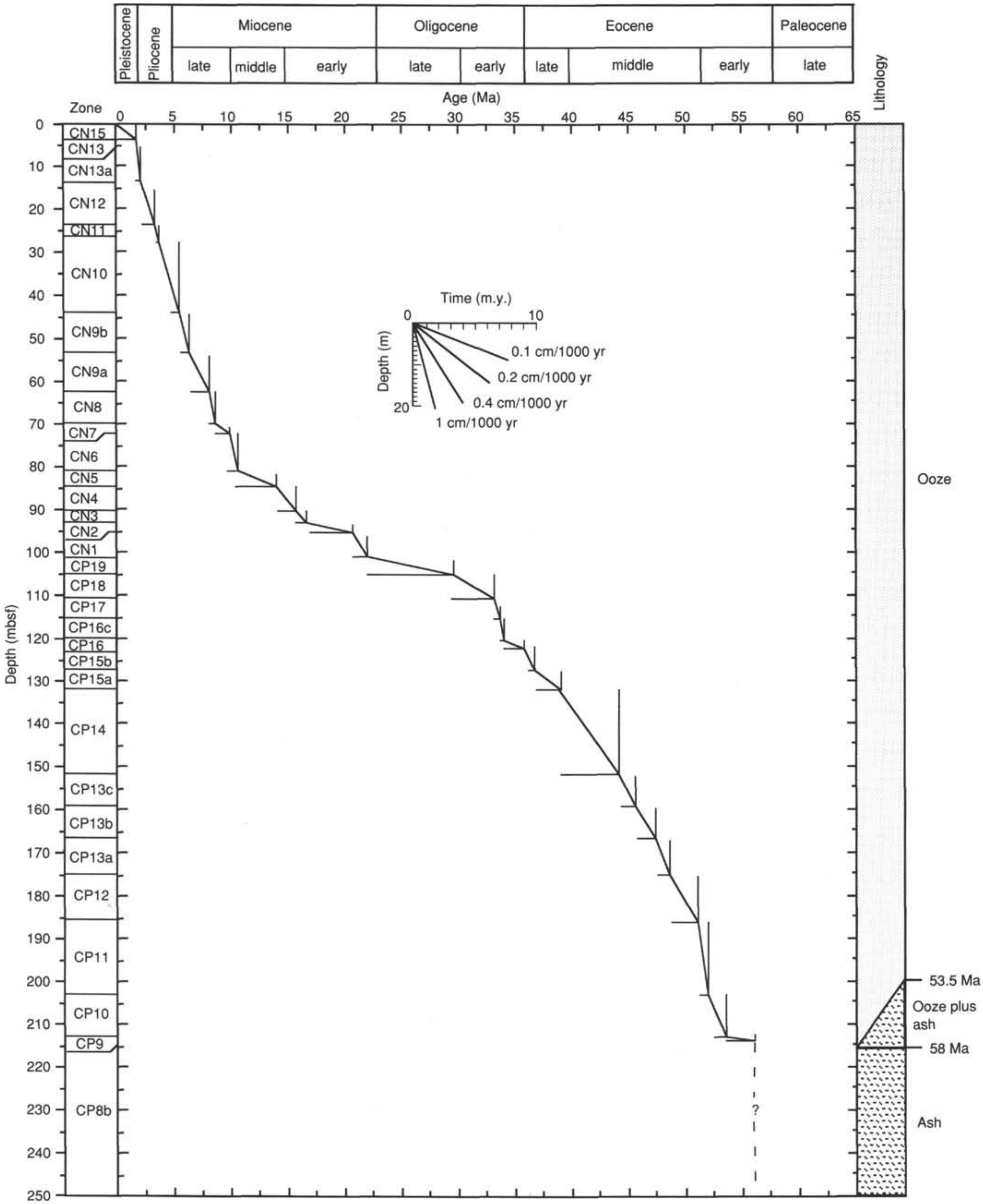

Figure 8. Age vs. depth plot for Site 757. Vertical bars represent the stratigraphic ranges and horizontal bars represent the ranges of the calcareous nannofossil zones.

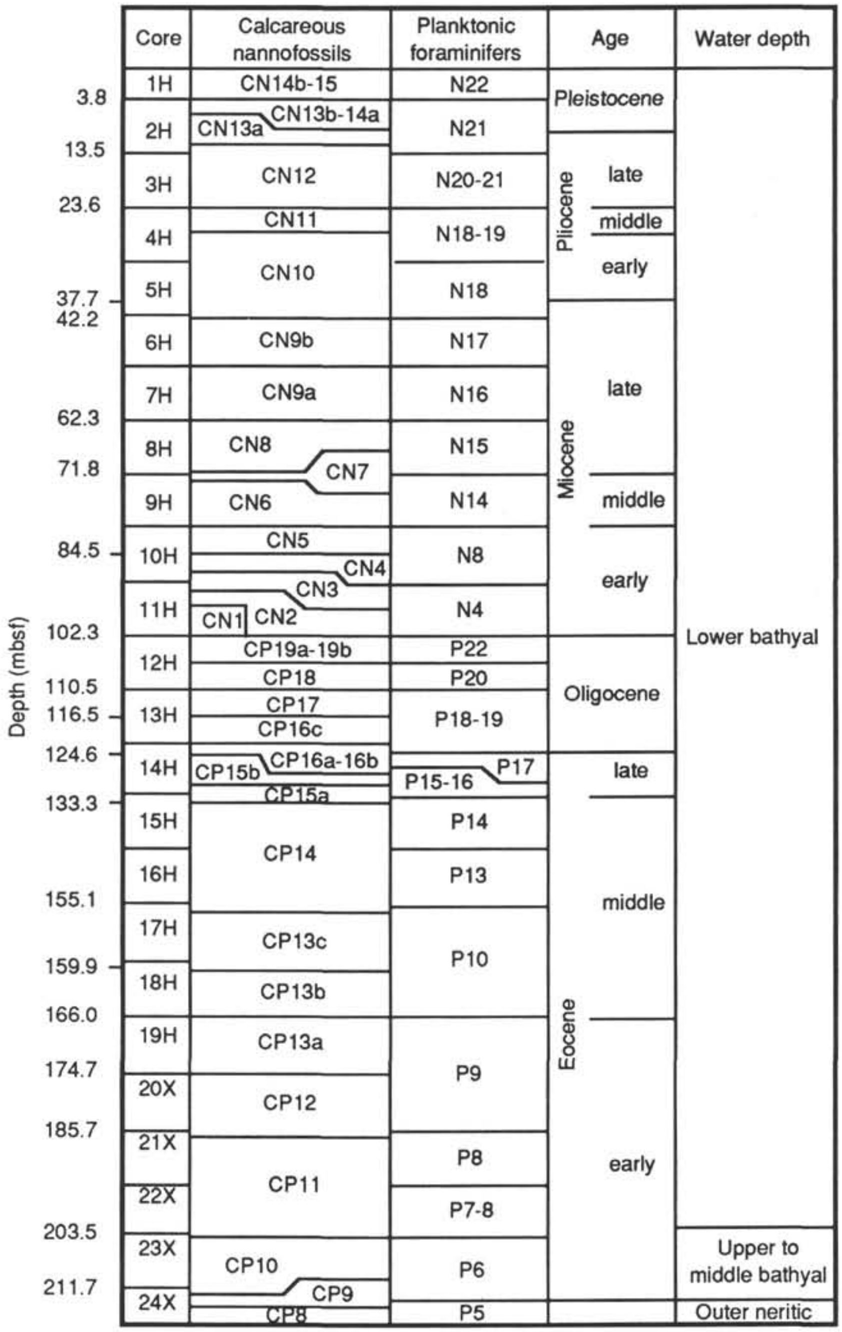

Figure 9. Calcareous nannofossil and planktonic foraminifer zones in Hole 757B.

The Paleogene nannofossil assemblages at Site 757 reflect temperate to subtropical conditions. Discoasters such as *D. lodoensis* and *D. saipanensis* are abundant, in contrast to few *Chiasmolithus solitus* and *Chiasmolithus altus*, which are usually in abundance in higher latitude sections such as those recovered from Broken Ridge. The late Eocene, high-latitude marker species *I. recurvus* is present, but it is not as abundant as at Broken Ridge. Another late Eocene age species, *Chiasmolithus oamaruensis*, is abundant in the Broken Ridge sediments but has not yet been noted in the sediments of Site 757.

Planktonic Foraminifers

The planktonic foraminifer assemblages recovered from the uppermost Eocene to Holocene sediments in Hole 757B have an affinity with other subtropical to tropical assemblages from the Indian Ocean. By contrast, only the late Miocene to Holocene age assemblages recovered at Site 756, the southernmost site drilled on Ninetyeast Ridge, show an affinity with subtropical faunas. The faunas from the middle Eocene to middle Miocene sediments at Site 757 are associated more closely with the temperate assemblages of the Southern Hemisphere. The change in the composition between the assemblages recovered from Broken Ridge and from Ninetyeast Ridge is not only a reflection of changing surface-water circulation patterns but also resulted from the northward motion of Ninetyeast Ridge bringing drill sites originally at high latitudes to lower latitudes.

Neogene to Holocene

A well-preserved early Miocene to Holocene age assemblage of planktonic foraminifers was recovered from Hole 757B. Domi-

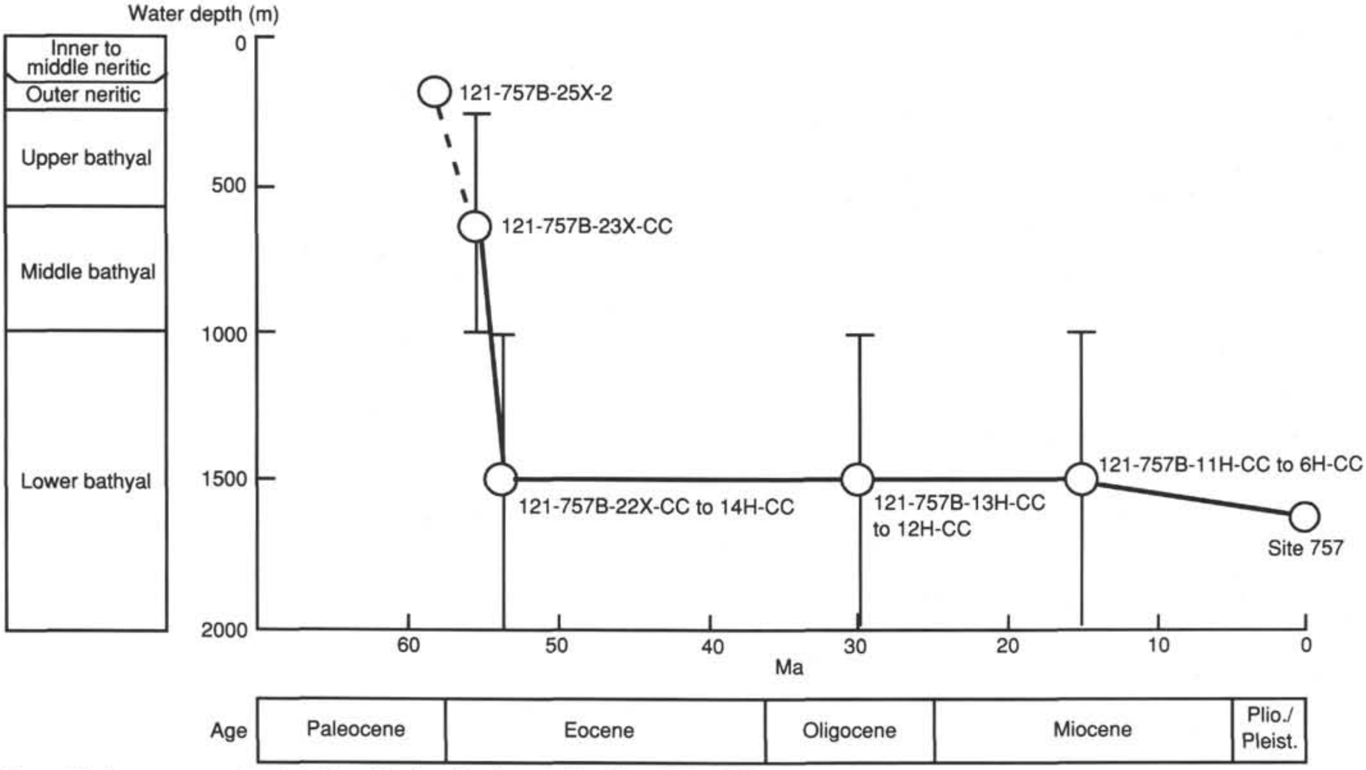

Figure 10. Age vs. water depth indicated by benthic foraminifers from Hole 757B.

nating the assemblage are typical, warm subtropical to tropical faunas. The abundance of low-latitude marker species made it possible to apply the zonation schemes of Banner and Blow (1965) and Blow (1969).

Pleistocene

A Pleistocene planktonic foraminifer assemblage was recovered from Sample 121-757B-1H-CC. Common throughout the fauna are the marker species *Globorotalia truncatulinoides* and the tropical species *Pulleniatina obliquiloculata, Globigerinoides obliquus, Globigerinoides trilobus*, and *Globorotalia menardii*.

Pliocene

A complete Pliocene sequence of sediments was recovered in Samples 121-757B-2H-CC to 121-757B-5H-CC. Faunas are dominated by the tropical to warm-subtropical species *G. obliquus, Globigerinoides extremus, Globigerinoides sacculifer, Globigerinoides conglobatus, Globorotalia tumida, G. trilobus, Sphaeroidinellopsis multiloba, G. menardii, Globorotalia limbata, Globigerinoides ruber, Globigerinoides ruber pyramidalis, Globoquadrina altispira altispira*, and *Globoquadrina altispira globosa*. Temperate to subtropical species similar to those recorded on Broken Ridge, such as *Globigerina bulloides* and *Globigerina woodi*, rarely occur. Rare throughout are the tropical *Pulleniatina* sp., *Neogloboquadrina* sp., *Globorotalia tumida flexuosa*, and *Globigerinoides fistulosus*. Preservation throughout the entire Pliocene is excellent.

Miocene

Upper Miocene sediments were recovered from Samples 121-757B-6H-CC and 121-757B-7H-CC. The continued presence of species from the *Globorotalia merotumida-G. tumida* lineage aids the subdivision of these sediments. The Miocene/Pliocene boundary is placed at the first appearance of *G. tumida* from *Globorotalia plesiotumida*, which is slightly below the first appearance of *Sphaeroidinella dehiscens* and slightly above the last appearance of *Globoquadrina dehiscens*.

A large proportion of the faunas is composed of more warm, subtropical to tropical forms such as *G. menardii, G. limbata, Globorotalia multicamerata, Sphaeroidinellopsis multiloba, G. altispira altispira*, and *G. altispira globosa*. Abundant throughout are *Orbulina universa, G. dehiscens, Globigerina nepenthes*, and *Sphaeroidinellopsis seminulina*.

Typical middle Miocene faunas were recovered only from Samples 121-757B-8H-CC and 121-757B-9H-CC. Only the N14 and N15 Zones of Banner and Blow (1965) were discerned. Species from the *Globorotalia fohsi* lineage were not recovered from spot samples taken between Samples 121-757B-8H-CC and 121-757B-9H-CC. Their absence, along with the absence of *Orbulina* sp., indicates that Zones N9 to N12 are missing. The faunas present are very similar to those in the upper Miocene.

Immediately below in Sample 121-757B-10H-CC, the faunas are characterized by the presence of *Praeorbulina glomerosa curva* and *Praeorbulina sicana*. This assigns the assemblage to Zone N8, of latest early Miocene age. Early Miocene age faunas were recovered from Sample 121-757B-10H-CC only. The species *Globigerina praedehiscens, Globigerina selli*, and *Globigerina venezuelana* are abundant. The co-occurrence of *Globorotalia kugleri* and *Globigerinoides primordius* assigns this sample to the earliest Miocene age Zone N4.

Paleogene

Oligocene

Early to late Oligocene age faunas were found in Cores 121-757B-12H-CC and 121-757B-13H-CC. Abundant throughout are *G. venezuelana, Globigerina galavisi*, and *Globigerina euapertura*. Only the latter sample could be assigned to the early Oligocene age Zones P18-19 of Blow (1969), based on the presence of *Pseudohastigerina micra* and *Pseudohastigerina naguewichiensis* and the absence of Eocene species *Turborotalia cerroa-*

zulensis, Globigerinatheka index, Hantkenina alabamensis, and *Cribrohantkenina inflata*.

Upper Eocene

Late Eocene age faunas were recovered from Sample 121-757B-14H, 140–142 cm. The faunas are tentatively assigned to the latest Eocene age Zone P17 of Blow (1969), based on the rare presence of *T. cerroazulensis* s.l. and *Turborotalia cerroazulensis cocoaensis* and the absence of *Globigerinatheka* sp. and *Cribrohantkenina inflata*. Common to the assemblages are *H. alabamensis, Globigerina eocaena, P. micra, P. naguewichiensis*, and *Chiloguembelina cubensis*.

Middle Eocene to Uppermost Paleocene

In Samples 121-757B-14H-CC to 121-757B-24X-1, 140 cm (129–213.1 mbsf), we found abundant planktonic foraminiferal assemblages of moderate to poor preservation. The marker species *T. cerroazulensis* s.l. is severely dissolved in the upper Eocene, in comparison with other species in the same samples.

A search for microtektites in the upper Eocene (five toothpick samples per section in Cores 121-757B-14H to 121-757B-16H) was unsuccessful.

The faunas are typical for austral, temperate assemblages (Toumarkine and Luterbacher, 1985) and lack most of the ornate, evolved low-latitude species, such as *Hantkenina* spp., *Morozovella lehneri, Planorotalites palmerae, Truncorotaloides topilensis*, and *Morozovella velascoensis*. The few warmer water species that were found, such as *Morozovella spinulosa* in the middle Eocene (Samples 121-757B-15H-CC to 121-757B-18H-CC) and *Morozovella aragonensis* (Samples 121-757B-18H-CC to 121-757B-22X-CC), *Morozovella marginodentata, Morozovella subbotina*, and *Morozovella caucasica* (Samples 121-757B-22X-CC to 121-757B-23X-CC) in the lower Eocene, occur in a very low abundance.

The late middle Eocene and late Eocene age assemblages are characterized by abundant *Globigerinatheca* spp. The middle Eocene assemblages are dominated by *Acarinina bullbrooki* and *Acarinina primitiva*, and the early Eocene age assemblages by *A. primitiva* and *Acarinina soldadoensis*. The earliest Eocene (Zone P6) and latest Paleocene age assemblages are characterized by common to abundant *G. velascoensis* and *A. soldadoensis*. Such assemblages are typical for austral/temperate areas (Jenkins, 1985). The assemblage of Sample 121-757B-23X-CC is identical to the assemblage found in lower Eocene Sample 121-752B-3R-CC from Broken Ridge.

The uppermost Paleocene was found only in Sections 2 through 4 of Core 121-757B-24X and is represented by *Acarinina mckannai, G. velascoensis, Planorotalites chapmani*, and *Morozovella aequa*.

Benthic Foraminifers

All core-catcher samples from Hole 757B were examined for $>125\mu$m-sized benthic foraminifers. Neogene to Eocene foraminifers are rare, but they are well preserved. However, Paleocene foraminifers near the top of the shell hash within the basalt volcaniclastics are poorly preserved. With the exception of a sample taken in Section 121-757B-25X-2, Samples 121-757B-24X-CC to 121-757B-38X-CC are barren of benthic foraminifers.

Pleistocene to Pliocene

Pliocene to Pleistocene faunas from Samples 121-757B-1H-CC to 121-757B-4H-CC are characterized by a low abundance of benthic foraminifers. *Globocassidulina subglobosa, Planulina wuellerstorfi*, and *Uvigerina* spp. are consistently found. According to the Holocene distribution of benthic foraminifers in the equatorial Indian Ocean (Peterson, 1984), these species are associated with the Indian Deep Water.

Miocene

Late Miocene age faunas (Samples 121-757B-5H-CC to 121-757B-8H-CC) are characterized by *Uvigerina proboscidea, Uvigerina hispida, Bulimina rostrata, Gyroidina soldanii*, and *Oridorsalis umbonatus*. Other elements of these faunas are similar to the Pliocene to Pleistocene faunas. Middle Miocene faunas (Sample 121-757B-9H-CC) contain a few specimens with low diversity. Early Miocene faunas (Samples 121-757B-10H-CC and 121-757B-11H-CC) contain the larger forms of *Cibicidoides, O. umbonatus*, and *Vulvulina pennatula. Favocassidulina favus* is common in Sample 121-757B-10H-CC, which is the first record of this species in the lower Miocene.

Oligocene

Oligocene faunas (Samples 121-757B-12H-CC and 121-757B-13H-CC) are generally similar to those of early Miocene age. However, the lower bathyal to abyssal species *Bulimina jarvisi* occurs consistently. The depth ranges of most of the taxa indicate lower bathyal depths through the Oligocene.

Eocene

Eocene faunas (Samples 121-757B-14H-CC to 121-757B-23X-CC) are characterized by the species diversification of the genera *Anomalinoides* and *Cibicidoides. Cibicidoides havanensis* is restricted to the upper Eocene. *Anomalinoides capita* is consistently found in lower to middle Eocene sediments.

Based on the upper and lower depth limits of *Alabamina dissonata, A. capita, Anomalinoides pseudogrosserugosa, B. jarvisi, Bulimina trinitatensis, Bulimina tuxpomensis, Cibicidina walli, Cibicidoides eocanus, C. havanensis, Nuttalides truempyi*, and *Turrilina brevispira* (van Morkhoven et al., 1986), the water paleodepth of Samples 121-757B-14H-CC to 121-757B-22X-CC is lower bathyal (about 1500 m) and that of Sample 121-757B-23X-CC is upper to middle bathyal (about 600 m).

Paleocene

Poorly preserved benthic foraminifers, ostracodes, bryozoans, and molluscan shell fragments are present in a shell hash sediment (Sample 121-757B-25X-2, 122–124 cm). The benthic foraminiferal assemblage consists of *Lenticulina* with thick-test walls and smaller-shaped *Cibicidoides* and is associated with more shallow-water elements such as *Stomatorbina* sp., *Coleites* sp., and *Guttulina* spp. This assemblage indicates an outer neritic environment (100–200 m in depth).

Diatoms

Rare and poorly preserved diatoms, silicoflagellates, radiolarians, and sponge spicules occur in the Pleistocene sediments of Holes 757A, 757B, and 757C.

Sample 121-757A-1H-CC contains a moderately to poorly preserved assemblage. The diatom floras are typical for low latitudes and consist of rare specimens of *Coscinodiscus nodulifer, Ethmodiscus rex, Rhizosolenia alata, Thalassiosira eccentrica, Thalassionema nitzschioides, Thalassionema bacillaris, Thalassiothix longissima, Nitzschia marina, Nitzschia fossilis*, and *Nitzschia reinholdii*(?).

IGNEOUS PETROLOGY

Drilling at Site 757 recovered basaltic rocks from Holes 757B and 757C. In Hole 757B, basaltic ashes encountered at 212 mbsf beneath calcareous sediments of late Paleocene age were drilled to 374.8 mbsf, when the hole was abandoned. Near the bottom of the hole, a highly plagioclase-phyric basalt unit was drilled between approximately 369 and 374 mbsf (Cores 121-757B-40X to 121-757B-42N). A total of 1.97 m of plagioclase-phyric basalt was recovered (excluding fragments of basalt in the tephra horizons), for a recovery of 39%. The basalt is immediately overlain and underlain by basaltic lapillistone and agglomerate of unknown age.

Hole 757C was washed and spot cored to 362.9 mbsf, close to predicted basement depth. Plagioclase-phyric basalt was found at 372.8 mbsf, beneath basaltic tephra, and drilled to 420.7 mbsf. The total drilled section is 48.3 m; based on drilling rates, the first 6 m is probably ash. Cores 121-757C-8R to 121-757C-12R contain 24.95 m of material, for a recovery of 52%. Basalts were observed in contact with overlying indurated tuffs.

The basalts form a series of discrete lava flows, distinguished on the basis of macroscopic features such as flow contacts, variations in the degree of alteration, and the distribution of plagioclase phenocrysts. The lavas appear to have been erupted in a subaerial environment.

Macroscopic Core Descriptions

Hole 757B: Basaltic Tephra

Details of the lithology of the basaltic tephra are given in the "Lithostratigraphy and Sedimentology" section (this chapter). Samples of basaltic fragments and ashes were taken for X-ray-fluorescence (XRF) analysis and thin-section studies.

Hole 757B: Flow Units 757B-F1 and 757B-F2

Highly plagioclase-phyric basalt was recovered in Sections 121-757B-40X-CC to 121-757B-43N-CC, representing a coring distance of approximately 5 m. However, only 1.97 m of basalt was recovered, together with 6 cm of buff-colored tuff adjacent to the upper margin of flow Unit 757B-F1 and approximately 15 cm of epiclastic basaltic agglomerate adjacent to the lower contact. Flow Unit 757B-F2 consists of approximately 20 cm of fragments of highly plagioclase-phyric basalt in Section 121-757B-43N-CC.

Both flow units contain up to 30% plagioclase phenocrysts, which range in size from 1 to >20 mm. Zonation of the phenocrysts is clearly seen even in hand specimen, being emphasized by faint, greenish alteration of the phenocryst rims. Unit 757B-F1 is sparsely vesicular, with rare, calcite-filled cavities approximately 20 mm across. Zeolites may also be present with the calcite. Alteration is slight to high, resulting in green smectites in the few vesicles and fractures, calcite (+ zeolites?) pockets, and partial replacement of the plagioclase phenocrysts by smectites and zeolites.

Flow Unit 757B-F1 is in direct contact with basaltic agglomerate or lapillistone at its lower margin, and similar rocks were recovered from above the unit, although the upper contact was not recovered. However, the lapillistone from above the unit, while preserving the textures of tephra underlying the unit, is of a much lighter color and unlike other tephra recovered from Hole 757B. Although this light coloration may be caused by chemical interaction with the underlying basalt, it could be the result of thermal induration, and the unit may be a sill. The presence of basaltic lithologies similar to the flows in Hole 757C indicates, however, that flow Unit 757B-F1 does not significantly post-date the sequence, and the distinction between sill and flow is probably not significant.

Hole 757C

Nineteen flow units were recognized in the core from Hole 757C, representing 24.95 m of recovered core and 25.85 m of curated core (Fig. 11). Twelve of the units each have recovered thicknesses less than 1 m; in several cases this represents the complete unit. The other units have recovered thicknesses of more than 2 m, and flow Unit 757C-F2 has a curated thickness of 5.51 m. The top flow, Unit 757C-F1 in Core 121-757C-8R-1, is overlain by red-brown indurated claystone.

In petrographic analysis, the units are all plagioclase-phyric basalts, most with over 20% plagioclase phenocrysts, but with

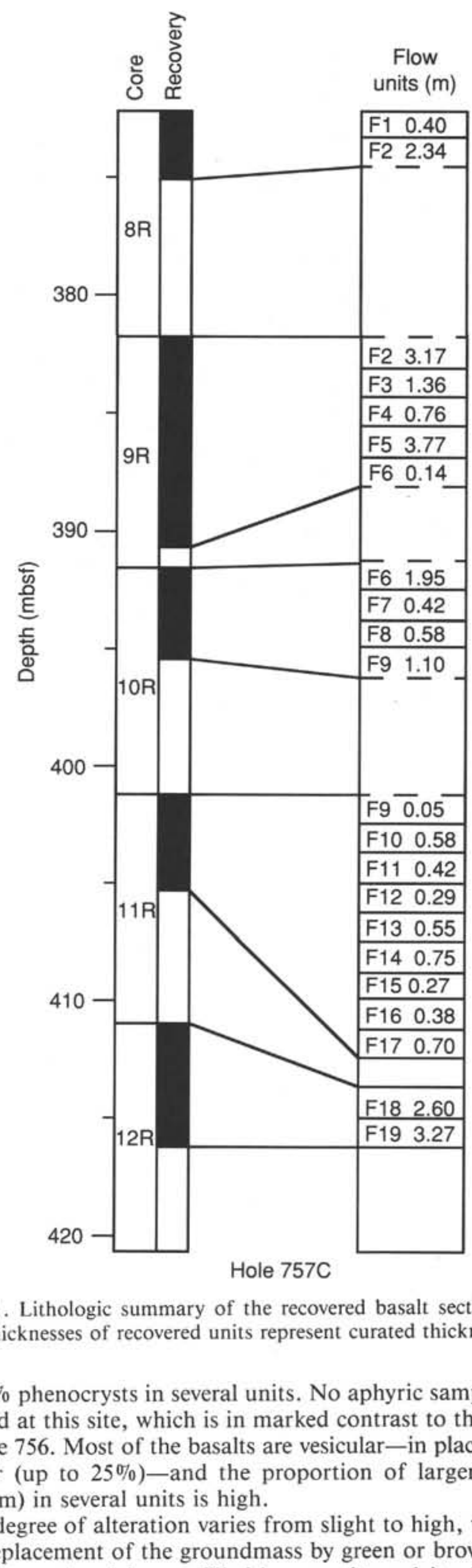

Figure 11. Lithologic summary of the recovered basalt section, Hole 757C. Thicknesses of recovered units represent curated thicknesses.

over 40% phenocrysts in several units. No aphyric samples were recovered at this site, which is in marked contrast to the basalts from Site 756. Most of the basalts are vesicular—in places highly vesicular (up to 25%)—and the proportion of larger cavities (>10 mm) in several units is high.

The degree of alteration varies from slight to high, with pervasive replacement of the groundmass by green or brown smectites. Veins and vesicles are filled by smectite, calcite, limonite, chalcedony, and, particularly in the lower units, at least two varieties of zeolite. The pronounced oxidative/nonoxidative alteration zones observed in the Site 756 basalts are restricted to the upper units. The occurrence of chalcedony and zeolites in the core from Hole 757C reflects alteration conditions different from those affecting the basalts at Site 756.

Flow units were distinguished on the basis of observed contacts (e.g., Figs. 12 and 13), color or other textural changes, dis-

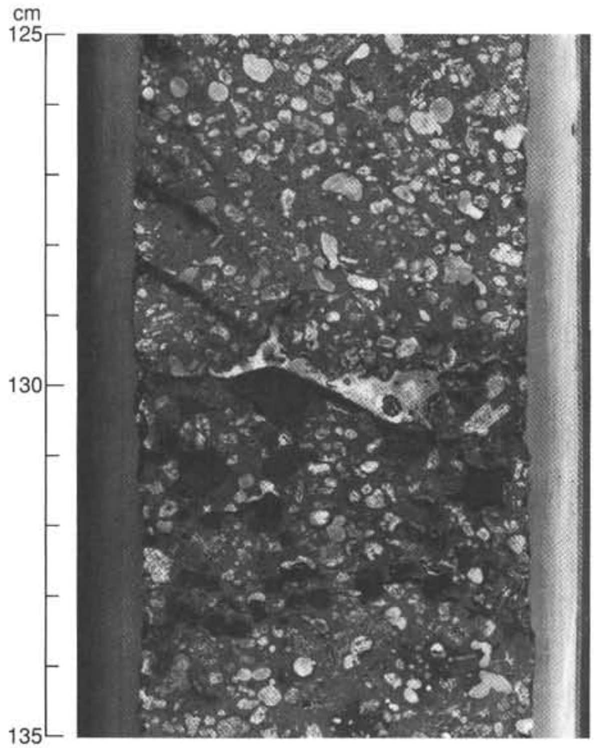

Figure 12. Vesicular zone at the top of flow Unit 757C-F12 (Section 121-757C-11R-1, 125-135 cm).

tribution of plagioclase phenocrysts, and distribution of vesicles. Thin brecciated and/or oxidized zones typically indicate a flow top, and in several instances we identified very thin flow units (<1 m). Either the flows were thin, and thus probably very fluid, or our "flow boundaries" are internal, brecciated oxidized layers within larger flows. Certainly in several units the distribution of phenocrysts (see the following text) and vesicles provides supporting evidence for our division; in other cases the identification is more equivocal.

In several units (e.g., flow Unit 757C-F5), the plagioclase phenocrysts are not uniformly distributed throughout the flow; a zone with fewer, smaller phenocrysts is present just below the top of the unit. On a larger scale, the proportion of plagioclase phenocrysts decreases slightly in Units 757C-F18 and 757C-F19. Such observations are detailed in the next section.

We believe that these are subaerial lavas. The absence of pillow rims, glassy selvages, and concentric, strongly zoned distribution of vesicles is evidence against eruption in deep water; the presence of narrow (<1 cm) flow contacts, large vesicles and gas cavities, massive structure, and oxidized flow tops supports the idea that these flows are subaerial (see "Paleomagnetics" section).

Petrography

Thirty-one thin sections from basement flow units and two thin sections from basalt fragments in ashes overlying the basement were studied. The detailed descriptions for each thin section are given with the visual core descriptions in this volume. The different mineral proportions in samples from Hole 757C are listed in Table 5 and shown graphically in Figure 14. The results of shipboard X-ray-diffraction (XRD) analyses are given in Table 6.

All of the rocks studied are moderately to highly plagioclase-phyric basalts. In contrast to Site 756 and the other Ninetyeast Ridge sites, no aphyric basalts were observed. They are all mi-

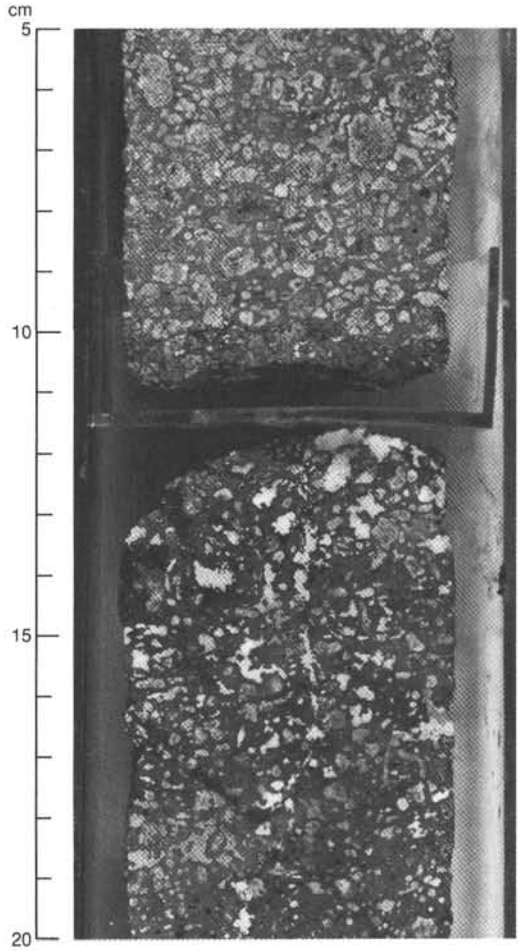

Figure 13. Vesicular and narrow breccia zone between flow Units 757C-F8 and 757C-F9 (Section 121-757C-10R-3, 5-20 cm).

crocrystalline to cryptocrystalline and holocrystalline to hypocrystalline, with hypidiomorphic texture. Most of these basalts have a porphyritic to glomeroporphyritic texture, and only some show a subophitic texture. The mesostasis is microcrystalline, or even cryptocrystalline, whereas the groundmass is entirely dominated by green smectites. This, in addition to the high degree of alteration of most samples, makes the accurate identification of the relative proportion of the mesostasis mineral phases extremely difficult.

Primary Igneous Mineralogy

Phenocrysts

The most obvious difference between these basalts and those from the other Ninetyeast Ridge sites, including Site 756, is the ubiquitous occurrence of plagioclase phenocrysts. In most units the proportion of phenocrysts exceeds 25%, and in several units, 40% (see Tables 5 and 7). In flow Units 757C-F18 and 757C-F19 at the base of the drilled section, phenocryst abundance decreases slightly, but still exceeds 10% (Fig. 14). The phenocrysts vary in size, generally exceeding 0.5 mm, with some crystals over 20 mm. The phenocrysts are subhedral to euhedral, some occur as glomerophyric clusters, and multistage histories are evident. Some of the phenocrysts are zoned, and some show two or more phases of resorption and overgrowth. Many of the phenocrysts are rimmed by a thin zone of more sodic feldspar. The composition of the cores of the phenocrysts is bytownitic (An_{82-90}) whereas the composition of the rims is labradorite

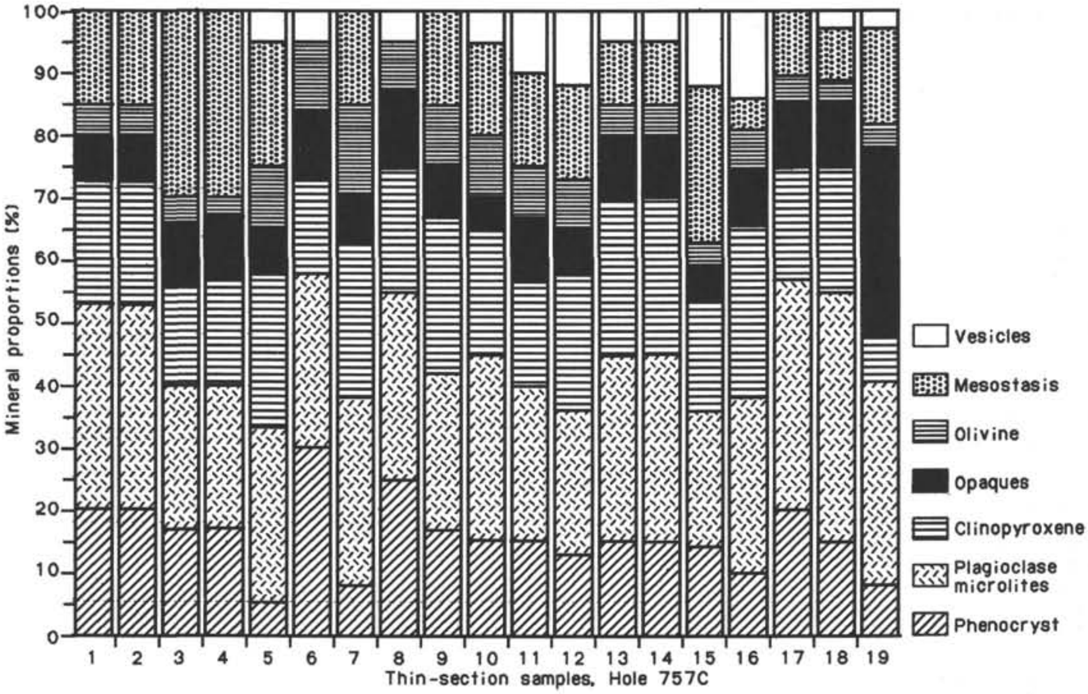

Figure 14. Estimated modal mineral proportions plotted for a downhole succession of basalt thin-section samples, Hole 757C. These visual estimations include the vesicles to sum to 100%. Sample numbers refer to intervals in Table 5.

(An_{65-70}). Many phenocrysts may have been derived from disaggregation of plagioclase-rich cumulates.

Flow Unit 757C-F5 was sampled to assess the role of crystal settling. In hand specimen, it is apparent that the distribution of plagioclase phenocrysts is not uniform. Approximately 15 cm below the top of the flow unit (Fig. 15), the proportion of plagioclase phenocrysts falls dramatically, from 40% to less than 10% (on a vesicle-free basis). An accurate modal analysis was performed by projecting the thin sections on 8.5 × 11 in. photographic paper (Fig. 16) and cutting out and weighing the relative proportions of phenocrysts, matrix, and vesicles (the other phenocryst phase present, olivine, is subordinate at <1% and negligible for this calculation). Our interpretation of this distribution is that the phenocrysts have undergone gravitational sinking—an unusual process in thin basaltic flows. Apparently the liquid had a low viscosity and was poor in iron (low density). Several other units in the drilled succession also show similar patterns of plagioclase distribution.

Other phenocryst phases include olivine and clinopyroxene. No unaltered olivine was found in any of the flow units, with the possible exception of Units 757C-F10 and 757C-F18, where less than 1% unaltered olivine may occur. Units 757C-F2, 757C-F4 through 757C-F6, 757C-F9, and 757C-F14 contain trace quantities of chlorite/smectite ± calcite and iddingsite pseudomorphs (usually one or two phenocryst pseudomorphs not larger than 1 mm per thin section). Olivine microphenocrysts are also in these units; these, too, are always replaced by green smectite with chlorite and iddingsite. Their abundance ranges up to 10% (e.g., Samples 121-757C-9R-6, 49-52 cm [Piece 1A], and 121-757C-9R-7, 18-21 cm [Piece 1A]).

The other mafic phenocryst phase is clinopyroxene, distinguished by its moderate birefringence, pale brown/green pleochroism, inclined extinction, rare twinning, and zoning. Precise identification of this phase is not possible, but the larger phenocrysts (0.5-1.5 mm) in flow Unit 757C-F18 are anhedral and belong to the diopside-augite series. In several instances the clinopyroxene phenocrysts are intimately intergrown with the plagioclase phenocrysts. The proportion of these larger clinopyroxene phenocrysts does not exceed about 2%-3%. In Units 757C-F10, 757C-F13, 757C-F14, and 757C-F19, the pyroxene phenocrysts are smaller (<0.1 mm) and appear subhedral. The larger clinopyroxene phenocrysts are restricted to the two lower flow units of Hole 757C, 757C-F18 and 757C-F19. No phenocrystal spinel was observed in these rocks.

Groundmass

The groundmass phases in the least altered rocks are plagioclase, clinopyroxene, olivine, opaques, and recrystallized volcanic glass. Plagioclase occurs as submillimeter (0.1 to 0.5 mm), euhedral to subhedral microlites or laths in relatively constant proportions (25% to 30%) throughout the core, except in flow Units 757C-F18 and 757C-F19, where the plagioclase microlite proportion reaches 40%. Clinopyroxene is always present in the mesostasis as relatively small, equant, anhedral to subhedral crystals of submillimeter size (0.1-0.2 mm). Its proportion also appears to be relatively constant, around 20%-25%, except again in Units 757C-F18 and 757C-F19, where it is distinctly less than 20%. Opaques occur as small anhedral to subhedral crystals, depending on the grain size of the mesostasis, disseminated throughout an invariably altered mesostasis in the cryptocrystalline samples, and as small, equant grains in the fine-grained samples. Magnetite (or titanomagnetite) and ilmenite are the dominant opaque minerals. The abundance of opaques rarely exceeds 10%, except in Sections 6 and 7 of Core 121-757C-9R (flow Unit 757C-F5), where it reaches 15% and is associated with a higher proportion of olivine in the groundmass. Many skeletal opaque grains were seen in reflected light, especially in the border areas of the flows, which is consistent with rapid cooling rates. The presence of exsolution lamellae of ilmenite-magnetite indicates high-temperature oxidation. Unaltered olivine is absent from these rocks, but, in general, the abundance of altered olivine or its alteration minerals is higher than in the basalts from Site 756, reaching up to 10%-15%. It is usually replaced by an association of smectites/chlorites and iddingsite.

Table 5. Modal analyses of basalt thin sections, Hole 757C.

	9R-1, 70–74 cm (Piece 3)	9R-2, 59–62 cm (Piece 1C)	9R-3, 50–54 cm (Piece 1A)	9R-3, 56–60 cm (Piece 1A)	9R-5, 80–82 cm (Piece 2)	9R-6, 49–52 cm (Piece 1A)	9R-7 18–21 cm (Piece 1A)	9R-7 89–93 cm (Piece 1B)	9R-7 107–110 cm (Piece 1C)
Flow unit	757C-F2	757C-F2	757C-F2	757C-F2	757C-F5	757C-F5	757C-F5	757C-F5	757C-F5
Phenocrysts									
Plagioclase (%)	20	20	15–20	15–20	5	>35	8	>25	17
diameter (mm)	5	5	2–8	2–8	1–7	2–10	2–8	2–6	2–8
Clinopyroxene	0	0	0	0	0	0	0	0	0
diameter (mm)	—	—	—	—	—	—	—	—	—
Groundmass									
Plagioclase (%)	33	33	25	25	28	30	30	30	25
length (mm)	0.3–0.4	0.3–0.4	0.3–0.4	0.3–0.4	0.1–0.5	0.2	0.2–0.4	0.2	0.2–0.3
Clinopyroxene (%)	20	20	15–20	15–20	25	15	25	20–25	25
diameter (mm)	0.2–0.4	0.2–0.4	0.1	0.1	0.1	<0.1	0.1–0.2	<0.1	0.1–0.2
Opaques (%)	7	7	10	10	7	10–15	7	10–15	8
[a]Secondary minerals									
Smectite after mesostasis	15	15	30	30	20	0	12.5	0	18
[b]Smectite after olivine	<5	<5	[c]<5	[c]<5	[c]10	10–15	10–15	5–10	10
Vesicles (%)	0	1	1	1	5	5	0	5	0
Alteration (%)	20	60	30–40	30–40	50	30–40	20–30	30	30–40
[d]Sample number	1	2	3	4	5	6	7	8	9

[a] In many thin sections, the phenocrystal plagioclase is partially replaced by clays and/or zeolites, and calcite and zeolites may be present in the groundmass.
[b] Mainly olivine phenocrysts and microphenocrysts.
[c] Includes iddingsite.
[d] Refers to samples plotted in Figure 14.
[e] Includes iron oxides and hydroxides resulting from alteration of the mesostasis.

The proportion of recrystallized volcanic glass varies greatly throughout the hole, between 0% (Samples 121-757C-9R-6, 49–52 cm [Piece 1A], and 121-757C-9R-7, 18–21 cm [Piece 1B]) and 30%. No fresh volcanic glass was observed because it was pervasively replaced by secondary green smectite (probably saponite) or brown smectites with iron oxides/hydroxides.

Secondary Mineralogy and Alteration Features

The basalts are all vesicular, although the proportion and size of the vesicles vary considerably, even within individual units. An example is provided by Figure 15, which shows the distribution of vesicles in flow Unit 757C-F5. The top of the unit has the highest vesicle content—over 20%—while the center of the unit has virtually no vesicles. The bottom of the unit has few vesicles (4%).

The proportion of vesicles is higher and they are also larger than in the Site 756 basalts, with sizes ranging from 0.5 to 20 mm. They are systematically lined by green smectites/chlorites (shipboard XRD determination) with a large variety of fillings: calcite, smectites, iron oxides/hydroxides, opal or chalcedony, and zeolites (including natrolite and analcite). Calcite is more common in the upper flow units and in Units 757C-F18 and 757C-F19, while zeolites predominate in Units 757C-F5 to 757C-F17. Where these two minerals are associated in a vesicle, calcite commonly occupies the lower part and zeolites fill the top part. The presence of zeolites and chalcedony indicates hydrothermal conditions during the alteration history of these basalts. This is distinct from the secondary mineral associations at DSDP Site 257 (Kempe, 1974) and from the assemblages at Site 756, where only calcite and smectites were observed and low-temperature alteration was the dominant process. It is possible that the thick, insulating (with very low thermal conductivity; see "Physical Properties" section, this chapter) ash section overlying the basalts at Site 757 resulted in an unusually high temperature gradient, with consequent zeolitization at relatively shallow depths. On the other hand, the pronounced oxidative/nonoxidative alteration zones, observed in the Site 756 basalts and corresponding respectively to brownish gray and dark blue gray macroscopic color of the rock, exist at this site, but they appear limited to the uppermost flow units of Holes 757B and 757C.

The degree of alteration is distinctly higher than in the Site 756 basalts, and locally, alteration completely obliterates the primary basalt mineralogy. Alteration varies from moderate to high, with pervasive replacement of the mesostasis by green or brown smectites/chlorites. Veins (up to 5 cm wide) and vesicles filled by secondary mineral associations also occur and are obviously well related to the flow contacts and the permeability of the rocks. For example, in flow Unit 757C-F5, the degree of alteration is between 30% and 50% in the center of the unit where the rock is massive, while it reaches up to 80% near the flow contacts where the rock is more vesicular and fractured. A detailed study (thin section and XRD) of the secondary mineral associations present at the flow contacts shows that the minerals are green and brown chlorite/smectite associations together with iron oxides/hydroxides and locally with calcite and/or zeolites.

Inter-Flow Unit Differences

Core 121-757C-12R, which corresponds to the flow Units 757C-F18 and 757C-F19, shows a different mineralogy from the overlying units, in agreement with the geochemistry. The mesostasis is much richer in plagioclase microlites and poorer in ferromagnesian minerals (clinopyroxene, opaques, and olivine altogether constitute less than 35% of the rock). In addition, the plagioclase phenocrysts are distinctly less abundant (<20%) than in the overlying units. There are also clinopyroxene (2%–4%) and olivine (<1%) phenocrysts; the former are not seen in the upper units.

Intersite Differences

The Site 757 basalts have very distinct petrographic characteristics from those of Site 756 (e.g., highly plagioclase-phyric and different secondary mineral paragenesis). They also appear to be petrographically distinct from the basalts recovered at the other Ninetyeast Ridge drill sites (Hekinian, 1974; Kempe,

Table 5 (continued).

9R-8 30–32 cm (Piece 2)	9R-8 72–75 cm (Piece 4B)	10R-1, 45–47 cm (Piece 1)	10R-1, 109–110 cm (Piece 2)	10R-3, 68–69 cm (Piece 2)	11R-1, 87–91 cm (Piece 9C)	11R-2, 116–120 cm (Piece 7A)	12R-1, 45–48 cm (Piece 2)	12R-2, 22–25 cm (Piece 1)	12R-2, 0–4 cm (Piece 1)
757C-F5	757C-F5	757C-F6	757C-F6	757C-F9	757C-F10	757C-F14	757C-F18	757C-F18	757C-F19
15	15–20	13	15	15	10–15	10	20	15	5–10
2–8	2–6	3–8	1–6	1–6	1–5	2–8	1–6	1–5	5
0	0	0	0	0	<2	0	<2	<2	<2
—	—	—	—	—	0.5	—	0.5–1.0	0.5–1.0	0.5–1.0
30	25	23	30	30	20–25	30	35–40	40	30–35
0.2–0.5	0.2–0.3	0.1	0.2–0.3	0.2–0.3	0.1–0.2	0.1–0.2	0.1	0.1–0.2	0.1–0.2
20	<20	22	25	25	15–20	30	15–20	15–20	<10
0.1–0.2	0.1	0.1–0.2	0.1	0.1	0.1	0.1–0.5	0.1	0.1	0.1
5	10	7	10	10	5	8	10	10	[c]10 + 25
15	18	15	<10	<10	25–30	<5	<10	5–10	>15
10	<10	8	[c]5	[c]5	<5	7	<5	<5	<5
5	10	12	5	5	10–15	15	0	<5	<5
50	80	60	>60	>60	>70	>70	50–60	>70	>80
10	11	12	13	14	15	16	17	18	19

Table 6. XRD mineral determinations of vein- and fracture-filling samples from basement, Hole 757C.

Core, section, interval (cm)	Shipboard data-base file number	Location	Minerals identified
8R-1, 43–44	184UBN	Flow contact	Chlorites/smectites
8R-1, 89–90	186UBN	Flow contact	Chlorites/smectites
8R-2, 37–38	185UBN	Vein	Feldspar, calcite, zeolites
8R-2, 50–51	187UBN	Vesicle	Opal, poorly crystalline clay
8R-3, 15–16	188UBN	Phenocryst	Chlorites/smectites, feldspar
9R-2, 55–56	194UBN	Veins	Calcite, feldspar, chlorites/smectites
9R-2, 61–62	190UBN	Veins	Opal, poorly crystalline clay
9R-4, 115–116	192UBN	Flow contact	Chlorites/smectites, zeolites
9R-5, 51–52	189UBN	Flow contact	Chlorites/smectites, zeolites
10R-3, 67–68	196UBN	Vein	Feldspar, zeolites
11R-1, 138–139	193UBN	Vesicle	Feldspar, zeolites
11R-3, 71–72	191UBN	Breccia contact	Chlorites/smectites, feldspar
12R-4, 102–103	195UBN	Vesicle	Chlorites/smectites, feldspar

Table 7. Phenocryst and vesicle data from flow Unit 757C-F5.

Core, section, interval (cm)	Depth[a] (cm)	Plagioclase[b] (%)	Matrix[b] (%)	Vesicles (%)
9R-5, 58–62	8	29	71	22
9R-5, 80–82	30	9	91	17
9R-6, 49–52	81	47	53	19
9R-7, 18–21	163	42	58	<1
9R-7, 88–93	233	46	54	1
9R-7, 107–110	252	49	51	0
9R-8, 72–75	355	39	60	4

[a] Below the top of the flow unit, estimated from the curated length (base of the unit is at 376 cm).
[b] Presented as vesicle-free proportions.

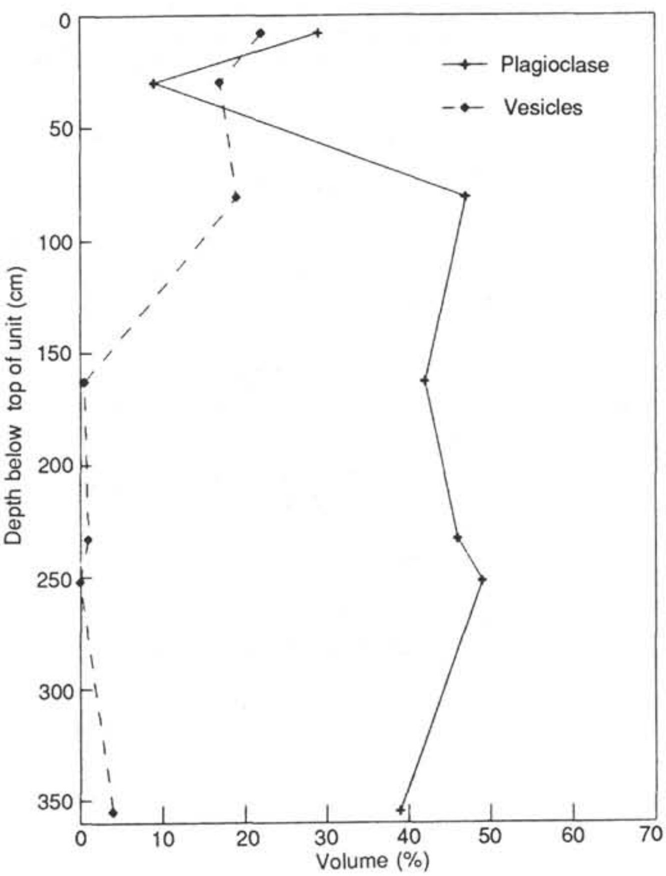

Figure 15. Profiles of vesicle and plagioclase phenocryst content of flow Unit 757C-F5. Plagioclase and vesicle abundance are calculated from accurate modal analysis (see text); plagioclase is plotted on a vesicle-free basis.

A

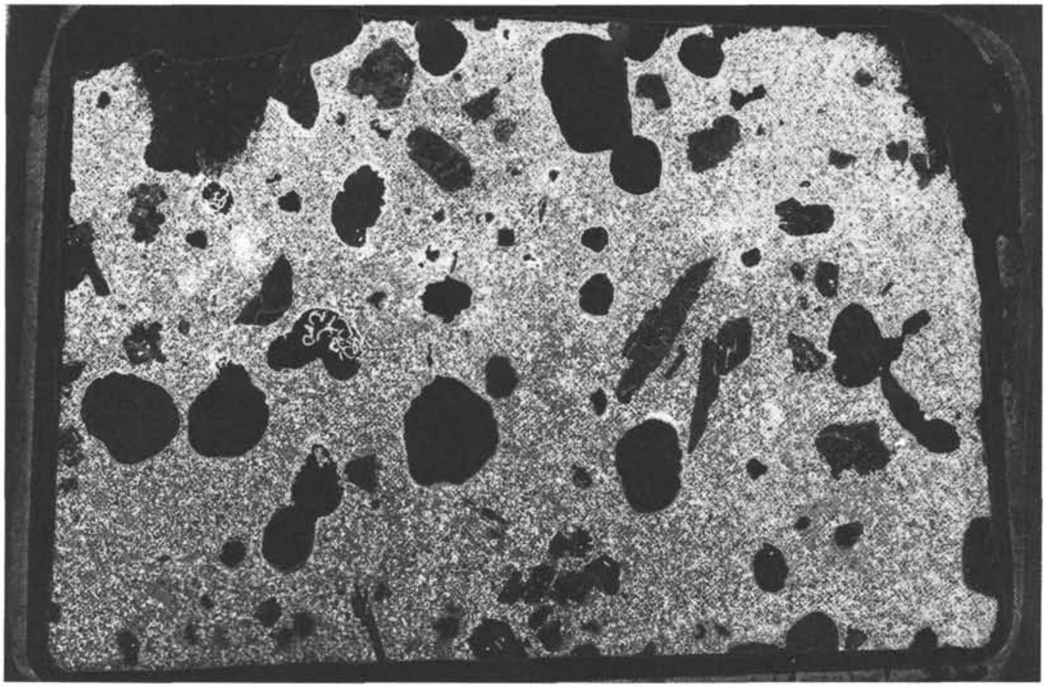

B

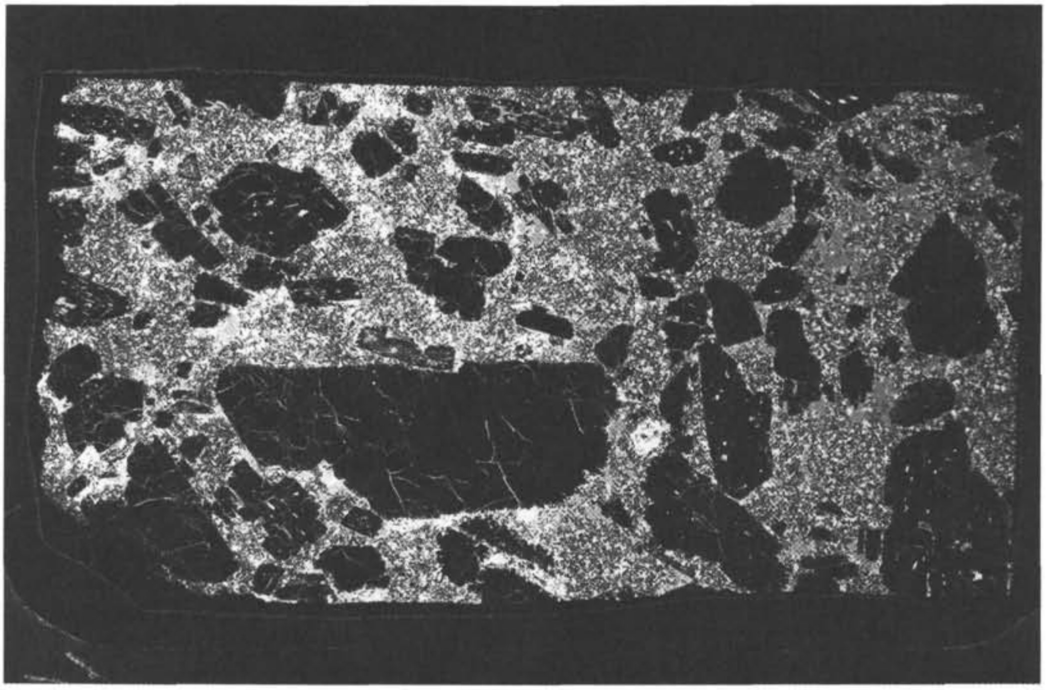

Figure 16. Projections of thin sections show variation within the flow units of plagioclase phenocryst and vesicle contents. **A.** Sample 121-757C-9R-5, 80–82 cm (Piece 2). **B.** Sample 121-757C-9R-7, 107–110 cm (Piece 1C).

1974). For example, basalts from Sites 214 and 216 of DSDP Leg 22 have higher proportions of clinopyroxene than plagioclase, quartz infillings to vesicles, and trachytic textures.

Geochemistry

Two samples of Hole 757B and 10 samples of Hole 757C basement basalts were analyzed by XRF for major and trace element abundances. In addition, 10 ash samples from the 157 m of ash overlying basement in Hole 757B were analyzed by XRF for trace element content, and four 1–4-cm samples of basaltic fragments within the ash were analyzed for major and trace element abundances. All samples were also analyzed for CO_2 content. The data are presented in Tables 8 through 10.

Following the discussion in the "Igneous Petrology" section of the "Site 756" chapter (this volume), we evaluate these data in terms of compositional variations of basalts and ashes within Holes 757B and 757C, compositional differences between basalts from different DSDP and ODP sites on Ninetyeast Ridge, and comparisons of Site 757 basalts with MORB and oceanic island basalts.

Table 8. XRF analyses of ashes, Hole 757B.

	24X-3, 36-39 cm	24X-5, 83-86 cm	26X-1, 90-93 cm	27X-4, 72-75 cm	29X-1, 138-139 cm	30X-3, 104-108 cm	31X-1, 67-71 cm	32X-1, 127-131 cm	36X-2, 40-42 cm	37X-3, 28-32 cm
$CaCO_3$ (wt%)	36.03	1.00	0.67	1.25	28.9	2.34	0.58	0.50	2.17	0.75
Trace elements (ppm)										
Rb	54	70	25	31	12	29	23	24	29	18
Sr	302	85	89	88	126	85	94	87	78	86
Ba	25	35	56	60	29	60	33	50	149	38
V	314	192	311	306	155	304	323	304	311	324
Cr	107	135	21	28	17	131	35	68	23	48
Ni	91	111	62	59	63	72	57	62	68	67
Cu	104	79	92	87	50	101	119	107	100	110
Zn	173	127	107	97	117	93	103	97	101	100
Y	30	20	16	18	72	23	28	25	28	25
Zr	81	72	125	134	106	87	115	109	107	102
Nb	8.8	4.9	8.9	8.3	8.0	7.5	7.7	8.6	8.4	8.0
Ce	15	12	8	12	53	11	15	12.1	17	15

Table 9. XRF analyses of basalts, Hole 757B.

	25X-3, 7-10 cm	28X-4, 50-52 cm	34X-1, 88-90 cm	35X-1, 9-11 cm	40X-CC, 12-14 cm	41X-1, 89-92 cm (Piece 1B)
Flow unit	—	—	—	—	—	757B-F1
Major elements (wt%)						
SiO_2	50.14	50.40	50.09	49.35	53.23	48.22
TiO_2	1.88	1.45	2.10	2.58	0.83	0.71
Al_2O_3	17.04	15.90	17.07	16.08	20.80	23.26
$^aFe_2O_3$	10.99	8.48	10.64	13.41	6.75	6.18
MnO	0.18	0.13	0.31	0.24	0.07	0.08
MgO	4.77	7.34	4.47	4.94	5.93	6.08
CaO	9.53	10.42	8.92	8.90	6.12	12.77
Na_2O	2.83	3.43	3.44	3.25	3.15	1.91
K_2O	1.55	1.26	1.09	0.90	2.89	0.37
P_2O_5	0.37	1.06	0.24	0.35	0.07	0.05
	99.28	99.85	98.38	100.00	99.85	99.62
Loss on ignition	1.95	6.46	0.59	1.15	4.94	1.81
$^bFeO/MgO$	2.07	1.04	2.14	2.44	1.02	0.91
CaO/Al_2O_3	0.56	0.66	0.52	0.55	0.29	0.55
Trace elements (ppm)						
Rb	30	—	12	22	32	2
Sr	205	—	192	194	164	189
Ba	31	—	86	37	69	15
V	330	—	370	419	268	190
Cr	116	—	29	23	169	162
Ni	69	—	55	52	49	78
Cu	47	—	179	167	25	77
Zn	302	—	313	265	86	45
Y	45	—	33	44	13	11
Zr	122	—	196	167	51	46
Nb	10.9	—	12.4	12.7	3.1	2.7
Ce	25	—	30	29	7	8

Note: Samples 121-757B-25X-3, 7-10 cm, to 121-757B-35X-1, 9-11 cm, are basaltic fragments from tephra layers. The other samples are from flow units.
[a] Total iron as Fe_2O_3.
[b] Total iron as FeO.

The major oxide content of the basement basalts from Hole 757C reflects the high abundance (5% to 40%) of plagioclase phenocrysts (Table 5). For example, the high Al_2O_3 contents (20.4% to 24.2%) and high Al_2O_3/CaO ratios in flow Units 757C-F1 through 757C-F17 (Figs. 17 and 18) are not typical of basaltic melts, but they can be interpreted as resulting from mixtures of melt and added plagioclase that crystallized from a different melt.

As at Site 756, the incompatible element abundances in basement basalts at Site 757 show well-defined positive correlations. Site 757, however, has a larger variation in incompatible element content; for example, Zr and Nb contents range by factors of 4.5 and 5.8, respectively (Fig. 19). These wide ranges encompass two compositional groups: flow Units 757C-F18 and 757C-F19 from Sections 1 through 3 of Core 121-757C-12R form an enriched group overlain by flow Units 757C-F1 through 757C-F17, which have lower incompatible element abundances (Fig. 19). These two compositional groups have similar V and P_2O_5 contents (Fig. 20 and Table 10), but differ in TiO_2 content (i.e., Cores 121-757C-11R and 121-757C-12R contain 0.88% to 0.96%

Table 10. XRF analyses of basalts, Hole 757C.

	9R-1, 70–74 cm (Piece 3)	9R-2, 0–10 cm (Piece 1A)	9R-3, 50–54 cm (Piece 1A)	9R-3, 56–60 cm (Piece 1A)	9R-7, 106–110 cm (Piece 1C)	10R-1, 106–109 cm (Piece 2A)	10R-3, 107–110 cm (Piece 5)	11R-2, 116–120 cm (Piece 7A)	12R-1, 45–48 cm (Piece 2)	12R-1, 104–110 cm (Piece 2)	12R-2, 22–25 cm (Piece 1)	12R-3, 0–4 cm (Piece 1)
Flow unit	757C-F2	757C-F2	757C-F2	757C-F5	757C-F6	757C-F6	757C-F9	757C-F14	757C-F18	757C-F18	757C-F18	757C-F19
Major elements (wt%)												
SiO_2	48.54	48.32	48.52	47.84	48.14	47.78	46.31	49.17	51.16	51.47	50.90	50.12
TiO_2	0.70	0.78	0.68	0.66	0.70	0.69	0.69	0.90	0.96	0.92	0.89	0.94
Al_2O_3	23.08	22.18	24.25	22.95	23.39	22.88	21.98	20.36	18.49	18.69	19.25	18.22
[a]Fe_2O_3	6.28	7.08	5.52	6.81	6.26	6.80	7.30	9.02	8.77	7.64	8.95	10.12
MnO	0.08	0.08	0.07	0.08	0.07	0.08	0.07	0.11	0.19	0.16	0.10	0.11
MgO	5.39	5.42	5.17	5.53	5.33	5.25	5.68	5.76	5.34	4.86	5.67	5.71
CaO	13.84	13.81	13.77	13.10	13.18	12.72	13.24	10.17	10.82	12.07	9.84	7.50
Na_2O	1.83	1.90	1.94	1.69	1.79	3.20	2.62	3.71	2.56	2.58	2.86	5.73
K_2O	0.25	0.15	0.25	0.93	0.98	1.01	1.34	1.05	1.27	0.76	1.88	1.88
P_2O_5	0.05	0.06	0.05	0.04	0.06	0.06	0.07	0.06	0.07	0.07	0.07	0.09
	100.02	99.78	100.24	99.61	99.90	100.43	99.31	100.29	99.60	99.20	100.39	100.41
Loss on ignition	1.26	1.36	1.66	1.70	2.08	5.40	8.03	4.28	0.37	1.19	1.79	6.93
$CaCO_3$	0.42	0.25	0.50	0.33	0.75	2.42	7.33	0.33	0.17	4.58	0.25	0.33
[b]FeO/MgO	1.05	1.18	0.96	1.11	1.06	1.17	1.16	1.41	1.48	1.41	1.42	1.60
CIPW norms												
Quartz							0.0	0.0	0.0	1.5	0.0	0.0
Nepheline	0.0	0.0	0.0	0.0	0.0	6.6	7.4	3.8	0.0	0.0	0.0	13.3
Orthoclase	1.4	0.89	1.5	5.6	5.8	5.9	8.0	6.2	7.5	4.6	11.2	11.2
Albite	15.6	16.2	16.4	14.3	15.2	14.9	8.8	24.5	21.9	22.1	24.3	24.1
Anorthite	54.3	51.9	56.8	52.8	53.1	45.1	44.8	35.9	35.6	37.6	34.2	18.5
Diopside	11.8	13.7	9.2	10.3	10.0	14.4	17.4	11.8	15.1	18.6	11.8	15.1
Hypersthene	12.2	11.7	10.4	7.2	6.0	0.0	0.0	0.0	15.3	12.2	4.1	0.0
Olivine	2.1	2.7	3.2	7.1	7.1	10.2	10.6	14.1	0.9	0.0	10.8	13.9
Apatite	0.11	0.13	0.11	0.09	0.13	0.13	0.15	0.13	0.13	0.16	0.15	0.20
Ilmenite	1.34	1.49	1.30	1.27	1.34	1.29	1.33	1.72	1.85	1.77	1.68	1.79
Magnetite	1.26	1.42	1.10	1.37	1.25	1.35	1.47	1.80	1.76	1.54	1.78	2.02
[c]Trace elements (ppm)												
Rb	1	1	2	20	15	14	18	17	14	8	20	15
Sr	197	179	202	189	195	356	348	343	176	166	177	113
Ba	19	20	24	24	23	14	17	27	93	72	99	39
V	187	172	223	151	157	142	130	200	200	218	185	149
Cr	149	157	159	136	129	115	119	80	81	86	83	80
Ni	74	74	76	72	65	59	56	50	53	57	54	58
Cu	54	49	64	50	50	43	26	39	39	64	29	47
Zn	52	52	51	45	43	43	41	55	66	73	69	84
Y	10	12	10	11	10	10	11	13	29	30	28	37
Zr	47	50	46	45	42	40	42	56	158	156	144	180
Nb	2.5	2.4	2.3	2.2	2.0	1.8	1.8	3.1	8.9	9.1	8.1	10.4
Ce	8	8	5	5	12	4	4	7	22	21	19	27

[a] Total iron as Fe_2O_3.
[b] Total iron as FeO.
[c] Data for Samples 121-757C-9R-1, 70–74 cm (Piece 3), 121-757C-9R-3, 50–54 cm (Piece 1A), 121-757C-9R-3, 56–60 (Piece 1A), 121-757C-9R-7, 106–110 cm (Piece 1C), and 121-757C-10R-1, 106–109 cm (Piece 2A), are averages of duplicate analyses.

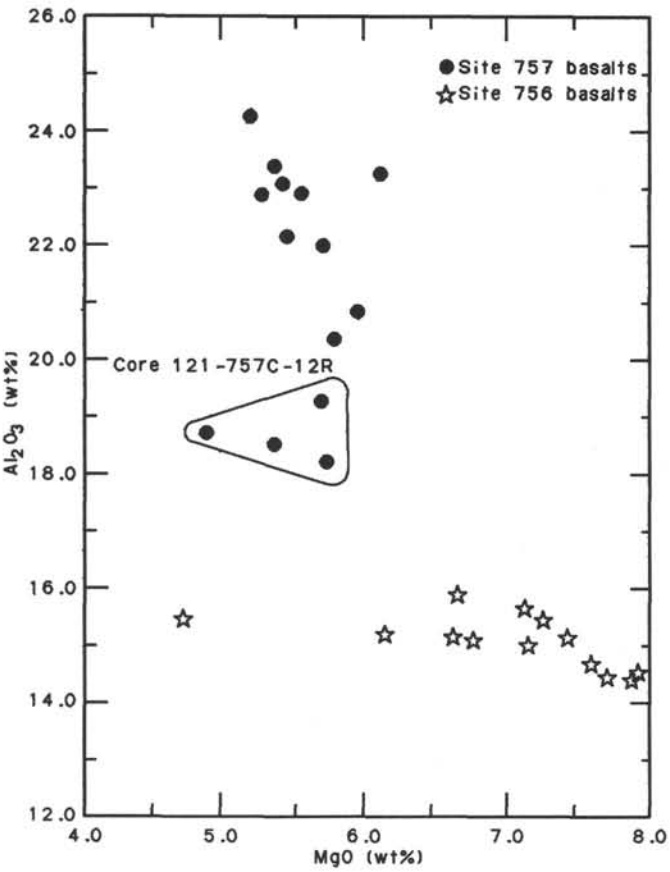

Figure 17. Al_2O_3 vs. MgO abundances in basement basalt from Sites 756 and 757. The higher Al_2O_3 content of the Site 757 basalts probably reflects plagioclase accumulation; however, Site 757 basalts may have also formed from an Al_2O_3-rich magma. Within the Site 757 field, samples from Core 121-757C-12R have the lowest Al_2O_3 contents.

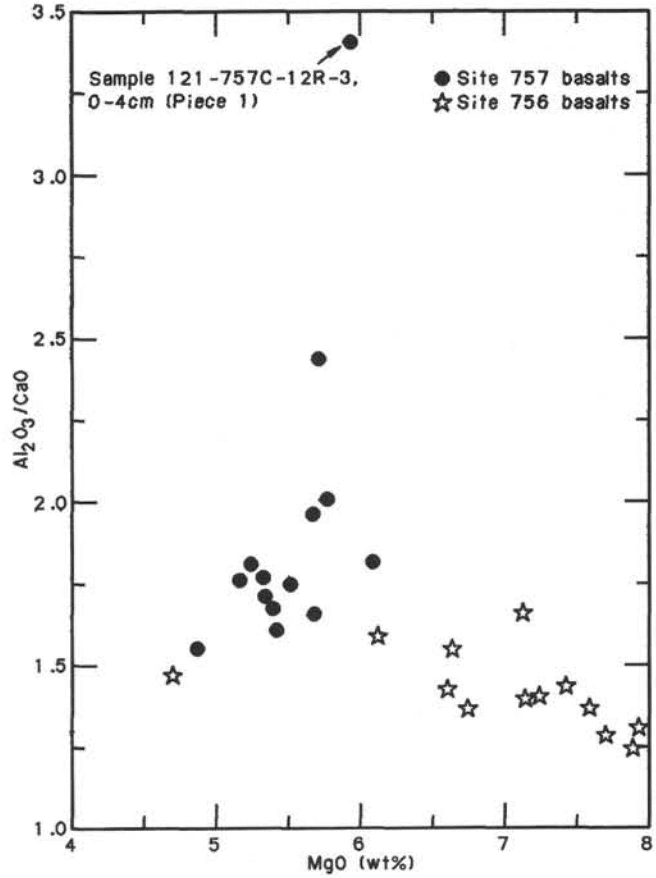

Figure 18. Al_2O_3/CaO ratio vs. MgO content in basement basalts from Sites 756 and 757. The higher Al_2O_3/CaO and lower MgO content of the basalts from Site 757 could result from plagioclase addition. Sample 121-757C-12R-3, 0-4 cm (Piece 1), is highly altered (loss on ignition = 6.93%), and its high Al_2O_3/CaO ratio probably reflects the loss of CaO during late-stage alteration.

TiO_2, whereas stratigraphically higher basalts have <0.78% TiO_2; Table 10 and Fig. 21). As a result, the two groups differ significantly in Ti/P and Ti/V ratios. They also differ in Ti/Zr ratios. As shown in Figure 22, basalts from Core 121-757C-12R are relatively depleted in Ti and P.

The geochemical differences of more than a factor of four in incompatible element content (Table 10) between the two compositional groups from Hole 757C cannot be explained by feldspar fractionation alone. This inference is supported by the V-Nb abundance trends (Fig. 20). Based on these major and trace element data, the simplest interpretation is that the two compositional groups from Hole 757C formed from different parental magmas. More complex models relating the two groups are possible, but they cannot be evaluated with only shipboard data. The presence of relatively enriched basalts at the bottom of the hole is the opposite of the trend in Hole 756B (compare Fig. 14 of the "Site 756" chapter with Fig. 23).

The stratigraphically younger basaltic ashes and fragments in Hole 757B extend the compositional range of the basement basalts (Tables 8 and 9 and Fig. 24), thereby possibly demonstrating temporal geochemical variations at a single site. For example, the Zr/Nb ratios of basaltic ashes and basalt fragments from Hole 757B overlap with those of the Site 756 basalts but are lower than those of basement basalts from Hole 757C (Fig. 25). However, some of the geochemical characteristics of these younger samples may reflect post-magmatic alteration, as indicated by the steep Ca gradients in the sedimentary pore waters (see "Inorganic Chemistry" section, this chapter). In particular, the high abundances of K_2O, P_2O_5 (Sample 121-757C-28X-4, 50-52 cm), Zn, and high Ce and Y (Sample 121-757C-29X-1, 138-139 cm) may be caused by secondary minerals (Tables 8 and 9 and Fig. 26).

Some basement basalts in Hole 757C are highly altered in thin-section analysis (over 80%; Table 5), and they have high loss on ignition (>4%; Table 10). As a result, abundances of alkali metals do not form coherent trends as a function of MgO content. One of the most altered samples (121-757C-12R-3, 0-4 cm [Piece 1]) is also depleted in CaO (Fig. 27). As at Site 756, basalts with a blue-gray color, interpreted as reflecting alteration in a nonoxidative environment, have low K_2O and Rb contents (Samples 121-757B-41X-1, 89-92 cm [Piece 1B], 121-757C-9R-1, 70-74 cm [Piece 3], and 121-757C-9R-3, 50-54 cm [Piece 1A]; see Tables 9 and 10).

Systematic geochemical differences between the basalts from the Ninetyeast Ridge sites are also evident in Figures 19, 20, and 24. An important question is whether these differences require different parental magmas and possibly mantle sources with different compositions or whether they reflect post-melting processes. For example, the low TiO_2 contents of the Hole 757C basalts relative to the Hole 756B basalts (Fig. 21) may in part be the result of the accumulation of plagioclase that contains negligible TiO_2. However, the difference, by a factor of two, in TiO_2 content between the basalts from Holes 756B and 757C cannot be explained only by plagioclase accumulation. Therefore, the compositions of the basalts from Hole 756B are not suitable for

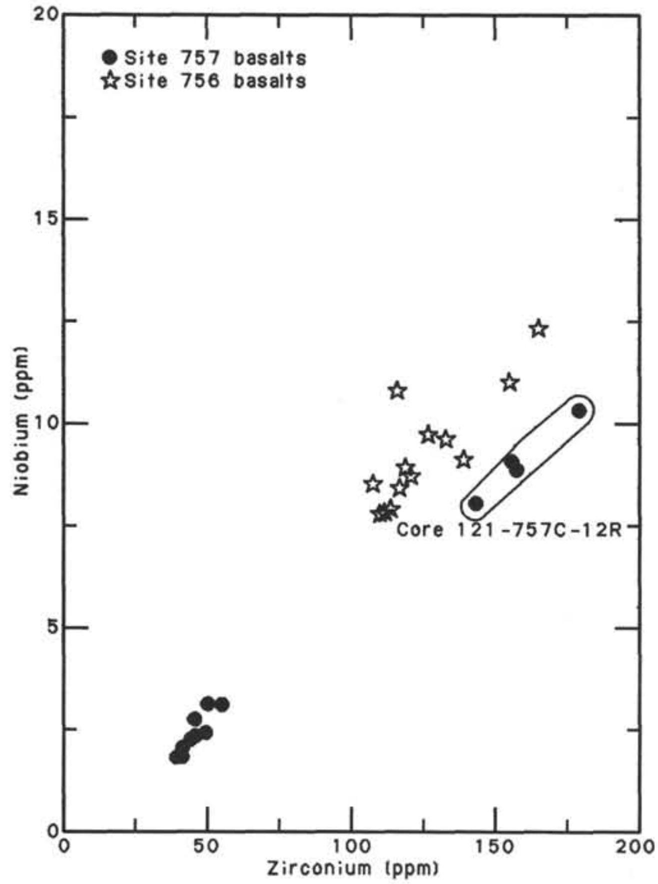

Figure 19. Nb vs. Zr abundances in basement basalts from Sites 756 and 757. The Site 757 basalts form two compositional groups, but the fields for the Site 756 and 757 basalts do not overlap.

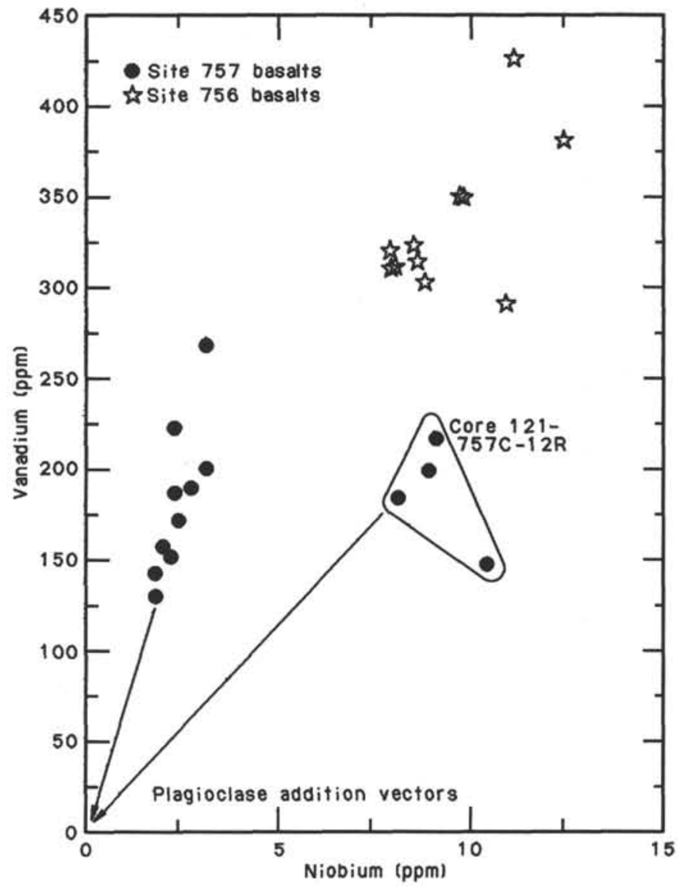

Figure 20. Abundances of V and Nb in basement basalts from Sites 756 and 757. Hole 757C basalts form two distinct fields differing in Nb content (and in abundances of other incompatible elements). As shown by the plagioclase addition vectors, these two groups cannot be related by plagioclase fractionation. Each of these Ninetyeast Ridge sites occupies a distinct region.

explaining the basalt compositions from Hole 757C. We conclude that the Hole 756B and 757C suites require compositionally different parental magmas, but with only shipboard data we cannot determine if the basalts require mantle sources with different compositions.

The trace element abundance ratios, Zr/Nb and Y/Nb, are relatively insensitive to the accumulation of plagioclase and to post-magmatic alteration. Relative to other Ninetyeast Ridge basalts (Frey et al., 1977), the uppermost basalts in Hole 757C have higher Zr/Nb and lower Y/Nb, and they define a distinct field (Fig. 25). However, many of these basalts have very low Nb contents (<3 ppm) which may result in large uncertainties in trace element ratios. These Hole 757C basalts apparently contain a larger component depleted in incompatible elements (MORB-like) than the previously recovered basalts from Ninetyeast Ridge.

In general, the variation of incompatible abundance ratios in Ninetyeast Ridge lavas (Figs. 24 and 28) can be explained by mixing, in various proportions, of sources enriched and depleted in incompatible elements. In the context of a hot-spot trace, this process can be identified as mixing of ascending plumes (i.e., sources of oceanic island basalts such as the transitional basalts of Kerguelen Island; Weis et al., 1988) with depleted (i.e., MORB-related) upper mantle.

Conclusions

1. Basalts of at least late Paleocene age were recovered at Site 757, under a thick overlying blanket of basaltic tephra. Two basaltic flow units were recognized in the core from Hole 757B, and 19 flow units from Hole 757C. The available data preclude any direct correlation between the flow units of the two holes.

2. The basalts form a series of discrete thin lava flows that were probably erupted in a subaerial environment.

3. All of the rocks studied are moderately to highly plagioclase-phyric basalts. Petrographically, they differ from the Site 756 basalts (Table 11). They are all vesicular, with a high proportion of large (>1-cm) vesicles. Both the plagioclase phenocryst and the vesicle contents vary downhole, as does the mineralogy: flow Units 757C-F18 and 757C-F19, corresponding to Core 121-757C-12R, have features distinct from those of the overlying units. Their plagioclase phenocrysts are slightly less abundant and have a slightly lower anorthite content; they have distinctly less ferromagnesian minerals than any of the overlying units, although clinopyroxene and olivine phenocrysts are present.

4. All of the basalts are moderately to highly altered. Different secondary mineral associations are present: blue green smectites, corresponding to nonoxidative alteration and limited to the upper units of the basalt section; calcite, brown smectites, and iron oxides/hydroxides, corresponding to more oxidative alteration processes and usually more limited in space, are mainly associated with large calcite veins and vesicles throughout the whole section; zeolites and opal/chalcedony, as well as chlorites/smectites, occur in vesicles and veins and at flow contacts. The zeolite and opal/chalcedony association indicates a higher temperature of alteration than in the Site 756 basalts.

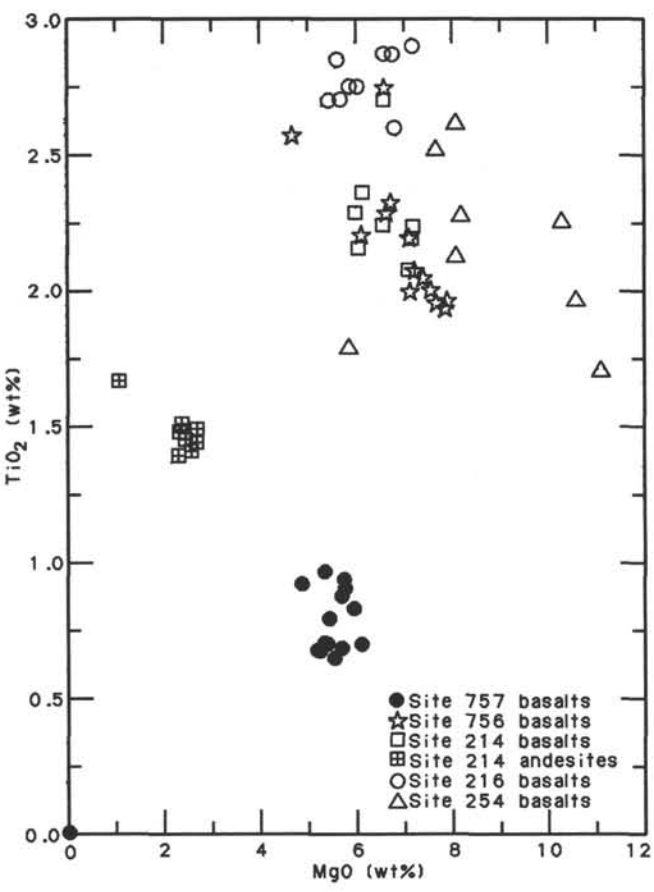

Figure 21. TiO_2 vs. MgO content in basement basalts from ODP Sites 756 and 757 and DSDP Sites 214, 216, and 254. The relatively low TiO_2 contents of the Site 757 basalts probably reflect, in part, plagioclase accumulation. Data for DSDP sites from Frey et al. (1977) and Thompson et al. (1974).

5. The basalts from Site 757 flow Units 757C-F1 through 757C-F17 have atypically high Al_2O_3 (18.2% to 24.2%) and Al_2O_3/CaO, coupled with low (<0.90 wt%) TiO_2 contents; these characteristics are consistent with the accumulation of abundant plagioclase phenocrysts. However, the parental melts possibly had higher Al_2O_3 contents than the basalts from the other Ninetyeast Ridge sites (Frey et al., 1977; Ludden et al., 1980).

6. There are two geochemical groups in basement basalt from Hole 757C. Relative to the upper flow units, in Cores 121-757C-9R through 121-757C-11R, the lowermost flow units in Core 121-757C-12R have higher FeO^*/MgO ratios and higher, by a factor of four, abundances of incompatible elements. The groups also differ in abundance ratios of incompatible elements (e.g., Ti/Zr and Zr/Nb). These geochemical groups cannot be related simply by plagioclase fractionation. They probably formed from different parental magmas.

7. Although there are distinct compositional and petrographic differences between the basalts from Sites 756 and 757 (see Table 11), the lower flow units from Hole 757C are more similar to the Site 756 basalts in Zr/Nb and Y/Nb than the upper flow units from Hole 757C (Figs. 25 and 28). In general, the Ninetyeast Ridge basalts appear to be mixtures of components related to MORB and of components related to ocean island basalts. The latter component dominates the trace element signature of the Ninetyeast Ridge basalts and has trace element characteristics similar to the transitional basalts from Kerguelen Archipelago (Weis et al., 1988). Data are not sufficient to evaluate if the MORB-ocean island basalt mixing proportions vary systematically with time.

PALEOMAGNETICS

Susceptibility

The initial susceptibilities of lithologic Subunit IA ("Lithostratigraphy and Sedimentology" section) are low (Fig. 29). The upper 75 m is characterized by a general decrease in susceptibility from about 3×10^{-6} cgs units in the very pale brown foraminifer-nannofossil ooze of Cores 121-757B-1H to 121-757B-4H (0–33.2 mbsf) to very low positive or slightly negative values in the underlying white nannofossil oozes. No visible changes in lithology accompany the susceptibility peaks in this section. The occurrence of peaks in the upper few meters of each core and the observation of rust flakes inside the core liner strongly suggest that these peaks result from rust contamination. Below 75 mbsf, susceptibilities increase to a base level of approximately 5×10^{-6} cgs units, reflecting the darker color, and presumably higher ferromagnetic content, of the sediments. Sustained peaks are as high as 4×10^{-5} cgs units, but are not obviously correlated with lithologic changes. The ashy calcareous chalks at the base of Unit I (Core 121-757B-23X, 208–211.7 mbsf) exhibit somewhat higher (as much as 10^{-4} cgs units) susceptibilities.

The Paleocene to lower Eocene ash and tuff sequence of lithologic Unit II (211.7–369.0 mbsf) and the basalts of lithologic Unit III (369.0–420.7 mbsf) have susceptibilities about two orders of magnitude higher than those of the overlying oozes (Figs. 29 and 30). The susceptibility of the foraminifer- and glauconite-bearing volcanic ash sequence of Subunit IIA (211.7–250.4 mbsf) decreases from a base level of 2×10^{-4} cgs units (peaks to 7×10^{-4} cgs units) in the upper part to 7×10^{-5} cgs units (peaks to 10^{-4} cgs units) in the basal portion. The upper part of Subunit IIB (250.4–340.0 mbsf) has a similar base level of 7×10^{-5} cgs units (peaks to 8×10^{-4} cgs units). Values in the lower part of this subunit (340.0–369.0 mbsf) are higher (up to 1.7×10^{-3} cgs units) and similar to those of the underlying basalts of Unit III. As a result, the contact between the volcanic ash and the basalts (Core 121-757C-8R; 372.8 mbsf) is not pronounced in the susceptibility data. Basalt susceptibility values are variable, ranging from 10^{-4} to 2.5×10^{-3} cgs units. These variations probably reflect variations in mineralogy, cooling, and alteration histories.

Remanence

Sediments

Variations in magnetization intensities in Unit I (0–211.7 mbsf) generally reflect the variations in susceptibility discussed in the preceding section (Fig. 31). Intensities after alternating field (AF) demagnetization at 9 mT are approximately 1 mA/m to a depth of 40 mbsf, where there is a significant decrease in intensity to 0.1 mA/m. Below 75 mbsf, intensities in the nannofossil oozes average 5–8 mA/m. Peaks in remanent intensity as high as 10^2 mA/m are apparently associated with rust contamination at the core tops. Average intensities in Unit II are generally 20 mA/m, with slightly lower (about 5 mA/m) values in Cores 121-757B-32X to 121-757B-37X (289–347 mbsf).

Although Cores 121-757B-3H to 121-757B-19H were oriented using the Eastman-Whipstock Multishot core orientation tool, the whole-core data from the poorly lithified sediments (0–180 mbsf) of Unit I yielded no polarity information. The Multishot tool performed well, as suggested by the consistent azimuth recorded for the drift of the hole (Table 12). The whole-core data, however, are characterized by consistent negative (normal) in-

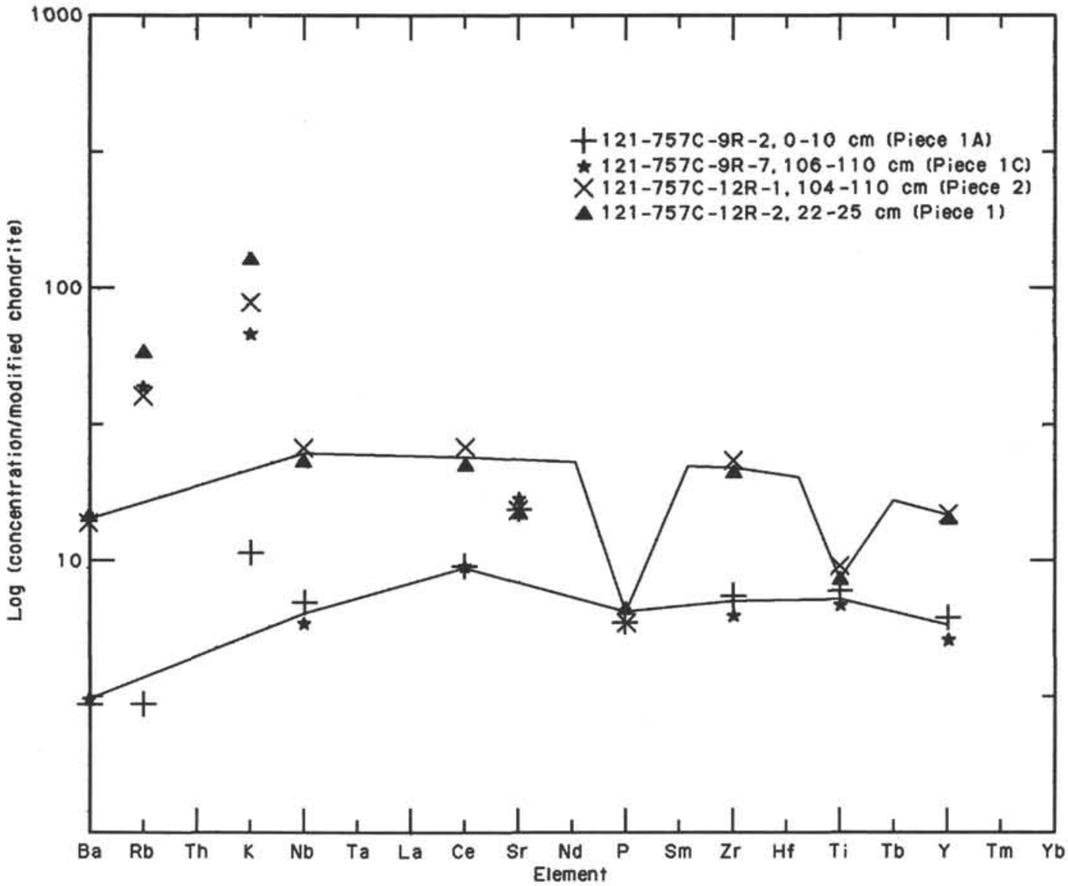

Figure 22. Abundances of incompatible elements in Hole 757C basalts normalized to modified chondritic meteorite abundances (Sun and McDonough, in press). Elements are arranged in order of increasing incompatibility from right to left. The most notable relative depletions of P and Ti are in Core 121-757C-12R basalts. The structure on the left side of the diagram may reflect post-magmatic alteration effects on Ba, Rb, and K abundances.

clinations and uncorrected declinations that cluster around 0° (Fig. 31).

The clustering of uncorrected declination values suggests that the sediments are being remagnetized after splitting. Comparison of working- and archive-half magnetization directions also supports this hypothesis. One possible explanation for this behavior is the acquisition of a viscous remanent magnetization (VRM). VRM may result from either mechanical reorientation of magnetic grains or thermal activation of magnetic moments in grains with very short thermal relaxation times. To test this hypothesis, we conducted a VRM-acquisition experiment with the archive half of Section 121-757C-2R-2. The core was measured after 2 hr of storage in the core rack, sealed in shrink wrap and inverted for 2 hr, and then remeasured. The significant change observed in the magnetization (inclination changed from $-40°$ to $-65°$) is a VRM acquired in the ambient laboratory field (about 0.5 Oe). The low shear strength of these sediments (approximately 5 kPa; "Physical Properties" section) suggests that physical reorientation of magnetic grains may be responsible for the VRM. This mechanism has been previously proposed to explain similar observations on Leg 108 (Shipboard Scientific Party, 1988).

Some corrected declinations within a single core show offsets between sections (Fig. 32), suggesting that rotation of the core with respect to the liner may occur during sectioning. In addition, systematic variations in direction and intensity within sections, similar to those described at Site 754 ("Paleomagnetics" section, "Site 754" chapter, this volume) were observed. We suspected that these effects might result from the high-frequency transducer and significant field gradient in the *P*-wave measurement unit. However, tests revealed no detectable effect of *P*-wave measurements on either water-rich (Core 121-757C-1R) or more consolidated (Core 121-757C-2R) sediments.

Whole-core measurements of the more indurated sediments of Unit I (180–211.7 mbsf) and the volcanogenic sediments of Unit II suggest the tentative polarity sequence shown in Figure 33. Discrete sample demagnetization was confined to four samples from Cores 121-757B-21X to 121-757B-23X because of the limited availability of suitable material and the DC bias present in the AF demagnetizer (see "Explanatory Notes" chapter, this volume). No detailed correlation with the geomagnetic reversal time scale (GRTS) is warranted at present. However, the presence of at least one normal and two reversed intervals in the volcanic ash and tuff sequence suggests a relatively long depositional duration. In particular, biostratigraphic data ("Biostratigraphy" section, this chapter) indicate that ash deposition continued into the latest Paleocene. The tentative identification of foraminifer Zone P5 and calcareous nannofossil Zone CP8 suggests that the normal interval beginning at 224 mbsf may represent Chron C25N (Berggren et al., 1985; Bolli et al., 1985). The duration of Chron C25N (0.64 m.y.) implies a sedimentation rate of 90–145 m/m.y. during this interval. Other possible correlations with the GRTS yield similar or lower sedimentation rates.

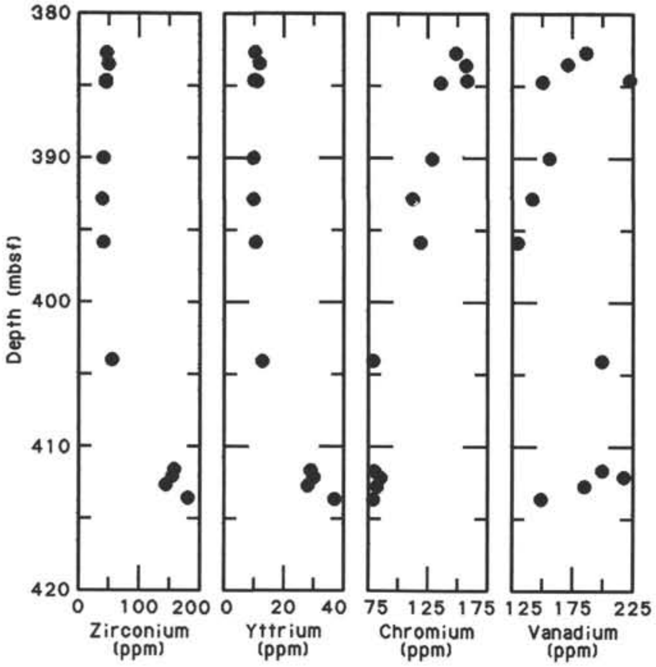

Figure 23. Abundances of Zr, Y, Cr, and V in basement basalts as a function of depth in Hole 757C. The lowest four samples from flow Units 757C-18 and 757C-19 have higher Zr and Y contents and lower Cr contents. This trend contrasts with that of basement basalts from Hole 756D (compare with Fig. 14 of the "Site 756" chapter).

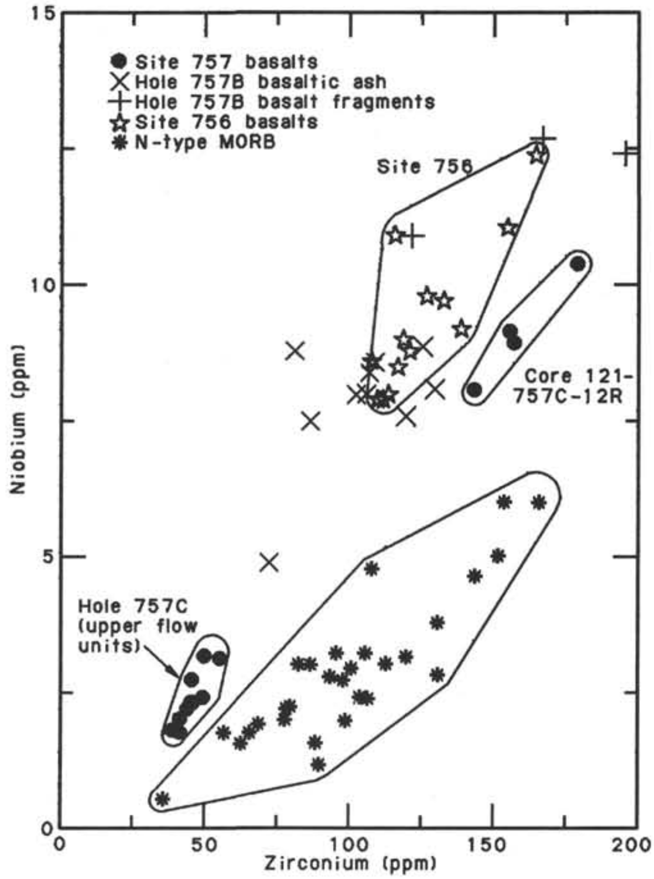

Figure 24. Nb vs. Zr for basaltic ashes and fragments from Hole 757B with a field for MORB (Bougault et al., 1979; Saunders, 1983; Price et al., 1986).

Basalts

Only natural remanent magnetizations (NRM) of basalts and volcaniclastic sediments from Unit III (369.0–421.0 mbsf) were measured aboard ship. NRM inclinations of the upper flow units (757B-F1–757C-F9) in Holes 757B and 757C are low (about +20°) and almost entirely of reversed polarity (Fig. 34). The lower flow units (757C-F10–757C-F19), in contrast, have very steep, reversed NRM inclinations (about +80°). These shipboard NRM observations are confirmed by preliminary shorebased AF demagnetization studies. The high inclination values of the lowermost flows probably represent a primary magnetization. The consistent low inclinations of the upper flow units cannot be explained at present and will be the subject of further shorebased studies. NRM intensities of the basalts range from 0.09 to 6.7 A/m, with an arithmetic mean of 1.2 A/m (Fig. 35). The average intensity is similar to that of "normal" MORB of similar age (Van Wagoner and Johnson, 1983) and slightly less than that of the younger basalts (2.1 A/m) from Site 756.

Magnetic Mineralogy of Basalts

Reflected light microscopy indicates the magnetic mineralogy of the basalts from Site 757 is dominated by oxides of the magnetite-ulvöspinel (titanomagnetite) solid-solution series. Observation of "trellis pattern" exsolution lamellae in many of the samples indicates that the composition has more than 10% to 20% of the ulvöspinel component. More accurate determination of composition will be made on shore. The two major features of interest are the habit and oxidation state of the oxides. Because magnetite typically forms late in the crystallization sequence, it commonly exhibits an anhedral, or less common subhedral, habit in basalts that are close to holocrystalline. These habits were observed in a number of the flows, especially in the interiors of flows. When rapidly cooled, however, titanomagnetite commonly exhibits a euhedral dendritic quench texture (skeletal habit). This habit is common but not unique to submarine basalts; it is common throughout the basalts of Site 757, especially near flow boundaries. Skeletal titanomagnetite grains are commonly associated with smectite, suggesting that they formed in regions of abundant glass. The evolution of habit was especially well exhibited in flow Unit 757C-F5, which has skeletal habits near the upper contact, grading into anhedral/subhedral habits in the interior, and back to skeletal forms at the lower contact.

Oxides may undergo either high- or low-temperature alteration. High-temperature alteration is distinguished by the presence of "trellis pattern" ilmenite lamellae (Haggerty, 1976). Low-temperature alteration leaves the grains optically homogeneous, but commonly causes cracking because of a reduction in volume with increasing oxidation. All of the basalts from Site 757 that have anhedral/subhedral habits exhibit varying degrees of high-temperature alteration. Some of the basalts with skeletal habits also show exsolution lamellae (observed in flow Units 757C-F6, 757C-F10, and 757C-F14), although most are optically homogeneous. Cracking caused by low-temperature alteration is light to moderate and generally much less advanced than at Site 756. The lesser degree of alteration is puzzling in light of the fact that the rocks from Site 757 are significantly older and presumably more altered than the basalts from Site 756. The presence of high-temperature alteration features in both anhedral and skeletal grains suggests that the basalts were subaerially erupted.

INORGANIC GEOCHEMISTRY

A major objective of the chemical measurements of pore waters on Leg 121 was to determine the horizontal uniformity of

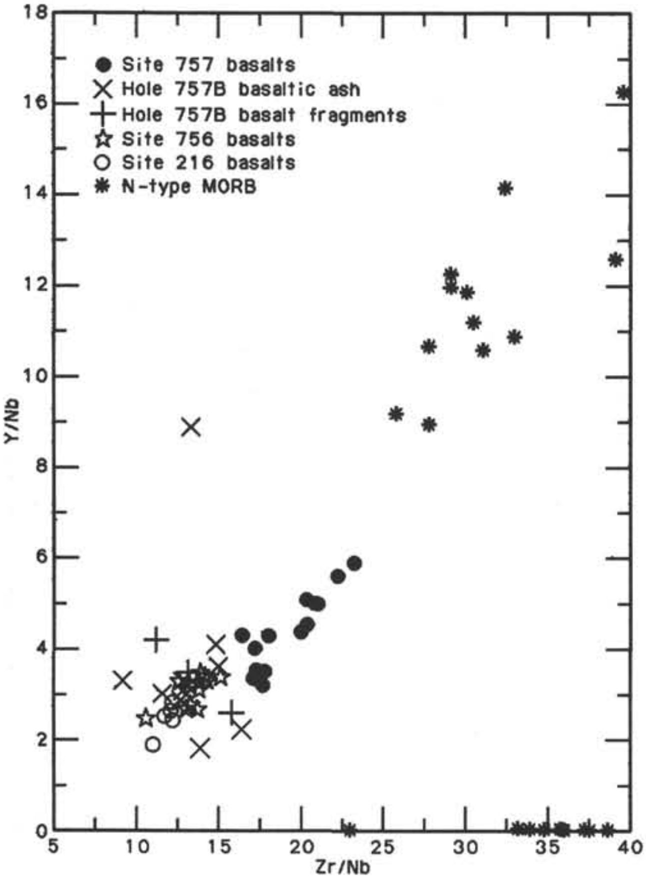

Figure 25. Y/Nb vs. Zr/Nb shows that basement basalts from Hole 757C have higher Zr/Nb than the other Ninetyeast Ridge basalts. However, the ashes and included basalt fragments in Hole 757B overlap with basalts from Sites 756 and 216 (A. D. Saunders and M. Storey, unpubl. data).

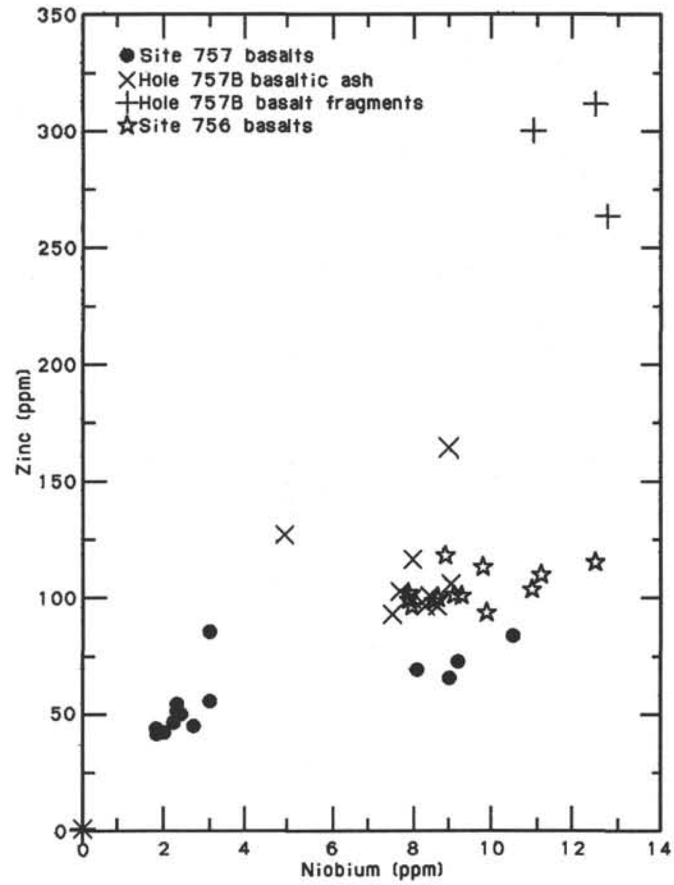

Figure 26. Zn vs. Nb contents in basement basalts from Holes 756D and 757C. The Zn contents have only small intrahole variations, but significant interhole differences. In contrast, four samples (three basalt fragments and one ash) from above the basement in Hole 757B have anomalously high Zn contents.

the chemical gradients in the pore fluids. Lateral changes in pore-water chemistry can be related to lithologic changes in the sediments or basalts, structural features of the basement, or the convection of fluids in the basement and possibly even sediments. For more detail, see the "Inorganic Geochemistry" section of the "Site 756" chapter. The overall results of the Ninetyeast Ridge sites are presented in the "Ninetyeast Ridge Summary" chapter (this volume).

Results

Site 757 is east of the crest of the Ninetyeast Ridge at 17°S. A pelagic cap about 200 m thick overlies volcanic ash and basaltic basement. The thickness of the volcanic ash varies from none present to about 200 m in the area surveyed. At Site 757 the carbonate sediment cover is 220 m thick and the ash is 140 m thick with basement below. About 2 km east of Site 757 is a normal fault with a vertical throw of about 100 m. Although the basement in the Site 757 area generally is steeply dipping, it is not as rough, irregular, and cut by as many faults as the basement at Site 756.

Three holes were drilled at Site 757. Holes 757A and 757B were drilled at one location, and Hole 757C was drilled 200 m northwest, upslope from the other two holes (see Fig. 3 and "Operations" section). The ash layer is slightly thicker under Hole 757C (for more detail, see "Lithostratigraphy and Sedimentology" section).

Very large changes in pore-water chemistry with depth were observed. The chemical compositions of the pore fluids from Site 757 are given in Table 13. The pore-water alkalinity, salinity, magnesium and calcium ion concentrations, chlorinity, and sulfate ion concentration measured for Hole 757B are plotted as a function of depth in Figure 36.

The calcium ion concentration measured at the deepest sample interval (366 mbsf) is the highest found in DSDP and ODP investigations. In addition, the calcium ion gradient, the change in calcium ion concentration per unit of depth change, is also the highest ever found in the history of DSDP and ODP. The magnesium ion concentration decreases with depth and reaches undetectable levels at 240 mbsf, slightly below the boundary between the carbonate ooze and the ash beneath. Alkalinity and sulfate ion concentrations also decrease strongly with depth. Salinities and chlorinities increase strongly with depth. Values of pH show a marked downward increase across the carbonate ooze/ash boundary.

Discussion

Changes in calcium and magnesium ion concentrations with depth in deep-ocean sediments reflect the alteration of volcanic material in the sediments or underlying basaltic basement (Lawrence and Gieskes, 1981; Gieskes, 1983). The unparalleled changes at Site 757 are undoubtedly the result of the alteration of the thick ash from 220 to 360 mbsf. The previous record high for calcium ion concentration was found at Site 253, also on the Ninetyeast Ridge, where the ash reaches a thickness of 400 m (Davies, Luyendyk, et al., 1974).

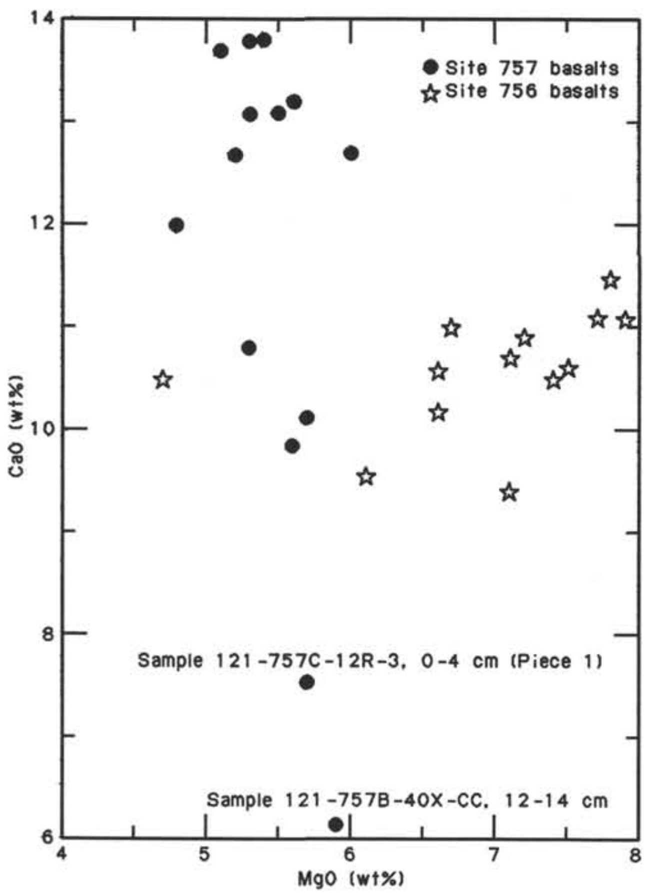

Figure 27. CaO vs. MgO in basement basalt from Sites 756 and 757. The samples with low CaO (121-757B-40X-CC, 12-14 cm, and 121-757C-12R-3, 0-4 cm [Piece 1]) may have lost CaO during post-magmatic alteration.

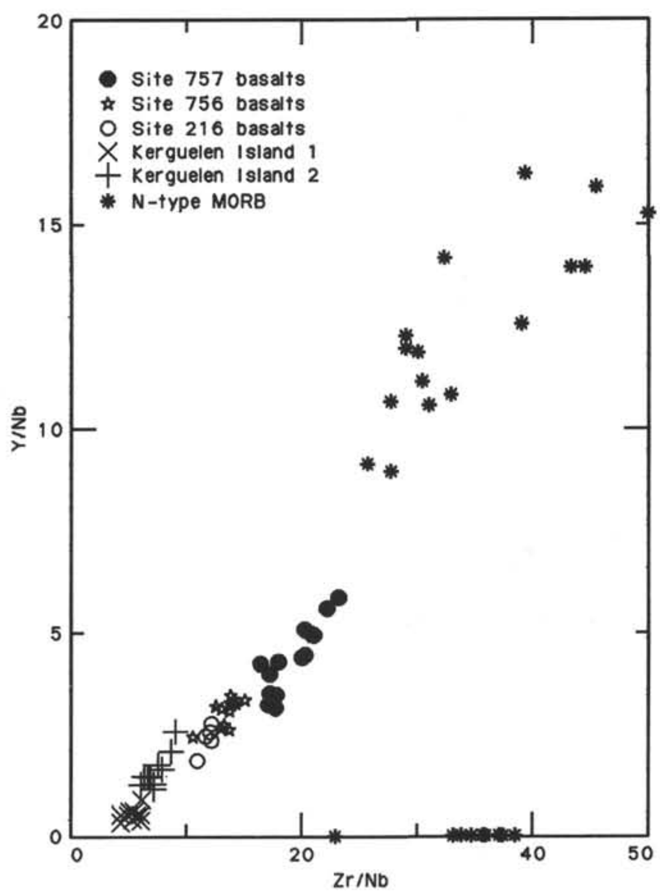

Figure 28. Y/Nb vs. Zr/Nb for the Ninetyeast Ridge basalts plotted with a MORB field (Bougault et al., 1979; Saunders, 1983; Price et al., 1986) and data for Kerguelen Island lavas (A. D. Saunders and M. Storey, unpubl. data).

All of the changes described in the preceding can be attributed to the alteration of volcanic ash to clay minerals and possibly zeolites. When ash alters to smectite, calcium is released into solution while magnesium is taken up by the smectite. This smectite is often saponite or chlorite-smectite interlayered clay, both of which are rich in magnesium. XRD studies of the clay minerals both in the ashes and basalts show the presence of 12 to 16 Å clay minerals, which expand when glycolated (Table 14).

The decrease in alkalinity and sulfate is caused by the supersaturation of the solution at depth with respect to calcite and gypsum, respectively. This supersaturation is driven by the increase in calcium concentration with depth. The ratio of the ion activity product to the solubility product (IAP/KSP) for calcite and gypsum was calculated from the chemical data (Table 13) using activity coefficients for seawater from Garrels and Christ (1965) and equilibrium constants from Drever (1982). The pore solutions are supersaturated with respect to calcite at all depths, with a marked jump in supersaturation occurring in the ashes. The IAP/KSP ratio for gypsum increases as a function of depth and reaches supersaturation at the ash boundary.

The salinities and chlorinities show an increase greater than 10% more than those of seawater as a result of water removal from solution as the ash is hydrated to form clay. A better quantitative estimate of the amount of ash alteration needed to produce the observed chemical changes will be possible when shore-based oxygen isotope measurements are made on the pore waters (see Lawrence and Gieskes, 1981).

Table 11. Differences between basalts from Sites 756 and 757.

	Site 756	Site 757
Ashes, breccias, and loose interflow material	Abundant	Absent
Number of flow units	14	19
Flow thickness	7 > 2 m and 4 > 4 m	12 < 1 m, 1 m < 2 < 2 m, and 4 > 2 m
Macroscopic and microscopic observations	Aphyric (maximum phenocrysts = 5%)	Highly plagioclase-phyric (up to 40%)
Alteration	About 40% (maximum 70%); low temperature	About 50%–60% low (maximum 90%); higher temperatures; (zeolites/quartz)
Compositional differences (e.g., Zr/Nb ratio)	<15	>16
Bulk-rock compositions correspond to:	Magmatic liquid plagioclase(?)	Liquid + cumulus
Within-hole variations reflect:	Fractionation from a single parental magma	At least two different magmas or mantle sources

Chemical measurements were made on pore-water samples from spot cores from Hole 757C, which is at a slightly thicker section of ash, 200 m northwest of and upslope from Holes 757A and 757B (see "Lithostratigraphy and Sedimentology" section). In general, the concentrations are comparable to those observed at Holes 757A and 757B. The calcium ion concentration is about 10% less for any given depth. The other chemical

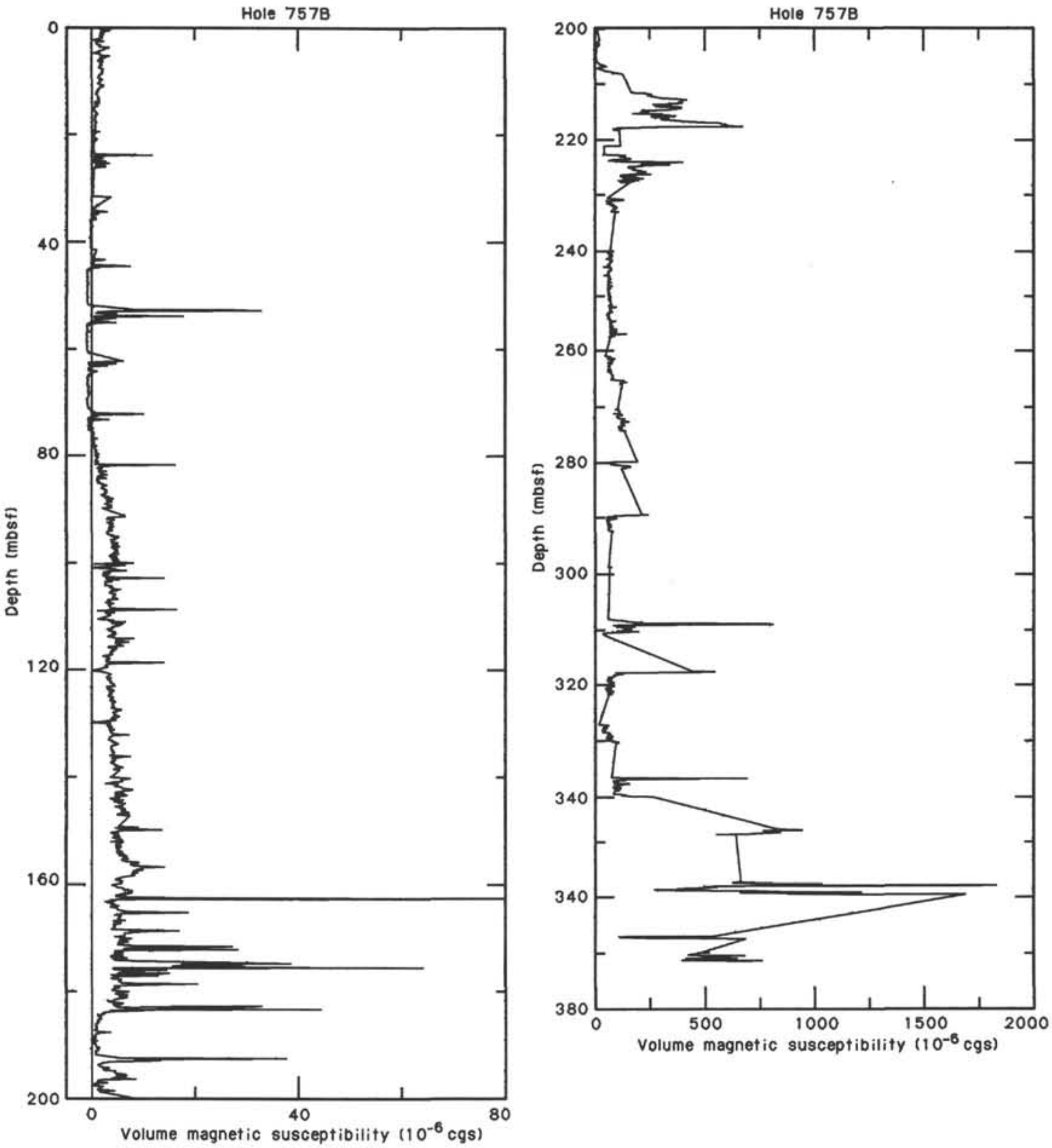

Figure 29. Volume magnetic susceptibility plot for Hole 757B.

constituents show variations that correspond to the calcium differences from Holes 757A and 757B.

The observed differences in calcium ion concentrations, expressed as percentages, at drill site locations 200 m apart are small in comparison with those observed at Site 756, as seems reasonable. Basement at Site 756, which is the source of the calcium signal in the pore waters, is more irregular and cut by more faults than basement at Site 757. The sediment cover is also thinner and varies more in thickness over comparable distances for the two sites. At Site 757, the ash layer is the source of the calcium signal, and although it varies in thickness between the two holes, the variation is relatively small. The ash layer is somewhat thicker at Hole 757C, which has the lower calcium gradient.

The causes of the differences in chemistry between the two holes at Site 757 are difficult to assess. The 10% change over 200 m, though small in comparison with the difference in values from Site 756, is still significant. Continued change on this order across Ninetyeast Ridge might reveal important information about basement structure, extent of ash alteration, or water transport mechanisms in basement and the overlying ash and pelagic sediments. The two pairs of holes are sufficient to demonstrate that studies of pore-water chemistry may be useful, but they are insufficient to justify larger scale interpretations.

ORGANIC GEOCHEMISTRY

Samples from Holes 757A, 757B, and 757C were studied for their carbonate carbon and organic carbon contents and for concentrations of hydrocarbon gases. Additionally, three samples were selected for Rock-Eval pyrolysis (see "Explanatory Notes" chapter and "Organic Geochemistry" section, "Site 752" chapter, this volume, for analytical details).

Gas Analyses

Concentrations of methane in the headspace gases did not exceed those in the laboratory air, 3 ppm. Ethane and propane were not detected.

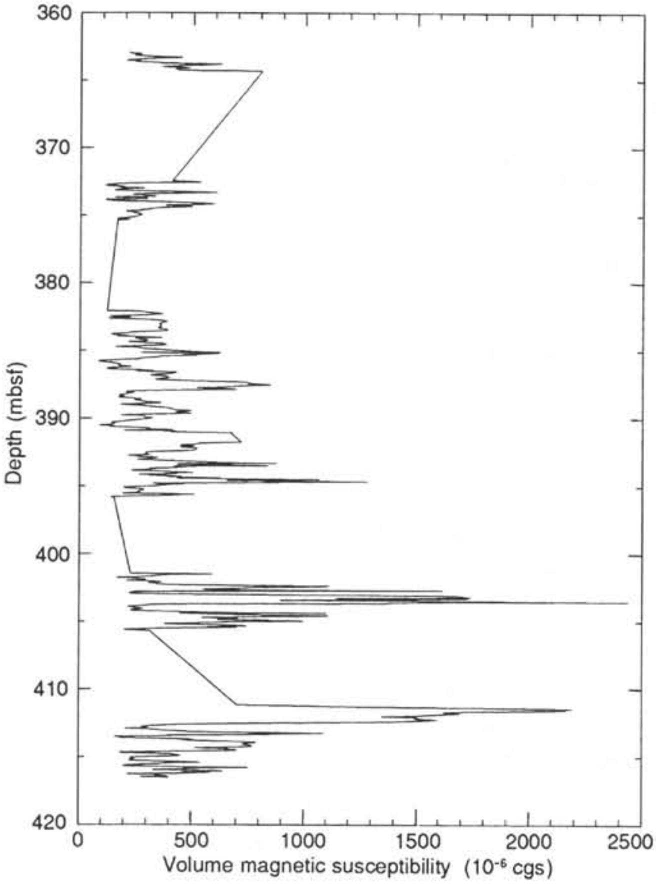

Figure 30. Volume magnetic susceptibility plot for Hole 757C.

Organic Carbon

Almost no organic matter was found in the Pleistocene to lower Eocene sediments drilled between 0 and 210 mbsf. In the Paleocene transition between the sediments and the ashes (210–225 mbsf, lithologic Subunit IIA), organic carbon percentages are slightly higher, with a maximum value of 0.45% immediately above the ash of lithologic Unit II. Little organic matter was detected in the ash drilled between 225 and 367 mbsf (Table 15 and Fig. 37).

Three samples were analyzed by Rock-Eval pyrolysis (Table 16). Their organic carbon contents vary between 0.1% and 0.45%. Some hydrocarbons were released from the two samples of the Paleocene transition unit, but none from the Eocene sample.

Carbonate Carbon

In the lower Eocene to Pleistocene section drilled between 210 mbsf and the seafloor, the average carbonate content is 96%. Slightly lower than average carbonate percentages occur between 0 and 15 mbsf, 144 and 164 mbsf, and immediately above the Paleocene transition zone separating biogenic sediments from the ash unit. These intervals correspond to the Pleistocene/uppermost Pliocene, middle Eocene, and lower Eocene, respectively. There is no decrease of carbonate percentage in the middle to lower Miocene, as was observed at Site 756 on the southern part of Ninetyeast Ridge.

Carbonate percentages are generally low in the ash unit drilled below 225 mbsf. However, some intervals contain up to 30% carbonate (Table 15 and Fig. 37). Samples from the interval between 255 and 271 mbsf are especially rich in carbonate in comparison with the average composition of the ash unit.

PHYSICAL PROPERTIES

The objectives of the physical-properties measurements at Site 757 were to study the consolidation of this calcareous section, provide ties between cored lithologies and seismic survey reflection profiles, and to tie these properties to the regional geologic history.

Hole 757B was cored with the APC to 174.7 mbsf, followed by the XCB and NCB systems. Hole 757C was rotary cored to 420.7 mbsf. The sediments cored at Site 757 consist of two units overlying basaltic basement (see "Lithostratigraphy and Sedimentology" section). Lithologic Unit I extends from 0 to 211.7 mbsf and consists of Pleistocene to lower Eocene nannofossil ooze. Two subunits are recognized in the upper 212 m of the section: Subunit IA extends from the mud line to 168.5 mbsf, and Subunit IIB, from 168.5 to 211.7 mbsf, is distinguished from the overlying subunit by its increased induration and micrite component. Lithologic Unit II consists of 157 m of ash with lapilli and tuff. Hole 757C penetrated over 45 m into basement, recovering highly plagioclase-phyric basalt flows (see "Igneous Petrology" section, this chapter).

Results

Index Properties

Measurements of water content (expressed as water weight relative to wet sample weight), porosity, bulk density, dry-bulk density, and grain (or matrix) density of the Site 757 sediments are listed in Table 17 and plotted relative to depth in Figures 38 and 39. Three units defined by their physical properties characterize the cored section. Physical-properties unit A (0–197 mbsf) corresponds to lithologic Unit I. Unit B (197–368 mbsf) overlaps with the base of lithologic Subunit IB and corresponds primarily to the tuffaceous sediments of lithologic Unit II. Unit C defines the underlying basalts of lithologic Unit III.

The upper 197-m-thick section consists of consolidating calcareous ooze. Porosity in unit A decreases from 72% near the mud line to 38% at 195 mbsf. Bulk density in unit A varies between 1.53 to 2.14 g/cm^3, with a mean value of 1.89 g/cm^3. Grain density within this upper unit does not vary much, with a mean value of 2.71 g/cm^3. The upper 45 m of unit A shows a trend of increasing bulk density that is interrupted by an interval between 49 and 69 mbsf (Figs. 38 and 39). This latter interval exhibits a high bulk density and low porosity relative to the surrounding sediments. Below 60 mbsf, however, the general increase of bulk density with depth is resumed. Other anomalies in the overall changing index properties of unit A are represented by a shift from high to lower densities at 90 mbsf and a high-density, low-porosity layer between 138 and 143 mbsf (Fig. 39).

Unit B, corresponding to lithologic Unit II, is evidenced in the index properties as a unit of higher water content and lower bulk densities relative to the base of overlying unit A. Index properties within unit B are nearly constant, as opposed to the trends observed in unit A, except for the interval between 197 and 246 mbsf. This short interval corresponds to the base of lithologic Subunit IB and all of Subunit IIA and represents a distinctive lithology and physical gradient from the nannofossil oozes with micrite of Unit I to the lapilli and tuffs of Subunit IIA. Within this short interval, bulk densities range from 1.76 to 2.20 g/cm^3, and grain densities decrease from a mean value of 2.71 g/cm^3 in unit A to 2.59 g/cm^3 in unit B. The lower grain and bulk densities of the volcaniclastic unit relative to calcareous sediments is typical of the lithologies sampled during Leg 121.

Below 368 mbsf, physical-properties unit C corresponds to the basement basalt flows of lithologic Unit III. The sampled basalts have bulk densities ranging between 2.32 and 2.99 g/cm^3, with a mean value of 2.59 g/cm^3. Porosities range from

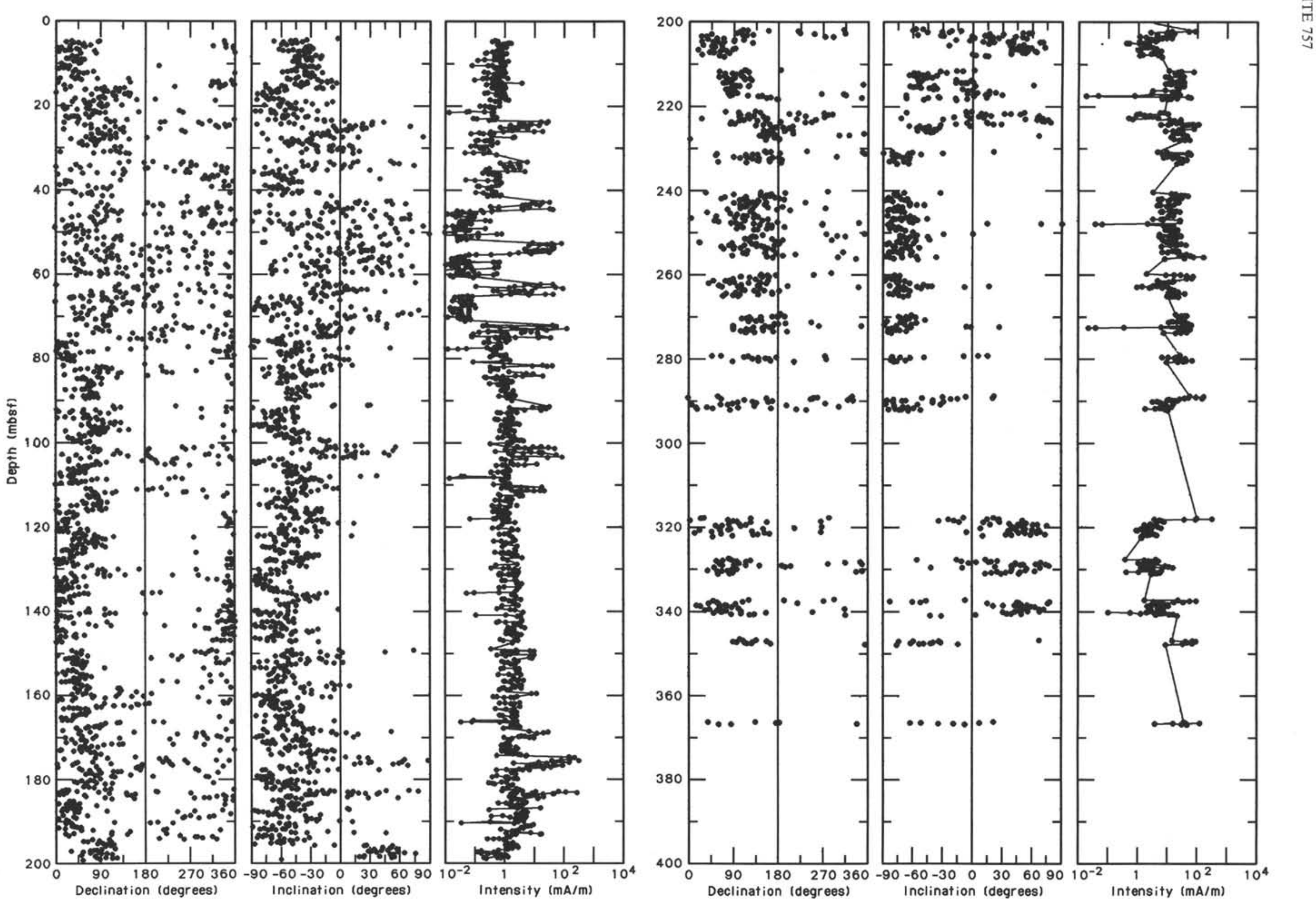

Figure 31. Unoriented remanence data after 9-mT AF demagnetization, Hole 757B.

Table 12. Multishot core orientation data, Hole 757B.

Core	Drift (degrees)	Direction of drift (degrees)	Declination (degrees)	Shot rate (min)	Half-hour delay	Instrument number
3H	2.0	345	82	0.5	N	1606
4H	1.8	316	18	0.5	N	1606
5H	2.0	317	67	0.5	N	1606
6H	2.0	330	267	0.5	N	EW40649
7H	1.8	325	186	0.5	N	EW40649
8H	1.8	330	243	0.5	N	EW40649
9H	1.8	315	200	0.5	N	1606
10H	1.8	325	265	0.5	N	1606
11H	1.8	325	127	0.5	N	1606
12H	1.6	327	35	0.5	N	EW40649
13H	1.6	320	280	0.5	N	EW40649
14H	1.4	320	235	0.5	N	EW40649
15H	1.5	330	303	1.0	N	1606
16H	1.2	320	173	1.0	N	1606
17H	1.1	327	173	1.0	N	1606
18H	1.1	325	92	1.0	N	1606
19H	1.2	325	355	1.0	N	1606

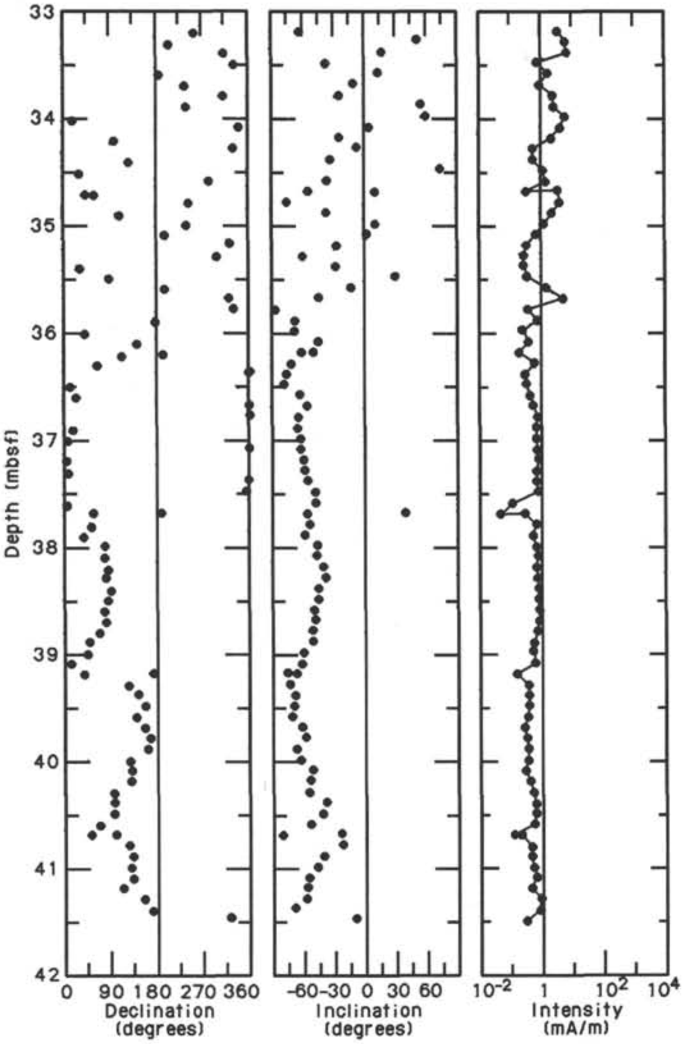

Figure 32. Remanence data for azimuthally oriented Core 121-757B-5H after 9-mT AF demagnetization. The higher intensity of random magnetization directions in the upper 2.5 m is probably the result of rust contamination. The declination is offset between successive sections.

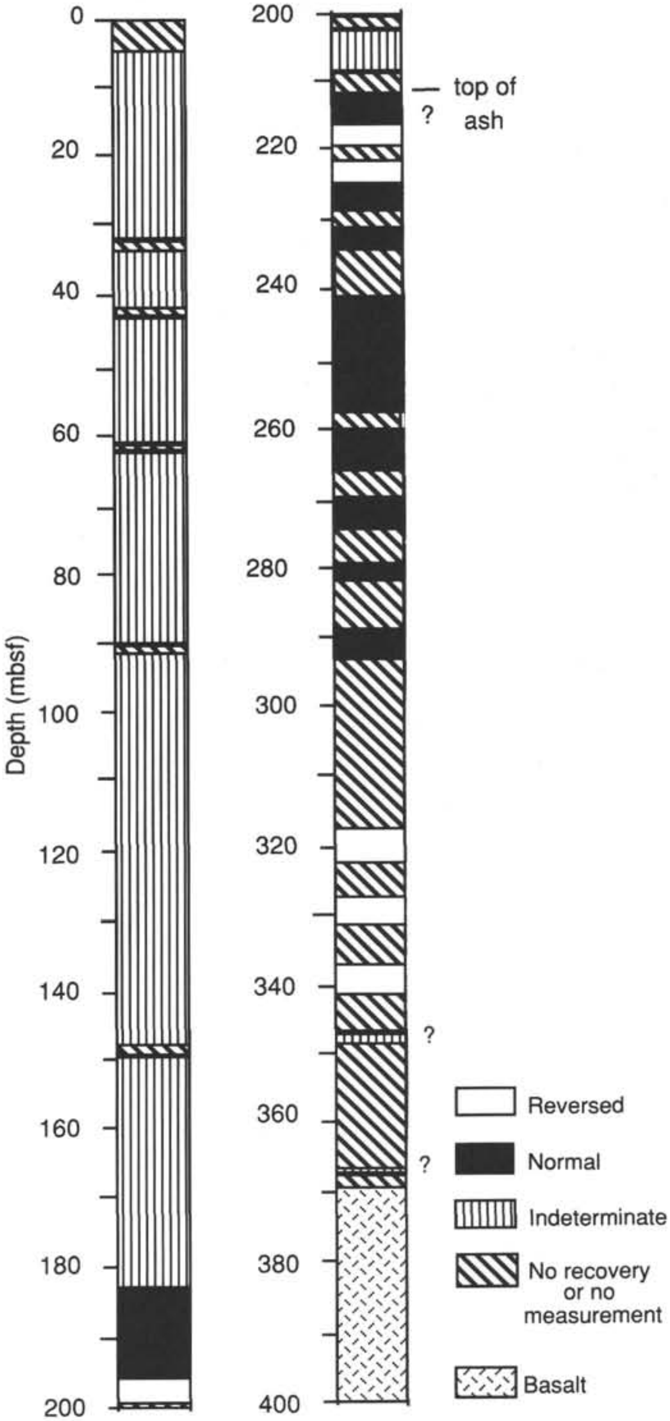

Figure 33. Magnetic polarity deduced from whole-core measurements from Hole 757B (cf. Fig. 31).

about 3% to 12.5%, values that are characteristic of fairly massive basalts. Although the recovered basement rock is fairly vesicular, the vesicles are generally filled with calcite, zeolites, or smectite. Very little interflow volcaniclastic material was recovered; hence, the index properties at the base of the holes lack an interbedded aspect.

Compressional-Wave Velocity

Velocity data obtained from laboratory samples are listed in Table 18 and displayed in Figures 38 through 40. The only mea-

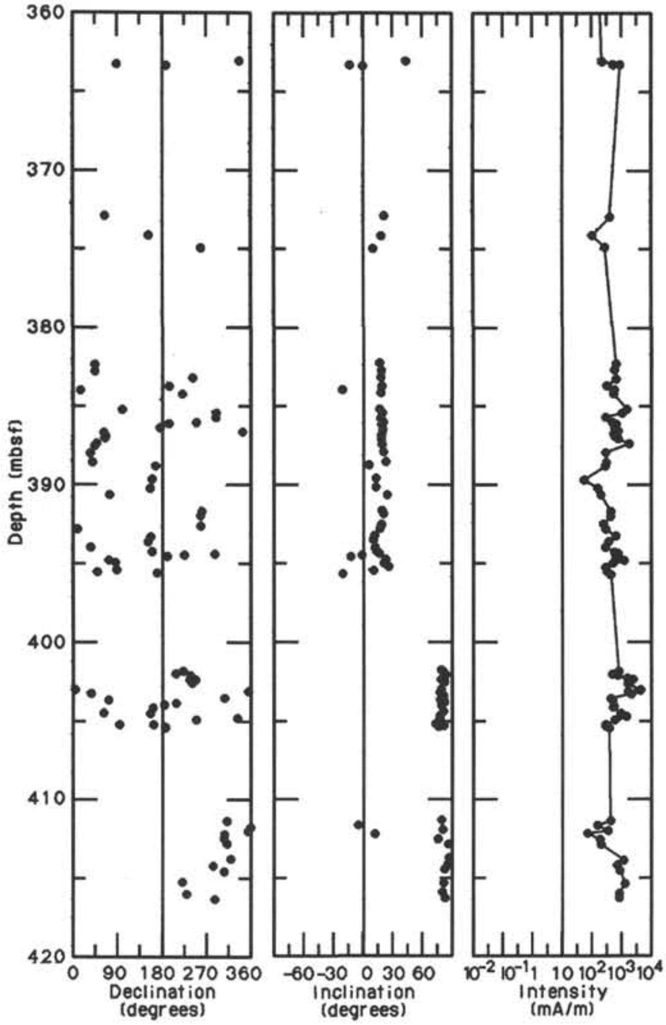

Figure 34. NRM declination, inclination, and intensity of discrete samples from Hole 757C.

surements made in the soft oozes of lithologic Unit I are *P*-wave-logger velocities, which range from values less than 1500 to 1670 m/s (Fig. 39). This slight velocity increase is sharply offset approximately 10 m below the physical-properties unit A/unit B boundary. The depth discrepancy of velocity and index properties demarcating the unit boundary is an artifact of *P*-wave logging of XCB cores from Core 121-757B-19H (174.7 mbsf) downward. Below 208 mbsf, velocities range from 1700 to near 3000 m/s.

Physical-properties unit C is marked by a distinct velocity increase from 3000 to 4500 m/s at 368 mbsf. A single, low value of 2230 m/s within this unit represents the volcaniclastic unit recovered below basalt in Hole 757B. The velocity range measured for the Site 757 basalts falls within that of the Site 756 basalts; however, the highly altered character of the basalts measured from Site 757 may explain why these do not reach the high velocities near 6 km/s obtained for some massive flows at Site 756.

The samples from this lower unit were tested by propagating a compressional wave through three mutually perpendicular directions to obtain measures of velocity anisotropy (Table 19 and Fig. 40). The vertical to horizontal anisotropy ranges from −2.2% to 6.3% in units B and C, with an average of 1.3%. This low value suggests that the volcanic units sampled at Site 757 have little to no anisotropy.

The impedance log, computed from GRAPE and compressional-wave-velocity data in the APC-cored section and from laboratory measurements in the remaining cores (below 210 mbsf), shows contrasts at 48, 80, 92, 210, 280, and 368 mbsf (Figs. 38 and 39). These impedance contrasts account for some of the reflectors in the seismic record (see "Seismic Stratigraphy" section, this chapter).

Vane Shear Strength

Records of torque vs. vane rotation were obtained from the APC-cored section in Hole 757B. Although these sediments contain small amounts of clay, their silty, noncohesive behavior results in extremely low strength values (Table 20 and Fig. 41). The sediments gain some strength in the lowermost part of the section, where the calcareous sediment contains greater amounts of micrite and ash. The lithologic definition of the top of Sub-

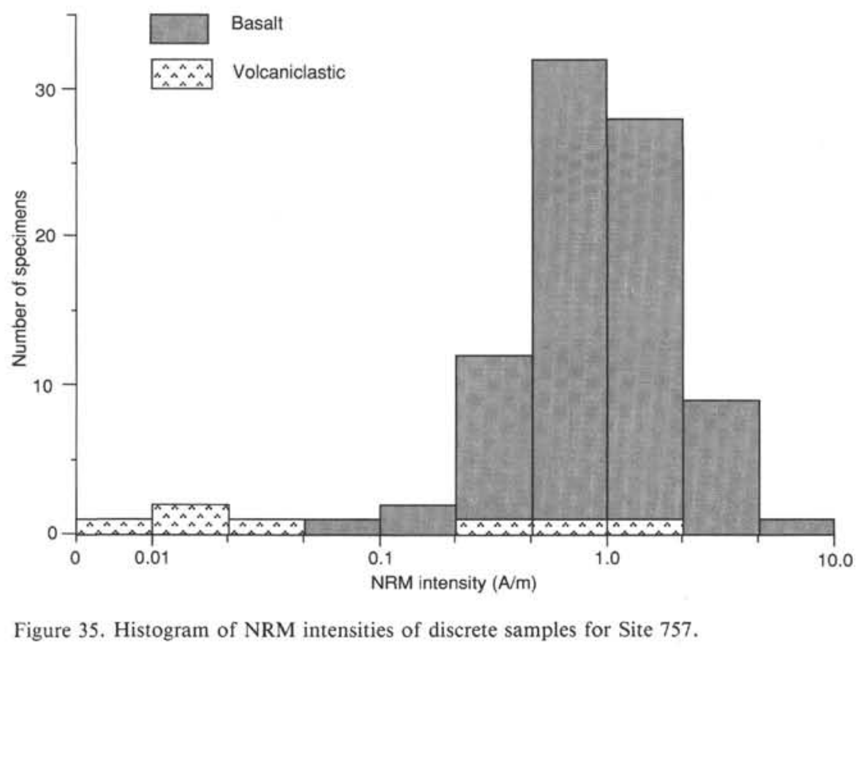

Figure 35. Histogram of NRM intensities of discrete samples for Site 757.

Table 13. Site 757 interstitial-water geochemistry data.

Sample (interval in cm)	Depth (mbsf)	Volume (mL)	pH	Alkalinity (mmol/L)	Salinity (g/kg)	Magnesium (mmol/L)	Calcium (mmol/L)	Chloride (mmol/L)	Sulfate (mmol/L)	Mg^{2+}/Ca^{2+}	IAP/KSP[b] Calcite	IAP/KSP[b] Gypsum	Temperature[c] (°C)
757A-1H-1, 0–1	0.00	13				52.60	10.10		25.60	5.21			
757C-1R-1, 148–150	1.48	14				51.50	11.40			4.52			
757B-1H-2, 140–150	2.73	32	7.60	2.670	35.5	50.50	12.30	542.00	27.30	4.11	1.90	0.13	5.1
757C-1R-4, 148–150	5.98	15			35.0	51.30	12.80	551.00	27.80	4.01			
757A-1H-5, 145–150	7.45	60	7.50	2.640	35.5	50.00	14.80	552.00	27.10	3.38	1.81	0.15	5.3
757C-1R-6, 148–150	8.98	13				51.50	13.20			3.90			
757B-2H-5, 148–150	11.98	7				49.10	18.50		27.30	2.65			
757B-3H-5, 145–150	21.45	27	7.30	2.130	36.2	46.80	23.80	557.00	27.30	1.97	1.53	0.25	5.9
757B-4H-4, 148–150	29.58	9				44.50	28.80		26.10	1.55			
757B-5H-4, 148–150	39.18	9				42.60	33.20		25.30	1.28			
757B-6H-5, 145–150	50.25	20	7.30	1.760	36.5	40.50	38.30	575.00	25.30	1.06	2.05	0.37	7.0
757B-7H-4, 148–150	58.48	7				38.90	42.70		24.60	0.91			
757B-8H-5, 148–150	69.68	7				38.00	47.90		25.30	0.79			
757B-9H-4, 145–150	77.75	30	7.30	1.690	37.0	34.80	51.90	568.00	24.30	0.67	2.95	0.53	8.1
757B-10H-5, 145–150	88.95	2				34.10	57.00		23.30	0.60			
757B-11H-5, 148–150	98.68	7				31.50	61.90		22.80	0.51			
757B-12H-5, 145–150	108.25	28	7.30	1.210	38.0	29.40	66.30	577.00	23.30	0.44	2.86	0.67	9.3
757B-13H-5, 138–140	117.88	4				26.10	72.00		21.40	0.36			
757C-2R-1, 148–150	122.98	10			37.5	30.00	70.00	581.00	22.30	0.43			
757B-14H-5, 148–150	127.58	7				24.60	76.10		22.80	0.32			
757C-2R-6, 148–150	130.48	8				27.90	72.00			0.39			
757C-3R-1, 148–150	132.58	8			38.5	26.70	75.70	583.00	21.80	0.35			
757B-15H-4, 145–150	135.75	17	7.20	1.090	38.2	23.00	79.50	579.00	22.40	0.29	2.59	0.81	10.4
757C-4R-1, 148–150	142.28	7				25.30	79.40			0.32			
757B-16H-4, 148–150	145.48	4				22.10	84.00		22.40	0.26			
757C-4R-6, 148–150	149.78	7			38.5	25.70	81.70	571.00	23.00	0.31			
757C-5R-3, 148–150	154.98	9				23.00	85.10			0.27			
757B-17H-5, 148–150	156.58	5				18.20	91.30		20.40	0.20			
757C-5R-6, 148–150	159.48	8			38.0	22.30	88.00	589.00	22.40	0.25			
[a]757C-6W-1, 0–5	160.10	2				24.50	71.80		20.60	0.34			
757B-18H-5, 145–150	166.25	12	7.11	0.661	39.0	18.30	93.80	583.00	19.10	0.20	1.61	0.85	11.7
757B-19H-3, 147–150	172.97	6				16.90	96.10		19.10	0.18			
757B-20X-5, 147–150	182.17	3				17.40	98.00		17.40	0.18			
757B-21X-5, 145–150	190.15	13	7.28	0.358	39.0	15.70	103.10	598.00	17.90	0.15	1.48	0.90	12.6
757B-24X-4, 140–150	217.60	55	8.35	0.535	39.0	9.10	109.60	593.00	18.40	0.08	29.00	1.02	13.7
757B-27X-5, 140–150	248.10	20	8.40	0.530	39.8	0.00	124.90	594.00	15.40	0.00	40.40	1.06	14.9
757B-30X-2, 140–150	272.60	17	8.20	0.500	40.0	0.00	131.60	598.00	14.60	0.00	25.70	1.05	15.9
757B-35X-CC, 0–1	322.23	5			40.5	0.00	149.30	604.00	14.10	0.00			
757B-37X-2, 140–150	340.20	11	8.00	0.650	40.2	0.00	150.70	598.00	14.40	0.00	27.60	1.31	18.6
757C-7R-1, 67–70	363.57	4			39.0	0.00	134.50	549.00	12.40	0.00			
757B-40X-1, 0–1	366.30	1					151.80						

[a] Contaminated with surface seawater.
[b] IAP = ion activity product; KSP = solubility product.
[c] Temperature = 5 + 4(depth/100).

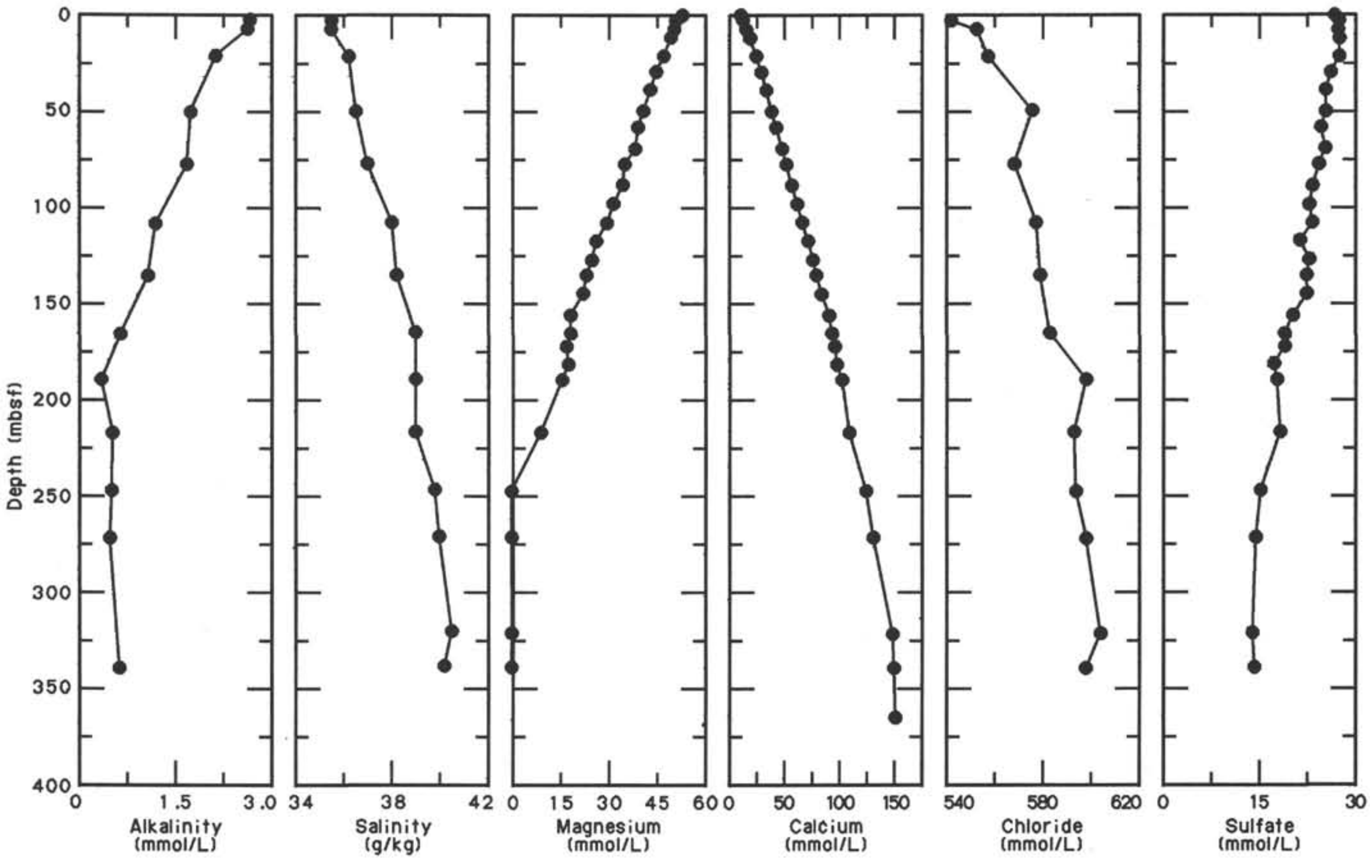

Figure 36. Interstitial-water profiles, Site 757.

Table 14. XRD patterns, Hole 757B.

Core, section, interval (cm)	Shipboard data-base file number	Minerals identified
24X-4, 145–150	175UBN.RD	Montmorillonite, unknowns (treated with 1 N HCl)
27X-5, 140–150	174UBN.RD 197UBG.RD	Chlorite/smectite (treated with 1 N HCl)
28X-2, 4–6	168UBN.RD	Chlorite/smectite, calcite
30X-2, 140–150	172UBN.RD	Chlorite/smectite, feldspar (treated with 1 N HCl)
37X-2, 140–150	183UBN.RD	Chlorite/smectite, feldspar (treated with 1 N HCl)

unit IB at 170 mbsf, based on sediment induration, is somewhat apparent in the shear-strength profile. However, evidence for bonding and strength is much clearer below 195 mbsf from these tests.

Formation Factor

Formation factor values measured in the upper 210 m of Hole 757B (Table 21 and Fig. 41) vary from 1.45 to near 2.85. The upper 70-m interval exhibits no systematic trend downhole, but instead varies around a mean value of 1.66. A peak at 50 mbsf matches the peak index-property values discussed previously. Below 70 mbsf, formation factor increases steadily with increasing depth, from 1.57 to 2.84 at approximately 180 mbsf. Values below 180 mbsf are more erratic, probably in response to the ash at the base of lithologic Unit I and the top of Unit II. Within the interval from 70 to 210 mbsf, the formation factor can be expressed as a function of depth by the following relationship:

$$\text{F factor} = 1.20 + (0.00675 \times \text{depth})$$

and

$$r = 0.844,$$

where depth is meters below seafloor and r is the regression coefficient.

Thermal Conductivity

Thermal conductivities are reported in Table 22 and displayed in Figure 42. Thermal conductivities in unit A range from 1.18 to 2.12 W/m°C and generally increase with increasing depth at a rate of 0.3 W/m°C per 100 m. The high conductivity at 50 mbsf corresponds to a higher density layer at this interval.

Thermal-conductivity values from 197 to 245 mbsf display the transitional nature observed in index properties across the same interval. Thermal-conductivity values drop to near 1 W/m°C over this 50-m-thick interval. Below 245 mbsf, thermal-conductivity values range from 1.07 to 1.46 W/m°C, with a mean of 1.28 W/m°C; all of these values are considerably lower than those of the overlying calcareous section. The ash unit overlying the basement basalts clearly results in a thermal impedance to heat flow through this part of the seafloor.

Discussion

Three physical-properties units are recognized for the samples recovered at Site 757.

Table 15. Percentages of total carbon, inorganic carbon, organic carbon, and calcium carbonate in samples from Holes 757B and 757C.

Core, section, interval (cm)	Depth (mbsf)	Total carbon (%)	Inorganic carbon (%)	Organic carbon (%)	Calcium carbonate (%)
121-757B-					
2H-2, 90-92	6.90	11.40	11.22	0.18	93.5
2H-4, 90-92	9.90	11.40	11.40	0.00	95.0
2H-6, 92-94	12.92		11.33		94.4
3H-2, 92-94	16.42	11.51	11.55	0.00	96.2
3H-4, 92-94	19.42	11.42	11.34	0.08	94.5
3H-6, 92-94	22.42		11.38		94.8
4H-2, 95-97	26.05		11.48		95.6
4H-4, 95-97	29.05	11.53	11.56	0.00	96.3
5H-2, 95-97	35.65		11.49		95.7
5H-4, 95-97	38.65	11.47	11.51	0.00	95.9
6H-1, 78-80	43.58		11.56		96.3
6H-3, 95-97	46.75		11.39		94.9
6H-5, 95-97	49.75		11.59		96.5
7H-2, 95-97	54.95		11.65		97.0
7H-4, 95-97	57.95	11.50	11.53	0.00	96.0
8H-2, 90-92	64.60		11.60		96.6
8H-4, 90-92	67.60	11.55	11.56	0.00	96.3
8H-6, 90-92	70.60		11.57		96.4
9H-2, 92-94	74.22		11.54		96.1
9H-4, 92-94	77.22	11.50	11.57	0.00	96.4
9H-6, 92-94	80.22		11.66		97.1
10H-2, 92-94	83.92		11.48		95.6
10H-4, 92-94	86.92	11.55	11.32	0.23	94.3
11H-2, 92-94	93.62		11.51		95.9
11H-4, 92-94	96.62	11.55	11.49	0.06	95.7
11H-6, 92-94	99.62		11.33		94.4
12H-2, 92-94	103.22		11.48		95.6
12H-4, 92-94	106.22	11.41	11.36	0.05	94.6
13H-2, 92-94	112.92		11.58		96.5
13H-4, 92-94	115.92	11.48	11.45	0.03	95.4
13H-6, 92-94	118.92		11.57		96.4
14H-2, 92-94	122.52		11.22		93.5
14H-4, 92-94	125.52	11.40	11.55	0.00	96.2
14H-6, 92-94	128.52		11.38		94.8
15H-2, 92-94	132.22		11.54		96.1
15H-5, 92-94	136.72	11.40	11.33	0.07	94.4
15H-6, 92-94	138.22		11.49		95.7
16H-3, 137-139	143.87		11.48		95.6
16H-4, 92-94	144.92	11.26	11.20	0.06	93.3
17H-2, 95-97	151.55		11.24		93.6
17H-4, 95-97	154.55	11.37	11.29	0.08	94.1
17H-6, 95-97	157.55		11.28		94.0
18H-2, 95-97	161.25		11.33		94.4
18H-4, 95-97	164.25	11.38	11.40	0.00	95.0
18H-6, 95-97	167.25		11.64		97.0
19H-2, 95-97	170.95		11.37		94.7
19H-4, 95-97	173.95	11.42	11.47	0.00	95.6
20X-2, 95-97	177.15		11.41		95.1
20X-4, 95-97	180.15	11.44	11.44	0.00	95.3
20X-6, 95-97	183.15		11.48		95.6
21X-2, 94-96	185.14		11.48		95.6
21X-4, 95-97	188.15	11.43	11.56	0.00	96.3
21X-6, 95-97	191.15		11.63		96.9
22X-2, 95-97	194.85		11.47		95.6
22X-4, 95-97	197.85	11.37	11.50	0.00	95.8
23X-2, 95-97	204.45		11.37		94.7
23X-4, 95-97	207.45	10.84	10.74	0.10	89.5
24X-1, 88-90	212.58	4.93	5.11	0.00	42.6
24X-2, 88-90	214.08		3.93		32.7
24X-3, 36-39	215.06		4.32		36.0
24X-3, 88-90	215.58	4.12	3.96	0.16	33.0
24X-4, 88-90	217.08		0.82		6.8
24X-5, 83-86	218.53		0.12		1.0
24X-5, 88-90	218.58		0.06		0.5
25X-2, 103-105	223.93	1.75	1.30	0.45	10.8
25X-4, 86-88	226.76		0.11		0.9
26X-1, 90-93	231.90		0.08		0.7
26X-1, 116-118	232.16		0.40		3.3
27X-2, 128-130	243.48		0.10		0.8
27X-4, 66-68	245.86		0.19		1.6
27X-4, 72-75	245.92		0.15		1.3
27X-6, 95-97	249.15		0.11		0.9
28X-3, 82-84	254.22		0.16		1.3
121-757B- (Cont.)					
28X-4, 88-90	255.78	1.14	1.19	0.00	9.9
29X-1, 138-139	261.38		3.47		28.9
29X-3, 53-54	263.53		0.87		7.3
29X-4, 37-38	264.87		1.13		9.4
30X-1, 41-42	270.11	1.88	1.79	0.09	14.9
30X-2, 113-114	272.33		0.12		1.0
30X-2, 140-150	272.60	0.44	0.35	0.09	2.9
30X-3, 104-108	273.74		0.28		2.3
31X-1, 67-71	280.07		0.07		0.6
31X-1, 88-90	280.28		0.12		1.0
32X-1, 125-127	290.25		0.06		0.5
32X-2, 46-48	290.96		0.09		0.8
33X-1, 2-4	298.62		0.08		0.7
34X-CC, 8-10	311.28		0.08		0.7
35X-3, 18-20	321.08		0.73		6.1
36X-1, 60-61	328.20		0.24		2.0
36X-2, 40-42	329.50		0.26		2.2
36X-3, 22-24	330.82	0.87	0.80	0.07	6.7
37X-1, 100-102	338.30		0.46		3.8
37X-3, 28-32	340.58		0.09		0.8
37X-3, 55-57	340.85		0.16		1.3
38X-1, 92-94	347.82		0.12		1.0
39X-2, 44-46	358.54		0.08		0.7
40X-1, 34-36	366.64		0.06		0.5
121-757C-					
7R-1, 33-34	363.23	1.58	1.47	0.11	12.3
7R-1, 98-100	363.88		0.09		0.8
7R-CC, 0-1	364.40	0.20	0.15	0.05	1.3
9R-1, 70-74	382.70		0.06		0.5
9R-2, 0-10	383.15		0.03		0.3
9R-3, 50-54	384.61		0.06		0.5
9R-7, 106-110	389.78		0.09		0.8
10R-1, 106-109	392.76		0.29		2.4
10R-3, 107-110	395.77		0.88		7.3
11R-2, 116-120	404.01		0.04		0.3
12R-1, 45-48	411.55		0.02		0.2
12R-1, 104-110	412.14		0.03		0.3
12R-2, 22-25	412.67		0.04		0.3
12R-3, 0-4	413.62		0.55		4.6

Physical-properties unit A corresponds to lithologic Unit I, in which the calcareous sediments exhibit a generally consolidating aspect of increasing bulk density and decreasing porosity. Throughout this section, grain size steadily decreases (see "Lithostratigraphy and Sedimentology" section) and may be responsible in part for the relative downhole changes described. Formation factor and thermal conductivity generally corroborate this compaction trend, although vane shear strength remains extremely low relative to typical values of most oceanic sediments. The upper 40 m of the section is described as having a larger foraminifer component than the remaining section. Thermal conductivity and formation factor within the same interval are fairly constant and low, only developing a positive downhole gradient below 50 mbsf. An interval at 48-60 mbsf has a higher density, formation factor, and thermal conductivity than the surrounding material. This particular horizon exhibits well-developed laminated structures, as opposed to the homogeneous, bioturbated adjacent lithologies. However, the other laminated parts of lithologic Unit I do not follow this behavior. Conversely, a high-density layer at 140 mbsf does not correspond to any evident lithologic change. The high density of the layers at 48-60 and 140 mbsf is weakly correlated with finer sediment texture and may represent subtle compositional changes and/or short periods of nondeposition to erosion.

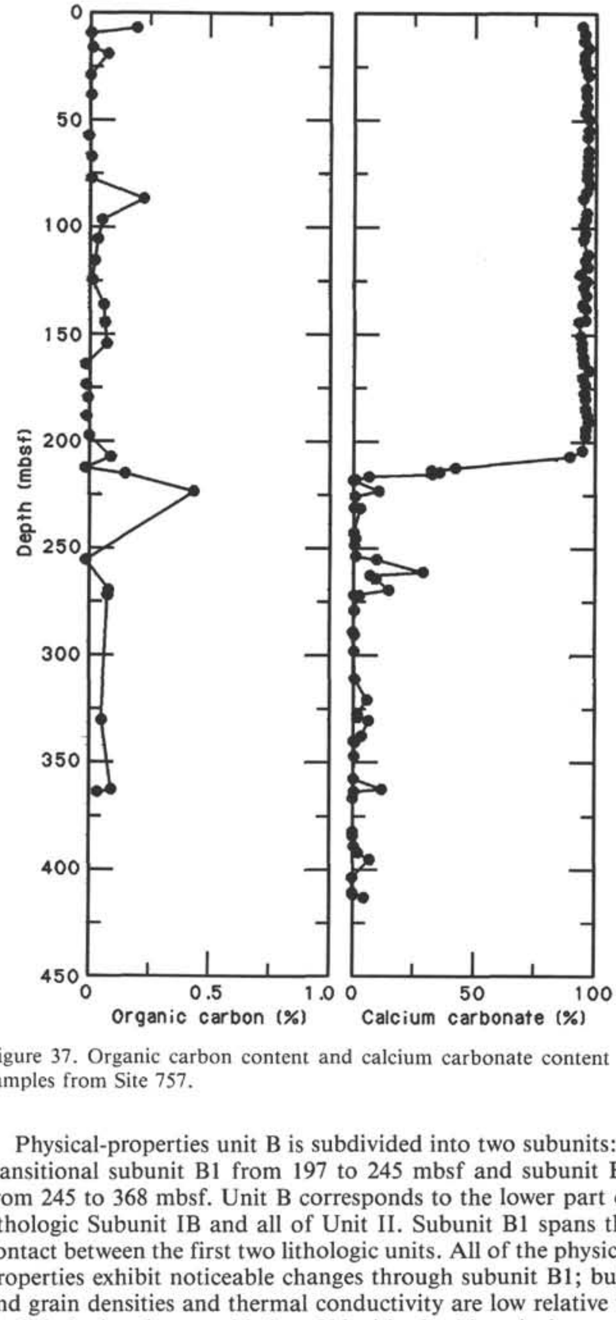

Figure 37. Organic carbon content and calcium carbonate content in samples from Site 757.

Physical-properties unit B is subdivided into two subunits: a transitional subunit B1 from 197 to 245 mbsf and subunit B2 from 245 to 368 mbsf. Unit B corresponds to the lower part of lithologic Subunit IB and all of Unit II. Subunit B1 spans the contact between the first two lithologic units. All of the physical properties exhibit noticeable changes through subunit B1; bulk and grain densities and thermal conductivity are low relative to the lithologies above and below. Velocities in this unit, however, are higher relative to the overlying carbonates. These characteristics suggest that the lapilli and tuffs retain a fairly porous, open network, but form a grain-to-grain structure with more structural integrity that leads to a greater bulk modulus and, hence, higher velocities. Vane-shear-strength results from the upper part of unit B also indicate a developed structural integrity. Low values of thermal conductivity in these tuffs result in a thermal impedance to heat flow, which may correlate with a zeolite alteration facies in the Site 757 basalts that was not found in Site 756 basalts (see "Igneous Petrology" section).

Physical-properties unit C corresponds to the basement basalts of lithologic Unit III. Hole 757B cored through a flow into interflow volcaniclastics, where the measured physical properties are similar to those recorded for the base of the overlying volcanics of Unit II. The basalts cored in Hole 757C contain very little interflow volcaniclastic material. Some well-recovered flow contacts may indicate that this lack of interflow material is not strictly a drilling artifact and instead may simply reflect short periods of time between flow emplacements. The basalts at Site 757 have velocities and densities similar to those cored at Site 756, except the former do not reach the peak velocities (i.e., 6 km/s) and densities of the more massive flows from Site 756. These physical differences probably reflect the more altered character and higher vesicularity of the Hole 757B basalts relative to those from Hole 756D (see "Igneous Petrology" section).

SEISMIC STRATIGRAPHY

General Setting

Site 757 is on the central part of Ninetyeast Ridge, on the eastern side of the crest of the ridge. The RC2707 site area survey in July 1986 was performed within a quadrangle bordered approximately by the coordinates 16°54′–17°12′S and 88°00′–88°18′E.

The bathymetry near Site 757 is dominated by the crest of the ridge (Fig. 43). The ridge crest is a comparatively flat hill rising to a water depth of about 1650 m. The maximum observed water depth does not exceed approximately 1800 m within the aforementioned region.

Site Survey

The site survey by the *JOIDES Resolution* was performed using a proton precession magnetometer, 3.5-kHz echo-sounder, and two 80-in.[3] water guns as a seismic source for the digital single-channel recording system. The analog records were filtered at two filter settings (65–160 and 40-160 Hz) and plotted at 75 and 50 lines/in., respectively. The analog record with the 60–160-Hz filter settings seems to be of better quality and was thus used for interpretation. The seismic profiles crossing Site 757 (Fig. 43) shown in Figures 44 (dip line) and 45 (strike line) are reprocessed *JOIDES Resolution* data (see backpocket foldout for entire pre-site seismic survey).

The approach site survey by *JOIDES Resolution* was planned to have dip lines oriented perpendicularly to the structural grain inferred from the RC2707 site survey. However, there was considerable uncertainty in this interpretation because the original survey grid was too coarse to correlate faults unambiguously from line to line. The ambiguity arose because the faulting is complex and variable. Furthermore, mis-ties between seismic sections at line intersections indicated that some lines had navigation errors of more than 1 km. In particular, the position of the proposed site location was estimated to be about 0.5 to 1 km

Table 16. Results of Rock-Eval pyrolysis of samples from Hole 757B.

Core, section, interval (cm)	Depth (mbsf)	Weight (mg)	T_{max} (°C)	S1 (mg HC/g rock)	S2 (mg HC/g rock)	S3 (mg CO_2/g rock)	Productivity index	S2/S3	Pyrolysized carbon (0.083[S1 + S2])	Total organic carbon (wt%)	Hydrogen index (mg HC/g C_{org})	Oxygen index (mg CO_2/g C_{org})
10H-4, 92–94	86.92	106.4	448	0.04	0.01	0.31	1.0	0.03	0.0	0.23	4	134
23X-4, 95–97	207.45	110.9	273	0.09	0.13	0.46	0.41	0.28	0.01	0.10	130	460
25X-2, 103–105	223.93	107.1	354	0.10	0.18	1.02	0.36	0.17	0.02	0.45	40	226

Table 17. Index properties of sediments from Site 757.

Sample (interval in cm)	Depth (mbsf)	Water content (%)	Porosity (%)	Density (g/cm³) wet bulk	dry bulk	grain
757B-2H-2, 90	6.90	48.92	71.65	1.53	0.78	2.67
757B-2H-4, 90	9.90	43.00	67.10	1.61	0.92	2.73
757B-2H-6, 90	12.90	44.00	68.14	1.59	0.89	2.75
757B-3H-2, 92	16.42	42.52	66.11	1.59	0.91	2.67
757B-3H-4, 92	19.42	40.95	65.25	1.64	0.97	2.74
757B-3H-6, 92	22.42	43.10	66.28	1.62	0.92	2.62
757B-4H-2, 95	26.05	42.05	65.57	1.64	0.95	2.65
757B-4H-4, 95	29.05	40.43	64.63	1.70	1.01	2.73
757B-5H-2, 95	35.65	38.85	63.30	1.72	1.05	2.75
757B-5H-4, 95	38.65	39.13	63.27	1.69	1.03	2.71
757B-6H-1, 78	43.58	39.61	63.86	1.69	1.02	2.73
757B-6H-3, 95	46.75	36.21	60.21	1.71	1.09	2.70
757B-6H-5, 95	49.75	31.09	54.99	1.83	1.26	2.75
757B-7H-2, 95	54.95	34.67	59.18	1.79	1.17	2.77
757B-7H-4, 95	57.95	31.82	56.20	1.83	1.25	2.79
757B-8H-2, 90	64.60	38.28	62.08	1.68	1.04	2.67
757B-8H-4, 90	67.60	36.73	61.17	1.69	1.07	2.75
757B-8H-6, 92	70.62	33.51	57.93	1.78	1.18	2.77
757B-9H-2, 92	74.22	34.52	58.96	1.77	1.16	2.76
757B-9H-4, 92	77.22	35.73	59.60	1.72	1.10	2.69
757B-9H-6, 92	80.22	28.71	51.83	1.86	1.32	2.71
757B-10H-2, 92	83.92	32.72	55.98	1.76	1.18	2.65
757B-10H-4, 92	86.92	29.75	53.50	1.84	1.30	2.75
757B-11H-2, 92	93.62	35.74	59.39	1.72	1.10	2.66
757B-11H-4, 92	96.62	30.34	54.51	1.83	1.28	2.79
757B-11H-6, 92	99.62	32.98	56.94	1.78	1.19	2.72
757B-12H-2, 92	103.22	28.86	51.64	1.86	1.33	2.67
757B-12H-4, 92	106.22	33.65	57.96	1.77	1.17	2.75
757B-13H-2, 92	112.92	30.07	53.33	1.84	1.28	2.69
757B-13H-4, 92	115.92	27.28	50.14	1.90	1.38	2.72
757B-13H-6, 92	118.92	28.31	50.85	1.86	1.33	2.66
757B-14H-2, 92	122.52	26.45	48.80	1.90	1.40	2.69
757B-14H-4, 92	125.52	28.03	51.50	1.91	1.37	2.77
757B-14H-6, 92	128.52	27.50	50.48	1.89	1.37	2.73
757B-15H-2, 92	132.22	27.14	49.97	1.90	1.38	2.72
757B-15H-5, 92	136.72	26.96	49.63	1.89	1.38	2.71
757B-15H-6, 92	138.22	18.05	37.44	2.11	1.73	2.76
757B-16H-3, 137	143.87	24.34	46.51	1.97	1.49	2.74
757B-16H-4, 92	144.92	26.46	49.31	1.91	1.40	2.74
757B-17H-2, 95	151.55	25.97	48.34	1.94	1.43	2.71
757B-17H-4, 95	154.55	24.26	46.37	1.97	1.40	2.70
757B-17H-6, 95	157.55	24.77	46.97	1.95	1.47	2.73
757B-18H-2, 95	161.25	21.78	42.49	2.04	1.60	2.69
757B-18H-4, 95	164.25	21.25	41.90	2.07	1.63	2.71
757B-18H-6, 95	167.25	18.61	37.71	2.09	1.70	2.69
757B-19H-2, 95	710.95	22.02	42.99	2.03	1.58	2.71
757B-19H-4, 95	173.95	21.66	42.56	2.04	1.60	2.72
757B-20X-2, 95	177.15	20.88	41.42	2.09	1.65	2.72
757B-20X-4, 95	180.15	19.57	39.50	2.08	1.68	2.72
757B-20X-6, 95	183.15	20.20	40.35	2.09	1.67	2.71
757B-21X-2, 94	185.14	19.68	39.19	2.12	1.70	2.67
757B-21X-4, 95	188.15	20.55	38.24	2.06	1.64	2.43
757B-21X-6, 95	191.15	21.79	42.18	2.03	1.59	2.66
757B-22X-2, 95	194.85	18.55	38.03	2.14	1.74	2.73
757B-22X-4, 95	197.85	23.80	45.60	2.00	1.50	2.70
757B-23X-2, 95	204.45	23.15	44.54	2.02	1.55	2.71
757B-23X-4, 95	207.45	27.72	50.24	1.93	1.39	2.67
757B-24X-1, 88	212.58	31.94	56.22	1.84	1.25	2.77
757B-24X-2, 88	214.08	37.91	62.41	1.73	1.08	2.75
757B-24X-3, 88	215.58	33.55	56.88	1.78	1.19	2.65
757B-24X-4, 88	217.08	38.50	63.03	1.76	1.08	2.76
757B-24X-5, 88	218.58	29.77	53.23	1.95	1.37	2.72
757B-25X-2, 103	223.93	38.82	61.35	1.69	1.04	2.53
757B-25X-4, 86	226.76	26.22	48.47	2.01	1.49	2.69
757B-26X-1, 116	232.16	28.61	50.41	1.92	1.37	2.57
757B-27X-2, 128	243.48	13.20	27.61	1.59	1.38	2.55
757B-27X-4, 66	245.86	27.64	48.60	1.90	1.37	2.50
757B-27X-6, 95	249.15	26.33	47.62	1.95	1.44	2.58
757B-28X-3, 82	254.22	25.61	46.29	1.96	1.45	2.54
757B-28X-4, 88	255.78	25.22	46.37	1.96	1.47	2.60
757B-29X-3, 52	263.52	23.38	42.54	2.01	1.54	2.46
757B-29X-4, 37	264.87	20.68	40.80	2.18	1.73	2.68
757B-30X-1, 42	270.12	19.93	38.46	2.11	1.69	2.55
757B-30X-2, 112	272.32	25.93	46.85	1.97	1.46	2.55
757B-31X-1, 88	280.28	28.23	50.09	1.96	1.40	2.59
757B-32X-2, 46	290.96	26.86	48.33	2.01	1.47	2.58
757B-33X-1, 2	298.62	32.76	57.38	1.95	1.31	2.80
757B-34X-CC, 8	311.28	30.68	51.76	1.86	1.29	2.46

Table 17 (continued).

Sample (interval in cm)	Depth (mbsf)	Water content (%)	Porosity (%)	Density (g/cm³) wet bulk	dry bulk	grain
757B-35X-3, 18	321.08	33.89	56.36	1.81	1.20	2.55
757B-36X-1, 60	328.20	32.50	53.98	1.81	1.22	2.47
757B-36X-3, 22	330.82	29.96	51.09	1.91	1.34	2.47
757B-37X-1, 100	338.30	28.79	49.88	1.91	1.36	2.50
757B-37X-3, 55	340.85	25.63	47.36	2.02	1.50	2.65
757B-38X-1, 92	347.82	26.68	49.46	2.03	1.49	2.73
757B-39X-2, 44	358.54	27.62	49.70	2.00	1.45	2.63
757C-7R-1, 33	363.23	16.28	33.48	2.20	1.84	2.63
757C-7R-1, 98	363.88	37.20	61.71	1.76	1.10	2.75
757B-40X-1, 34	366.64	28.96	51.32	1.93	1.37	2.62
757B-41X-1, 87	370.17	2.67	7.82	2.99	2.91	3.15
757B-42N-1, 28	370.58	3.55	10.09	2.89	2.79	3.10
757C-8R-2, 89	374.79	2.85	6.57	2.54	2.47	2.44
757C-9R-2, 92	384.07	1.90	4.70	2.60	2.60	2.60
757C-9R-4, 86	386.30	2.86	6.47	2.48	2.41	2.39
757C-9R-6, 66	388.26	1.65	3.91	2.54	2.50	2.47
757C-9R-8, 71	390.81	1.31	3.29	2.67	2.63	2.61
757C-10R-2, 70	393.90	5.57	11.15	2.32	2.19	2.16
757C-10R-3, 7	394.77	5.67	12.68	2.37	2.24	2.46
757C-11R-3, 115	405.40	3.40	8.20	2.52	2.44	2.58
757C-12R-1, 2	411.12	2.31	5.92	2.66	2.60	2.71
757C-12R-3, 108	414.70	2.84	6.86	2.54	2.47	2.56

north of its plotted position (Fig. 43) when navigation errors were minimized.

During the seismic survey, fault correlation between the first three strike lines was completed, and the primary direction of faulting is now interpreted as N21°E. The site location was revised to be in the same relative structural position as the original prospectus location in accordance with Pollution Prevention and Safety Panel instructions. The strike line of the approach survey was also moved to cross this new location in a direction parallel to the new interpretation of the structural grain (Figs. 43 and 45).

Correlation between Seismic Stratigraphy and Lithostratigraphy

Lithostratigraphy

The lithologic sequence is divided into three units. Unit I (0 to 211.7 mbsf) is lower Eocene to Pleistocene ooze, Unit II (211.7 to 367.0 mbsf) is upper Paleocene to lower Eocene water-lain ash and tuff, and Unit III (367.0 to 420.7 mbsf) is basalt. These units are further divided into subunits as follows: Subunit IA (0 to 168.5 mbsf) consists of nannofossil ooze with foraminifers; Subunit IB (168.5 to 211.7 mbsf) is a calcareous ooze with chalk and ash; Subunit IIA (211.7 to 250.4 mbsf) is ash with lapilli, foraminifers, glauconite, and pebbles; and Subunit IIB (250.4 to 367.0 mbsf) is tuff with lapilli, pebbles, and shells (see "Lithostratigraphy and Sedimentology" section). The lithology predicted for this location based on a seismic stratigraphic evaluation of the RC2707 site survey (Newman and Sclater, 1988) agrees closely with the cored section.

Reflectors

Ten reflectors, numbered 1 through 10 in Figures 44 through 46, were used to interpret the stratigraphy of this site. Water bottom is reflector 1, which is followed by two sea-surface reflections of the outgoing pulse of the water gun. The distance to the seafloor reflector is 1652 m (uncorrected), the same depth as calculated from the length of the drill pipe. Dip and strike line reflector two-way traveltimes (TWT) are shown in Table 23. Most of the reflectors have associated water gun sea-surface "ghosts."

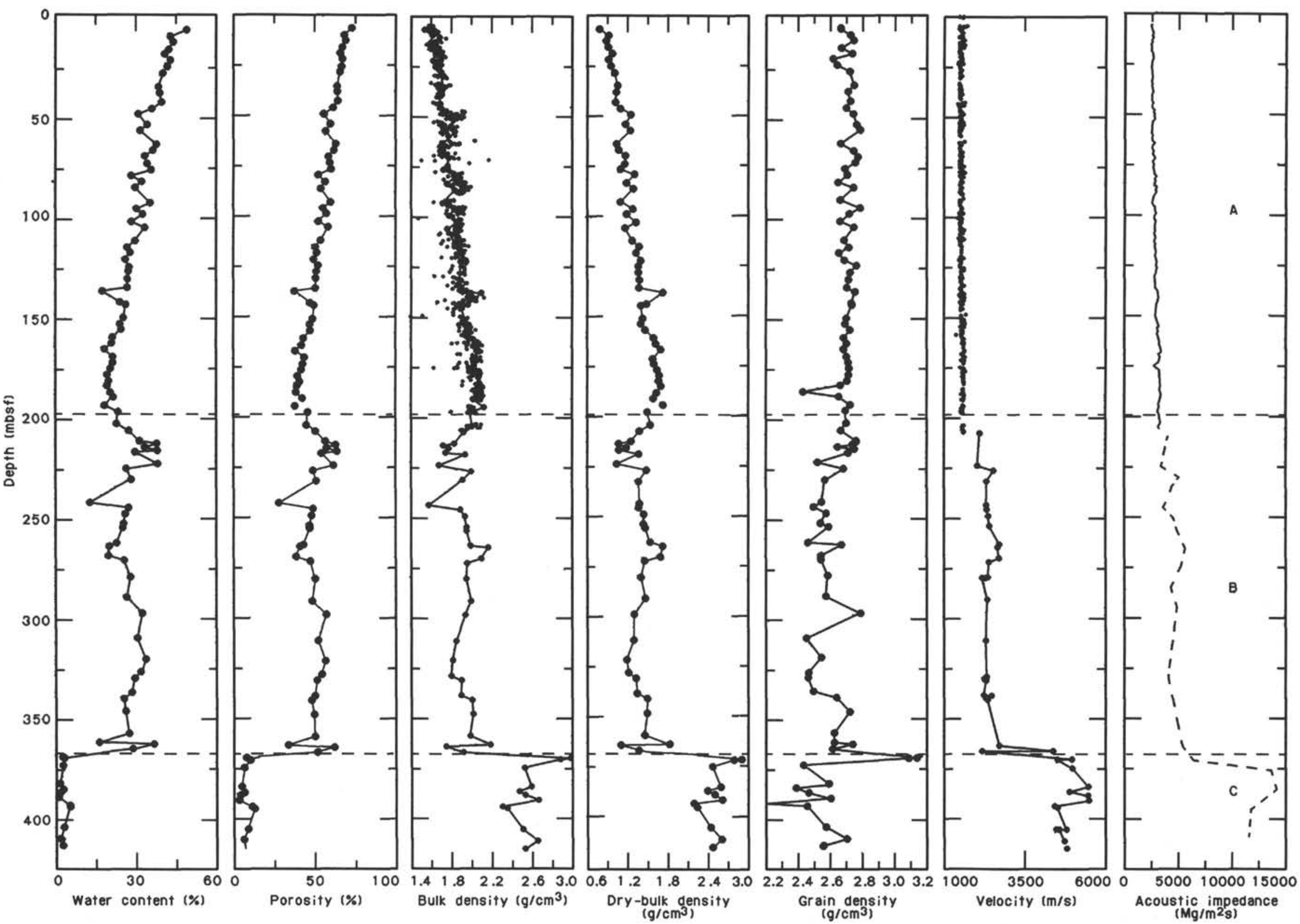

Figure 38. Water content, porosity, bulk density, dry-bulk density, grain density, compressional-wave velocity, and acoustic impedance profiles of sediments and basement from Site 757. *A*, *B*, and *C* refer to physical-properties units, defined by dashed lines.

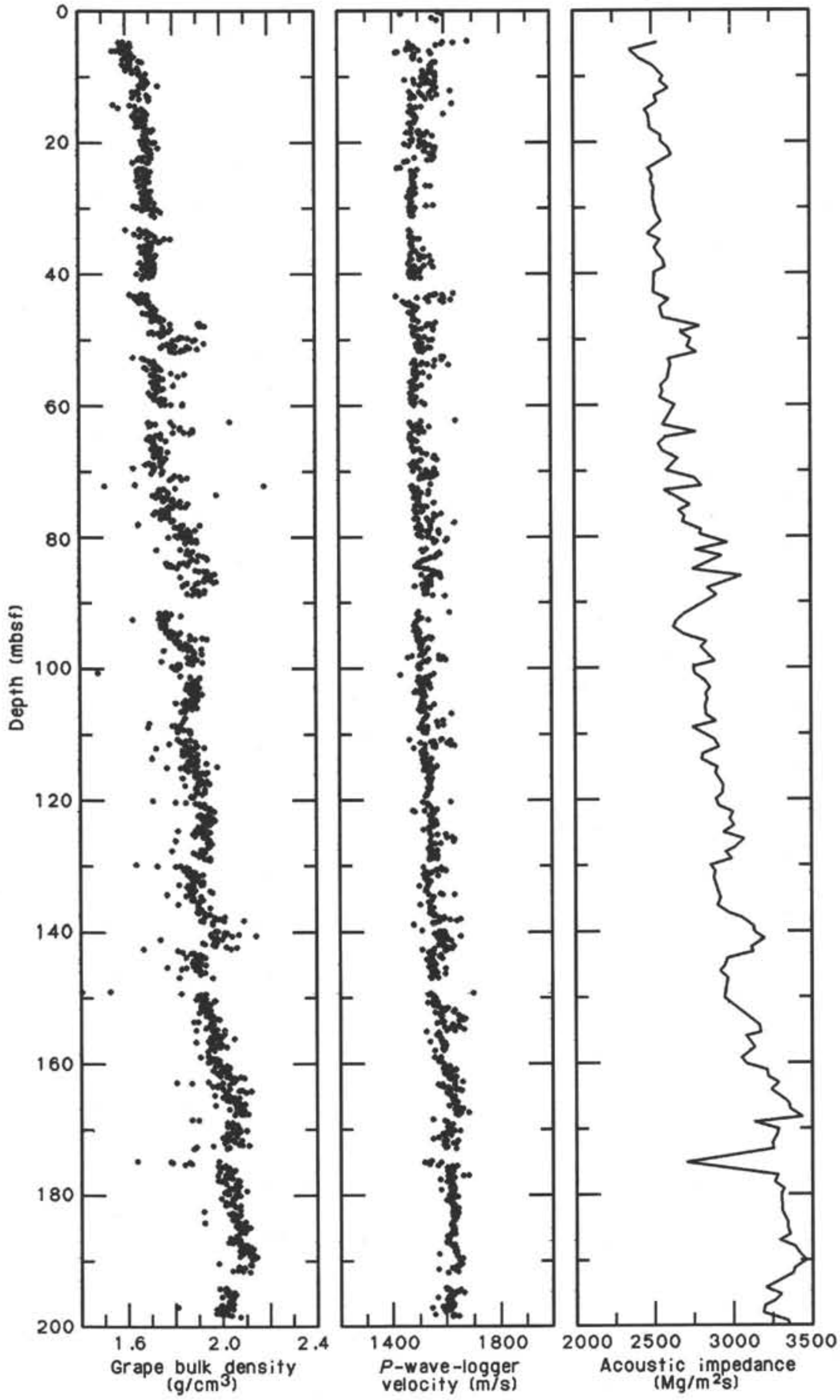

Figure 39. GRAPE densities and *P*-wave-logger velocities from physical-properties unit A, Site 757.

Velocities

Velocities measured aboard ship with the *P*-wave logger and on a Hamilton Frame velocimeter (see "Physical Properties" section) range from about 1500 to about 1600 m/s in the soft sediments (ooze), from 2000 to 2800 m/s for tuffs, and from 4500 to 5500 m/s for basalts. The velocity model used for reflector depth calculations is shown in Table 24.

Acoustic Impedance

Acoustic impedance was calculated throughout the section (see "Physical Properties" section). The impedance ranges from 2300 to 2500 Mg/m^2s between 0 and 207 mbsf, increases to a range between 3500 and 6000 Mg/m^2s between 210 and 367 mbsf, and increases again to a range from 11,700 to over 14,000 Mg/m^2s between 373 and 420 mbsf, the total depth of the hole.

Table 18. Compressional-wave velocity of sediments from Site 757.

Sample (interval in cm)	Depth (mbsf)	Direction[a]	Compressional-wave velocity (m/s)
757B-23X-2, 140	204.90	C	1702.4
757B-23X-5, 8	208.08	A	2140.0
757B-23X-5, 32	208.32	C	1964.2
757B-25X-2, 103	223.93	B	2080.4
757B-25X-2, 103	223.93	A	2086.4
757B-25X-2, 103	223.93	C	2082.8
757B-25X-4, 86	226.76	C	2636.7
757B-25X-4, 86	226.76	A	2569.7
757B-25X-4, 86	226.76	B	2610.6
757B-26X-1, 116	232.16	A	2360.7
757B-26X-1, 116	232.16	C	2382.8
757B-26X-1, 116	232.16	B	2391.6
757B-27X-2, 128	243.48	B	2367.2
757B-27X-2, 128	243.48	C	2402.5
757B-27X-2, 128	243.48	A	2334.1
757B-27X-4, 66	245.86	B	2433.2
757B-27X-4, 66	245.86	C	2398.9
757B-27X-4, 66	245.86	A	2357.0
757B-27X-6, 95	249.15	B	2417.4
757B-27X-6, 95	249.15	C	2398.9
757B-27X-6, 95	249.15	A	2402.9
757B-28X-3, 82	254.22	C	2404.8
757B-28X-3, 82	254.22	B	2461.3
757B-28X-3, 82	254.22	A	2447.9
757B-29X-3, 52	263.52	A	2746.2
757B-29X-3, 52	263.52	B	2773.1
757B-29X-3, 52	263.52	C	2771.2
757B-29X-4, 37	264.87	C	2698.1
757B-29X-4, 37	264.87	B	2758.6
757B-29X-4, 37	264.87	A	2702.5
757B-30X-1, 42	270.12	A	2742.1
757B-30X-1, 42	270.12	B	2838.6
757B-30X-1, 42	270.12	C	2818.4
757B-30X-2, 112	272.32	C	2446.1
757B-30X-2, 112	272.32	A	2440.1
757B-30X-2, 112	272.32	B	2480.5
757B-31X-1, 39	279.79	A	2391.8
757B-31X-1, 81	280.21	A	2330.5
757B-31X-1, 91	280.31	B	2287.7
757B-31X-1, 91	280.31	A	2226.8
757B-31X-1, 91	280.31	C	2283.5
757B-32X-2, 47	290.97	A	2396.0
757B-34X-CC, 8	311.28	B	2372.8
757B-34X-CC, 8	311.28	A	2349.6
757B-34X-CC, 8	311.28	C	2383.1
757B-36X-1, 144	329.04	A	2366.0
757B-36X-2, 75	329.85	A	2306.6
757B-36X-2, 126	330.36	A	2320.0
757B-36X-3, 22	330.82	A	2369.1
757B-36X-3, 22	330.82	B	2362.1
757B-36X-3, 22	330.82	C	2371.4
757B-37X-1, 102	338.32	A	2298.1
757B-37X-1, 119	338.49	A	2528.0
757B-37X-2, 98	339.78	A	2361.1
757B-37X-3, 51	340.81	A	2406.5
757C-7R-1, 47	363.37	A	2777.3
757C-7R-1, 47	363.37	C	2816.4
757C-7R-1, 47	363.37	B	2872.3
757B-40X-1, 7	366.37	A	4410.6
757B-40X-1, 33	366.63	A	2228.9
757B-41X-1, 87	370.17	C	4931.5
757B-41X-1, 87	370.17	A	4983.8
757B-41X-1, 87	370.17	B	5377.2
757B-42N-1, 28	370.58	A	4557.0
757B-42N-1, 28	370.58	C	4589.5
757B-42N-1, 28	370.58	B	4878.9
757C-8R-2, 89	374.79	C	4891.4
757C-8R-2, 89	374.79	B	4949.5
757C-8R-2, 89	374.79	A	4997.7
757C-9R-2, 92	384.07	A	5477.2
757C-9R-2, 92	384.07	B	5482.2
757C-9R-2, 92	384.07	C	5591.7
757C-9R-4, 86	386.30	C	5020.9
757C-9R-4, 86	386.30	B	4895.9
757C-9R-4, 86	386.30	A	4920.1

Table 18 (continued).

Sample (interval in cm)	Depth (mbsf)	Direction[a]	Compressional-wave velocity (m/s)
757C-9R-6, 66	388.26	C	5559.0
757C-9R-6, 66	388.26	A	5478.5
757C-9R-6, 66	388.26	B	5385.6
757C-9R-8, 71	390.81	C	5439.7
757C-9R-8, 71	390.81	A	5493.6
757C-9R-8, 71	390.81	B	5517.9
757C-10R-2, 70	393.90	C	4579.1
757C-10R-2, 70	393.90	B	4375.3
757C-10R-2, 70	393.90	A	4460.6
757C-10R-3, 7	394.77	B	4651.0
757C-10R-3, 7	394.77	C	4254.4
757C-10R-3, 7	394.77	A	4554.9
757C-11R-3, 115	405.40	C	4814.2
757C-11R-3, 115	405.40	A	4494.6
757C-11R-3, 115	405.40	B	4592.9
757C-12R-1, 2	411.12	A	4744.8
757C-12R-1, 2	411.12	B	4971.4
757C-12R-1, 2	411.12	C	5117.4
757C-12R-3, 108	414.70	C	5047.8
757C-12R-3, 108	414.70	B	4750.0
757C-12R-3, 108	414.70	A	4817.8

[a] A = vertical propagation; B = propagation perpendicular to the split-core face; C = propagation parallel to the split-core face.

Reflections occur at large impedance vs. depth gradients (Fig. 46).

Grain Size

Grain size varies greatly throughout the sedimentary section. The grain size ranges from approximately 5 to 50 μm. The grain size in phi units (see "Lithostratigraphy and Sedimentology" section) is plotted as a three-value centered running average for the upper 200 m of the section (Fig. 46). Grain-size peak values are at 7, 20, 65, 90, 114, 130, 160, and 185 mbsf. Seismic reflectors correlate with subtle local grain-size minima, except for the reflector at 76 mbsf.

Correlation

Correlation of seismic record reflections with grain size, impedance, and lithology is shown in Figure 46. The velocity structure in Table 24 was used in this correlation. Reflectors based on this velocity structure show good correlation to the lithologic units and grain size and possibly to impedance.

Reflector 2 at 40 mbsf can be correlated with an increase (beginning of a peak in a broader sense) in the impedance profile. This reflector can also be correlated to a low between two plateaus in a thermal-conductivity plot (see "Physical Properties" section) and a low in the grain-size profile. However, this reflector does not coincide with a lithology change. Reflector 3 (76 mbsf) can be correlated with an increase in impedance and an interval of low vane shear strength. There is no correlation between any other physical property or lithology. Reflectors 4 and 5 (122 and 150 mbsf) can be correlated with increases of impedance and grain-size lows.

Reflector 6 (174 mbsf) cannot be correlated with a change in the impedance profile (the low in the profile is an artifact probably caused by measuring a water-saturated sediment in the top of a core section with the GRAPE and *P*-wave logger), but reflector 6 does correlate with a low grain-size value and high values in vane shear strength (see "Physical Properties" section). This reflector correlates with a lithology change from nannofossil ooze with foraminifers (Subunit 1A) to calcareous ooze with

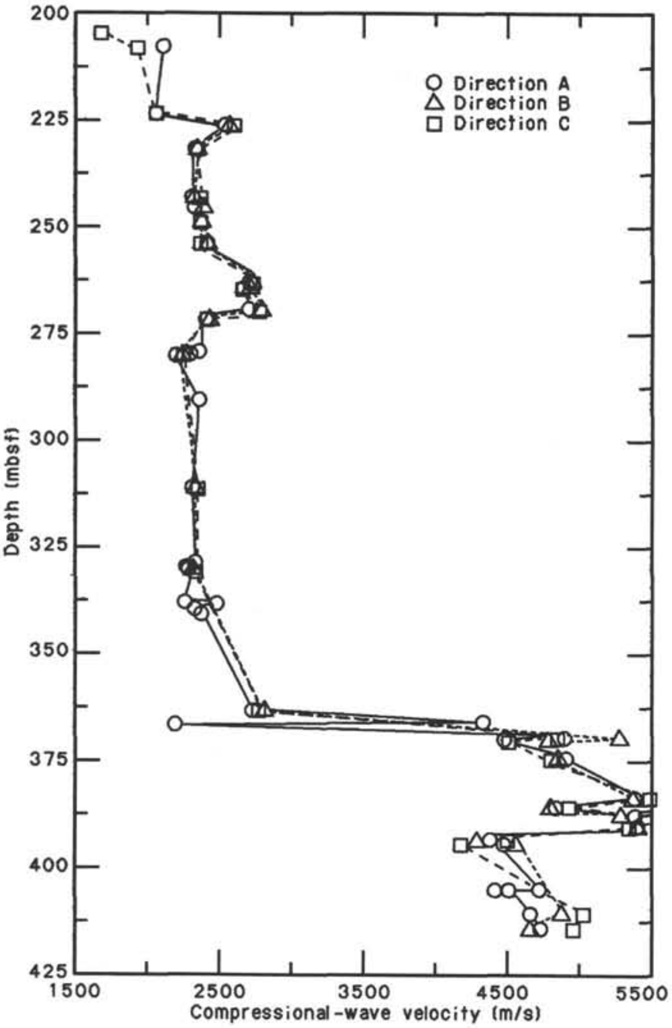

Figure 40. Velocity anisotropy in sediments from lithologic Unit II and the basalts of Unit III, Site 757. The lack of consistently higher horizontal velocities suggests little, if any, anisotropic character to these lithologies.

chalk and ash (Subunit IB) at 168.5 mbsf (see "Lithostratigraphy and Sedimentology" section). The depth difference between the seismic reflector and the lithology change is possibly caused by a gradual change in lithology. Errors in the velocity model and errors in resolving the two-way traveltime to this reflector could account for this observed discrepancy.

Reflector 7 (211 mbsf) correlates with increases in impedance and velocity, a decrease in porosity, and increases in densities. This reflector also correlates with a major lithology change between calcareous ooze (Subunit IB) and ash with lapilli (Subunit IIA). Reflector 8 (251 mbsf) can be correlated with another increasing trend in the impedance curve and with the lithology change from ash with lapilli (Subunit IIA) to tuff with lapilli (Subunit IIB). Reflector 9 (367 mbsf) marks a change between the last sedimentary layer (Subunit IIB) and the first basaltic flows (Unit III). This reflector correlates with major changes in all of the physical properties. Reflector 10 at 2.600 s (390 mbsf) correlates with a decrease in impedance. It can also be correlated with decreases in density and thermal conductivity and with an increase in porosity. This last reflector is the first reflector of a "reverberant layer."

Table 19. Velocity anisotropies calculated for physical-properties units B and C in Holes 757B and 757C.

Sample (interval in cm)	Depth (mbsf)	ANIS1[a] (%)	ANIS2[b] (%)
757B-23X-2, 140	204.90		
757B-23X-5, 8	208.08		
757B-23X-5, 32	208.32		
757B-25X-2, 103	223.93	−0.2	0.1
757B-25X-4, 86	226.76	2.1	1.0
757B-26X-1, 116	232.16	1.1	−0.4
757B-27X-2, 128	243.48	2.2	1.5
757B-27X-4, 66	245.86	2.5	−1.4
757B-27X-6, 95	249.15	0.2	−0.8
757B-28X-3, 82	254.22	−0.6	−2.3
757B-29X-3, 52	263.52	0.9	−0.1
757B-29X-4, 37	264.87	1.0	−2.2
757B-30X-1, 42	270.12	3.2	−0.7
757B-30X-2, 112	272.32	1.0	−1.4
757B-31X-1, 39	279.79		
757B-31X-1, 81	280.21		
757B-31X-1, 91	280.31	2.6	−0.2
757B-32X-2, 47	290.97		
757B-34X-CC, 8	311.28	1.2	0.4
757B-36X-1, 144	329.04		
757B-36X-2, 75	329.85		
757B-36X-2, 126	330.36		
757B-36X-3, 22	330.82	−0.1	0.4
757B-37X-1, 102	338.32		
757B-37X-1, 119	338.49		
757B-37X-2, 98	339.78		
757B-37X-3, 51	340.81		
757C-7R-1, 47	363.37	2.4	−1.9
757B-40X-1, 7	366.37		
757B-40X-1, 33	366.63		
757B-41X-1, 87	370.17	3.4	−8.3
757B-42N-1, 28	370.58	3.9	−5.9
757C-8R-2, 89	374.79	−1.5	−1.2
757C-9R-2, 92	384.07	1.1	2.0
757C-9R-4, 86	386.30	0.8	2.6
757C-9R-6, 66	388.26	−0.1	3.2
757C-9R-8, 71	390.81	−0.3	−1.4
757C-10R-2, 70	393.90	0.4	4.7
757C-10R-3, 7	394.77	−2.2	−8.5
757C-12R-1, 2	411.12	6.3	2.9
Maximum		6.3	4.7
Minimum		−2.2	−8.5
Average		1.3	−0.7
Absolute average		1.7	2.2

[a] ANIS1 = ([Vb + Vc]/2 − Va)/Va or ([Vb or Vc] − Va)/Va.
[b] ANIS2 = (Vc − Vb)/Vb.

Seismic Stratigraphy Interpretation

The basaltic flows drilled at Site 757 dip to the south on the seismic section. The reflections within the flows probably arise from different velocity zones, which are caused by varying degrees of basalt alteration. The tuff sequence above the basalts also dips toward the south. The tuff layers were deposited in shallow water (see "Lithostratigraphy and Sedimentology" section) and are shown in the dip line section onlapping the underlying basalt layers (Fig. 44). The ash deposited onto the tuffs exhibits a complex stratigraphic pattern (Fig. 44). The clinoforms observed within the ash unit dip away from the paleostructural high toward both the southeast and the northwest. Overlying the ash horizons is calcareous ooze with chalk and ash, which is overlain by nannofossil ooze. The calcareous ooze and nannofossil ooze units appear to be deposited in roughly parallel layers; however, onlap relationships are observed away from the site toward the southeast (Figs. 44 and 45; Newman and Sclater, 1988).

Table 20. Vane shear strength of sediments from Hole 757B.

Sample (interval in cm)	Depth (mbsf)	Undrained shear strength (kPa)
757B-2H-2, 90	6.90	0.7
757B-2H-4, 90	9.90	3.3
757B-2H-6, 90	12.90	4.3
757B-3H-2, 92	16.42	5.4
757B-3H-4, 92	19.42	4.1
757B-3H-6, 92	22.42	4.7
757B-4H-2, 95	26.05	8.3
757B-4H-4, 95	92.05	5.5
757B-5H-2, 99	35.69	4.9
757B-5H-4, 100	38.70	5.2
757B-6H-1, 92	43.72	4.2
757B-6H-3, 80	46.60	6.4
757B-6H-5, 95	49.75	4.1
757B-7H-2, 95	54.95	6.1
757B-7H-4, 95	57.95	7.2
757B-8H-2, 90	64.60	4.4
757B-8H-4, 92	67.62	3.2
757B-8H-6, 92	70.62	2.1
757B-9H-2, 92	74.22	3.5
757B-9H-4, 92	77.22	1.7
757B-9H-6, 92	80.22	1.6
757B-10H-2, 92	83.92	3.7
757B-10H-4, 92	86.92	5.3
757B-11H-2, 92	93.62	1.9
757B-11H-2, 92	93.62	4.7
757B-11H-4, 92	96.62	4.7
757B-11H-6, 92	99.62	1.9
757B-12H-2, 92	103.22	10.7
757B-12H-4, 92	106.22	2.8
757B-13H-2, 92	112.92	6.1
757B-13H-4, 92	115.92	7.3
757B-13H-6, 92	118.92	3.3
757B-14H-2, 92	122.52	3.0
757B-14H-4, 92	125.52	1.4
757B-14H-6, 92	128.52	2.0
757B-15H-2, 92	132.22	3.6
757B-15H-5, 92	136.72	2.4
757B-15H-6, 92	138.22	7.3
757B-16H-3, 136	143.86	3.3
757B-16H-4, 92	144.92	5.2
757B-17H-2, 94	151.54	2.4
757B-17H-4, 97	154.57	6.1
757B-17H-6, 102	157.62	14.7
757B-18H-2, 97	161.27	8.5
757B-18H-4, 95	164.25	2.2
757B-18H-6, 95	167.25	1.9
757B-19H-2, 97	170.97	9.0
757B-19H-4, 95	173.95	18.3
757B-20X-2, 96	177.16	13.0
757B-20X-2, 105	177.25	5.1
757B-20X-6, 95	183.15	6.7
757B-21X-2, 98	185.18	8.6
757B-21X-4, 98	188.18	5.8
757B-21X-6, 96	191.16	4.8
757B-22X-2, 87	194.77	13.3
757B-22X-4, 94	197.84	15.8
757B-23X-2, 100	204.50	27.3
757B-23X-4, 95	207.45	114.0

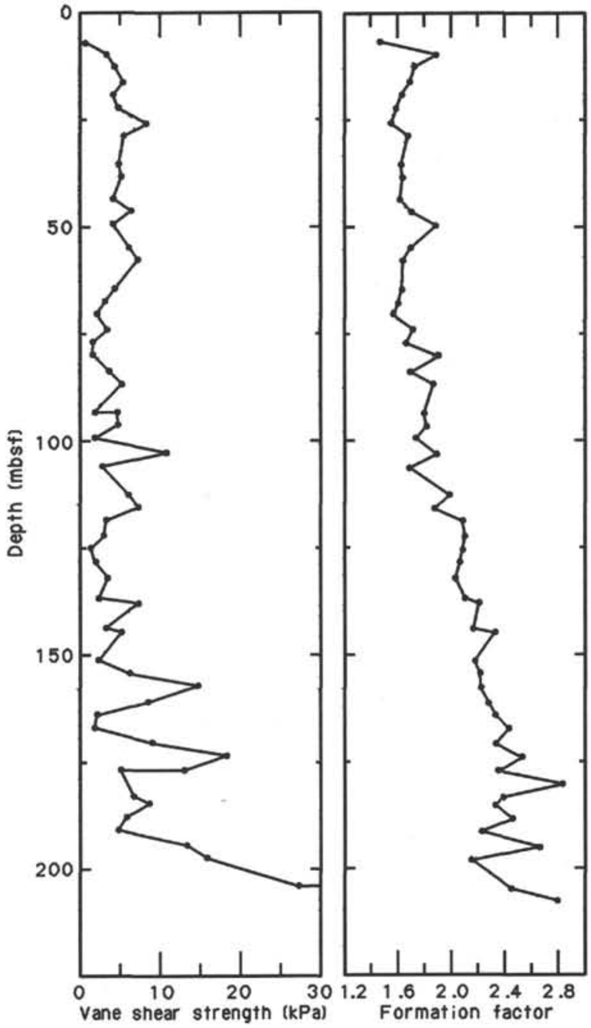

Figure 41. Vane shear strength and formation factor of sediments from Hole 757B.

Conclusions

The basalt flows, the last episode of the constructional phase of the ridge, are subaerial and are overlain by tuffs and ashes that were deposited in a shallow-water environment. The seismic stratigraphic patterns (i.e., clinoforms) observed within these units suggest a complex depositional environment. Rounded basalt pebbles, shelly layers, scoured contacts, and cross laminations in the cores from this ash unit also suggest a complex shallow-water depositional environment (see "Lithostratigraphy and Sedimentology" section). Site 757 was slightly deeper toward the end of the ash deposition because of continued thermal subsidence. Open-ocean pelagic conditions existed at the end of the eruptive episodes, as evidenced by the deposition of calcareous and nannofossil oozes. A distinct change in seismic character and stratal patterns corresponds to the contact between the ashes and the overlying oozes, which suggests a change in the depositional environment from shallow-water to more open-ocean conditions (Fig. 44).

The reflectors at Site 757 are well tied to the subtle increases in impedance and to local grain-size minima (Fig. 46). The lithologic units also correlate very well with the seismic stratigraphic units. The main seismic reflectors are interpreted as follows:

1. 174 mbsf: corresponds to the 168.5 mbsf boundary between nannofossil ooze and calcareous ooze;
2. 211 mbsf: coincides with the boundary between calcareous ooze and ash (212 mbsf);
3. 251 mbsf: coincides with the ash and tuff boundary;
4. 367 mbsf: correlates to the boundary between tuff and basalt.

REFERENCES

Banner, F. T., and Blow, W. H., 1965. Progress in the planktonic foraminiferal biostratigraphy of the Neogene. *Nature*, 208:1164–1166.

Berggren, W. A., Kent, D. V., Flynn, J. J., and Van Couvering, J. A., 1985. Cenozoic geochronology. *Geol. Soc. Am. Bull.*, 96:1407–1418.

Blow, W. H., 1969. Late middle Eocene to Recent planktonic biostratigraphy. *In* Bronnimann, P., and Renz, H. H. (Eds.), *Proc. Int. Conf. Planktonic Microfossils, 1st, Geneva, 1967*, 1:199–421.

Bolli, H. M., Saunders, J. B., and Perch-Nielsen, K. (Eds.), 1985. *Plankton Stratigraphy*: Cambridge (Cambridge Univ. Press).

Bougault, H., Treuil, M., and Joron, J.-L., 1979. Trace elements in basalts from 23°N and 36°N in the Atlantic Ocean: fractional crystallization, partial melting, and heterogeneity of the upper mantle. *In* Melson, W. G., Rabinowitz, P. D., et al., *Init. Repts. DSDP*, 45: Washington (U.S. Govt. Printing Office), 493–506.

Davies, T. A., Luyendyk, B. P., et al., 1974. *Init. Repts. DSDP*, 26: Washington (U.S. Govt. Printing Office).

Drever, J. I., 1982. *The Geochemistry of Natural Waters*: Englewood Cliffs, NJ (Prentice Hall).

Duncan, R. A., 1978. Geochronology of basalts from the Ninetyeast Ridge and continental dispersion in the eastern Indian Ocean. *J. Volcanol. Geotherm. Res.*, 4:283–305.

Duncan, R. A., Backman, J., Macdonald, A., et al., in press. Réunion hotspot activity through Tertiary time: initial results from the Ocean Drilling Program, Leg 115. *J. Volcanol. Geotherm. Res.*

Frey, F. A., Dickey, J. S., Thompson, G., and Bryan, W. B., 1977. Eastern Indian Ocean DSDP sites: correlations between petrography, geochemistry and tectonic setting. *In* Heirtzler, J. R., and Sclater, J. G. (Eds.), *A Synthesis of Deep Sea Drilling in the Indian Ocean*: Washington (Am. Geophys. Union), 189–257.

Garrels, R. M., and Christ, C. L., 1965. *Solutions, Minerals and Equilibria*: San Francisco (Freeman, Cooper).

Gieskes, J. M., 1983. The chemistry of interstitial waters of deep sea sediments: interpretation of Deep Sea Drilling data. *Chem. Ocean.*, 8:221–269.

Haggerty, S. E., 1976. Opaque mineral oxides in terrestrial igneous rocks. *In* Rumble, D. (Ed.), *Oxide Minerals*: Short Course Notes Mineral. Soc. Am., 3:101–104.

Hekinian, R., 1974. Petrology of igneous rocks from Leg 22 in the northeastern Indian Ocean. *In* von der Borch, C. C., Sclater, J. G., et al., *Init. Repts. DSDP*, 22: Washington (U.S. Govt. Printing Office), 413–447.

Jenkins, D. G., 1985. Southern mid-latitude Paleocene to Holocene planktic foraminifera. *In* Bolli, H. M., Saunders, J. B., and Perch-Nielsen, K. (Eds.), *Plankton Stratigraphy*: Cambridge (Cambridge Univ. Press), 263–283.

Kempe, D.R.C., 1974. The petrology of the basalts, Leg 26. *In* Davies, T. A., Luyendyk, B. P., et al. *Init. Repts. DSDP*, 26: Washington (U.S. Govt. Printing Office), 465–503.

Lawrence, J. R., and Gieskes, J. M., 1981. Constraints on water transport and alteration in the oceanic crust from the isotopic composition of pore water. *J. Geophys. Res.*, 86:7924–7934.

Ludden, J. L., Thompson, G., Bryan, W. B., and Frey, F. A., 1980. The origin of lavas from the Ninetyeast Ridge, eastern Indian Ocean: an evaluation of fractional models. *J. Geophys. Res.*, 85:4405–4420.

Molnar, P., and Tapponnier, P., 1975. Cenozoic tectonics of Asia: effects of a continental collision. *Science*, 198:419–426.

Morkhoven, F.P.C.M. van, Berggren, W. A., and Edwards, A. S., 1986. Cenozoic cosmopolitan deep-water benthic foraminifera. *Bull. Cent. Rech. Explor. Prod. Elf-Aquitaine*, 11:1–421.

Newman, J. S., and Sclater, J. G., 1988. Site surveys of the central and southern Ninetyeast Ridge for the Ocean Drilling Program, Leg 121. *Tech. Rep. Univ. Tex. Austin Inst. Geophys.*, 74.

Okada, H., and Bukry, D., 1980. Supplementary modification and introduction of code numbers to the low latitude coccolith biostratigraphy (Bukry, 1973; 1975). *In* Haq, B. U. (Ed.), *Nannofossil Biostratigraphy*: Stroudsburg, PA (Hutchison Ross), 321–377.

Patriat, P., and Achache, J., 1984. India-Eurasia collision chronology has implications for crustal shortening and driving mechanism of plates. *Nature*, 311:615–621.

Peirce, J. W., 1978. The northward motion of India since the Late Cretaceous. *Geophys. J. R. Astron. Soc.*, 52:277–312.

Peterson, L. C., 1984. Recent abyssal benthic foraminiferal biofacies of the eastern equatorial Indian Ocean. *Mar. Micropaleontol.*, 8:479–579.

Price, R. C., Kennedy, A. K., Riggs-Sneeringer, M., and Frey, F. A., 1986. Geochemistry of basalts from the Indian Ocean triple junction: implications for the generation and evolution of Indian Ocean Ridge basalts. *Earth Planet. Sci. Lett.*, 78:379–396.

Rea, D. K., Leinen, M., and Janecek, T. R., 1985. Geologic approach to the long-term history of atmospheric circulation. *Science*, 227: 721–725.

Royer, J.-Y., Sclater, J. G., and Sandwell, D. T., in press. A preliminary tectonic chart of the Indian Ocean. *Proc. Indian Acad. Sci., Earth Planet. Sci.*

Saunders, A. D., 1983. Geochemistry of basalts recovered from the Gulf of California during Leg 65 of the Deep Sea Drilling Project. *In* Lewis, B.T.R., Robinson, P., et al., *Init. Repts. DSDP*, 65: Washington (U.S. Govt. Printing Office), 591–622.

Shipboard Scientific Party, 1988. Site 661. *In* Ruddiman, W., Sarnthein, M., et al., *Proc. ODP, Init. Repts.*, 108: College Station, TX (Ocean Drilling Program), 419–420.

Sun, S.-S., and McDonough, W. F., in press. Chemical and isotopic systematics of oceanic basalts: implications for mantle composition and processes. *In* Saunders, A. D., and Norry, M. J. (Eds.), *Magmatism in Ocean Basins*: Spec. Publ. Geol Soc. London.

Thompson, G., Bryan, W. B., Frey, F. A., and Sung, C. M., 1974. Petrology and geochemistry of basalts and related rocks from Sites 214, 215, and 216, DSDP Leg 22, Indian Ocean. *In* von der Borch, C. C., Sclater, J. G., et al., *Init. Repts. DSDP*, 22: Washington (U.S. Govt. Printing Office), 459–468.

Toumarkine, M., and Luterbacher, H., 1985. Paleocene and Eocene planktic foraminifera. *In* Bolli, H. M., Saunders, J. B., Perch-Nielsen, K. (Eds.), *Plankton Stratigraphy*: Cambridge (Cambridge Univ. Press), 87–154.

Van Wagoner, N. A., and Johnson, H. P., 1983. Magnetic properties of three segments of the Mid-Atlantic Ridge at 37°N: Famous, Narrowgate, and AMAR:AMAR2. *J. Geophys. Res.*, 88:5065–5082.

Weis, D., Beaux, J. F., Gautier, I., Giret, A., and Vidal, P., 1988. Kerguelen Archipelago: geochemical evidence for recycled material. *In* Hart, S. R., and Gülen, L. (Eds.), *Crust/Mantle Recycling at Convergence Zones*: Nato ASI Workshop, Abst., May 25–29, Antalaya, Turkey, 122–125.

Ms 121A-111

Table 21. Formation factor of sediments from Hole 757B.

Sample (interval in cm)	Depth (mbsf)	Formation factor
757B-2H-2, 92	6.92	1.47
757B-2H-2, 92	6.92	1.47
757B-2H-4, 92	9.92	1.89
757B-2H-6, 88	12.88	1.73
757B-3H-2, 90	16.40	1.69
757B-3H-4, 90	19.40	1.63
757B-3H-6, 90	22.40	1.59
757B-4H-2, 98	26.08	1.55
757B-4H-4, 98	29.08	1.68
757B-5H-2, 97	35.67	1.63
757B-5H-4, 97	38.67	1.64
757B-6H-1, 83	43.63	1.62
757B-6H-3, 100	46.80	1.71
757B-6H-5, 98	49.78	1.89
757B-7H-2, 97	54.97	1.70
757B-7H-4, 98	57.98	1.64
757B-8H-2, 90	64.60	1.63
757B-8H-4, 94	67.64	1.60
757B-8H-6, 94	70.64	1.57
757B-9H-2, 92	74.22	1.72
757B-9H-4, 92	77.22	1.67
757B-9H-6, 92	80.22	1.91
757B-10H-2, 92	83.92	1.70
757B-10H-4, 92	86.92	1.87
757B-11H-2, 92	93.62	1.80
757B-11H-4, 92	96.62	1.82
757B-11H-6, 92	99.62	1.74
757B-12H-2, 92	103.22	1.89
757B-12H-4, 92	106.22	1.69
757B-13H-2, 92	112.92	1.99
757B-13H-4, 92	115.92	1.88
757B-13H-6, 92	118.92	2.09
757B-14H-2, 92	122.52	2.11
757B-14H-4, 92	125.52	2.09
757B-14H-6, 92	128.52	2.07
757B-15H-2, 92	132.22	2.04
757B-15H-5, 92	136.72	2.11
757B-15H-6, 92	138.22	2.21
757B-16H-3, 137	143.87	2.17
757B-16H-4, 92	144.92	2.33
757B-17H-2, 90	151.50	2.18
757B-17H-4, 92	154.52	2.22
757B-17H-6, 93	157.53	2.23
757B-18H-2, 94	161.24	2.29
757B-18H-4, 94	164.24	2.34
757B-18H-6, 94	167.24	2.44
757B-19H-2, 94	170.94	2.34
757B-19H-4, 94	173.94	2.54
757B-20X-2, 95	177.15	2.36
757B-20X-4, 102	180.22	2.84
757B-20X-6, 90	183.10	2.40
757B-21X-2, 94	185.14	2.34
757B-21X-4, 97	188.17	2.47
757B-21X-6, 95	191.15	2.23
757B-22X-2, 95	194.85	2.67
757B-22X-4, 95	197.85	2.16
757B-23X-2, 93	204.43	2.46
757B-23X-4, 92	207.42	2.80

Table 22. Thermal conductivity of samples of sediments and basement from Site 757.

Sample (interval in cm)	Depth (mbsf)	Thermal conductivity (W/m°C)
757B-2H-2, 70	6.70	1.176
757B-2H-4, 70	9.70	1.358
757B-2H-6, 70	12.70	1.329
757B-3H-2, 87	16.37	1.420
757B-3H-4, 87	19.37	1.344
757B-3H-6, 87	22.37	1.365
757B-4H-2, 70	25.80	1.336
757B-4H-4, 70	28.80	1.380
757B-5H-2, 85	35.55	1.305
757B-5H-4, 85	38.55	1.259
757B-6H-2, 85	45.15	1.245
757B-6H-4, 85	48.15	1.560
757B-6H-5, 85	49.65	1.452
757B-6H-6, 85	51.15	1.753
757B-7H-2, 85	54.85	1.656
757B-7H-4, 85	57.85	1.473
757B-8H-2, 85	64.55	1.428
757B-8H-4, 85	67.55	1.395
757B-8H-6, 85	70.55	1.597
757B-9H-2, 85	74.15	1.536
757B-9H-4, 85	77.15	1.447
757B-9H-6, 85	80.15	1.544
757B-10H-2, 85	83.85	1.594
757B-10H-4, 85	86.85	1.670
757B-10H-6, 50	89.50	1.824
757B-11H-2, 85	93.55	1.343
757B-11H-4, 85	96.55	1.715
757B-11H-6, 85	99.55	1.552
757B-12H-2, 85	103.15	1.576
757B-12H-4, 85	106.15	1.630
757B-12H-6, 85	109.15	1.529
757B-13H-2, 80	112.80	1.641
757B-13H-4, 80	115.80	1.662
757B-13H-6, 80	118.80	1.732
757B-14H-2, 80	122.40	1.552
757B-14H-4, 80	125.40	1.781
757B-14H-6, 80	128.40	1.607
757B-15H-2, 80	132.10	1.498
757B-15H-4, 80	135.10	1.640
757B-15H-6, 80	138.10	2.039
757B-16H-2, 80	141.80	1.872
757B-16H-4, 80	144.80	1.471
757B-17H-2, 80	151.40	1.788
757B-17H-4, 80	154.40	1.852
757B-17H-6, 80	157.40	1.906
757B-18H-2, 80	161.10	1.881
757B-18H-4, 80	164.10	2.124
757B-18H-6, 80	167.10	1.504
757B-19H-2, 80	170.80	1.909
757B-19H-4, 80	173.80	1.954
757B-20X-2, 80	177.00	1.720
757B-20X-4, 80	180.00	1.787
757B-20X-6, 80	183.00	1.995
757B-21X-2, 80	185.00	1.770
757B-21X-4, 80	188.00	1.511
757B-21X-6, 80	191.00	2.070
757B-22X-2, 80	194.70	1.716
757B-22X-4, 80	197.70	1.377
757B-23X-2, 80	204.30	1.728
757B-23X-4, 80	207.30	1.661
757B-24X-2, 85	214.05	1.158
757B-24X-4, 85	217.05	1.001
757B-25X-2, 38	223.28	1.370
757B-25X-2, 81	223.71	1.255
757B-25X-4, 81	226.71	1.264
757B-26X-2, 85	233.35	1.158
757B-27X-1, 94	241.64	1.240
757B-27X-2, 85	243.05	1.100
757B-27X-4, 85	246.05	1.200
757B-28X-3, 92	254.32	1.070
757B-29X-3, 88	263.88	1.290
757B-30X-2, 103	272.23	1.260
757B-31X-1, 88	280.28	1.330
757B-32X-2, 41	290.91	1.280

Table 22 (continued).

Sample (interval in cm)	Depth (mbsf)	Thermal conductivity (W/m°C)
757B-34X-CC, 6	311.26	1.250
757B-35X-CC, 7	322.30	1.240
757B-37X-3, 47	340.77	1.440
757C-7R-1, 35	363.25	1.460
757B-41X-1, 0	369.30	1.730
757B-42N-1, 26	370.56	1.600
757C-8R-2, 71	374.61	1.970
757C-9R-2, 82	383.97	1.900
757C-9R-4, 83	386.27	1.730
757C-10R-2, 65	393.85	1.410
757C-10R-3, 0	394.70	1.630
757C-11R-2, 27	403.12	1.450
757C-11R-3, 115	405.40	1.740
757C-12R-1, 4	411.14	1.860
757C-12R-3, 111	414.73	1.570

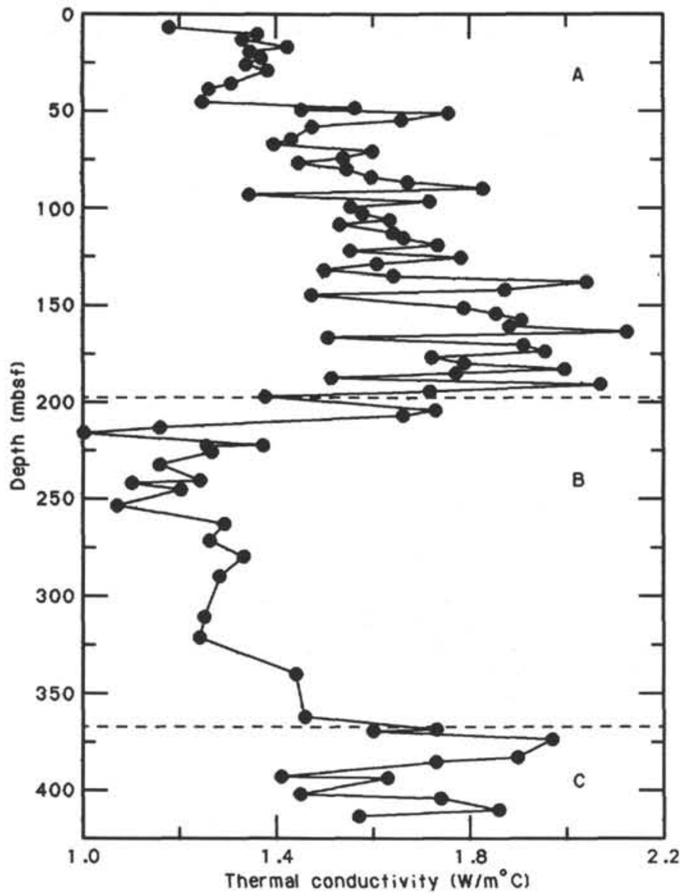

Figure 42. Thermal conductivity of sediments from Site 757. *A*, *B*, and *C* refer to physical-properties units, defined by dashed lines.

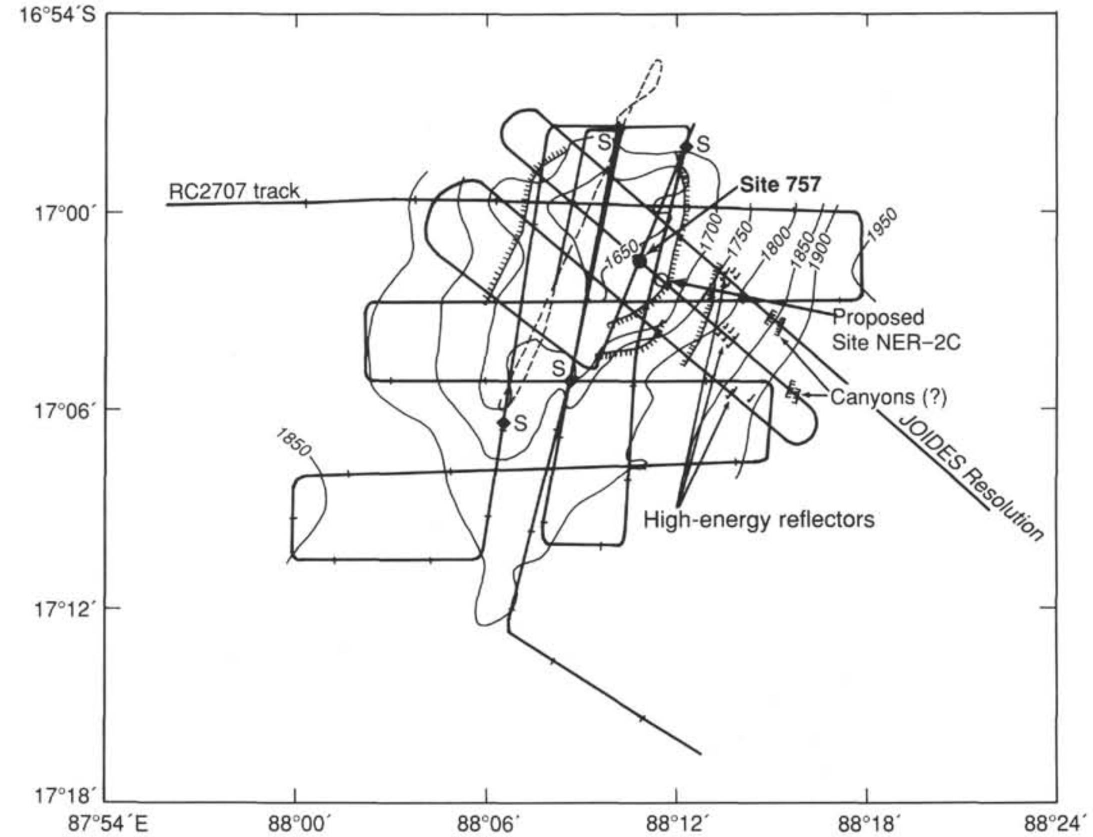

Figure 43. Central Ninetyeast Ridge survey area. Solid lines delineate RC2707 and *JOIDES Resolution* tracks. Bathymetry contour interval is 50 m. Diamonds labeled *S* show positions of RC2707 sonobuoy refraction survey. The location of Site 757 is approximately 2.8 km northwest of proposed Site NER-2C at *Resolution* track crossing. High-energy reflectors labeled along the eastern flank of the ridge possibly indicate coarse-sediment deposits in small intraslope basins (Newman and Sclater, 1988).

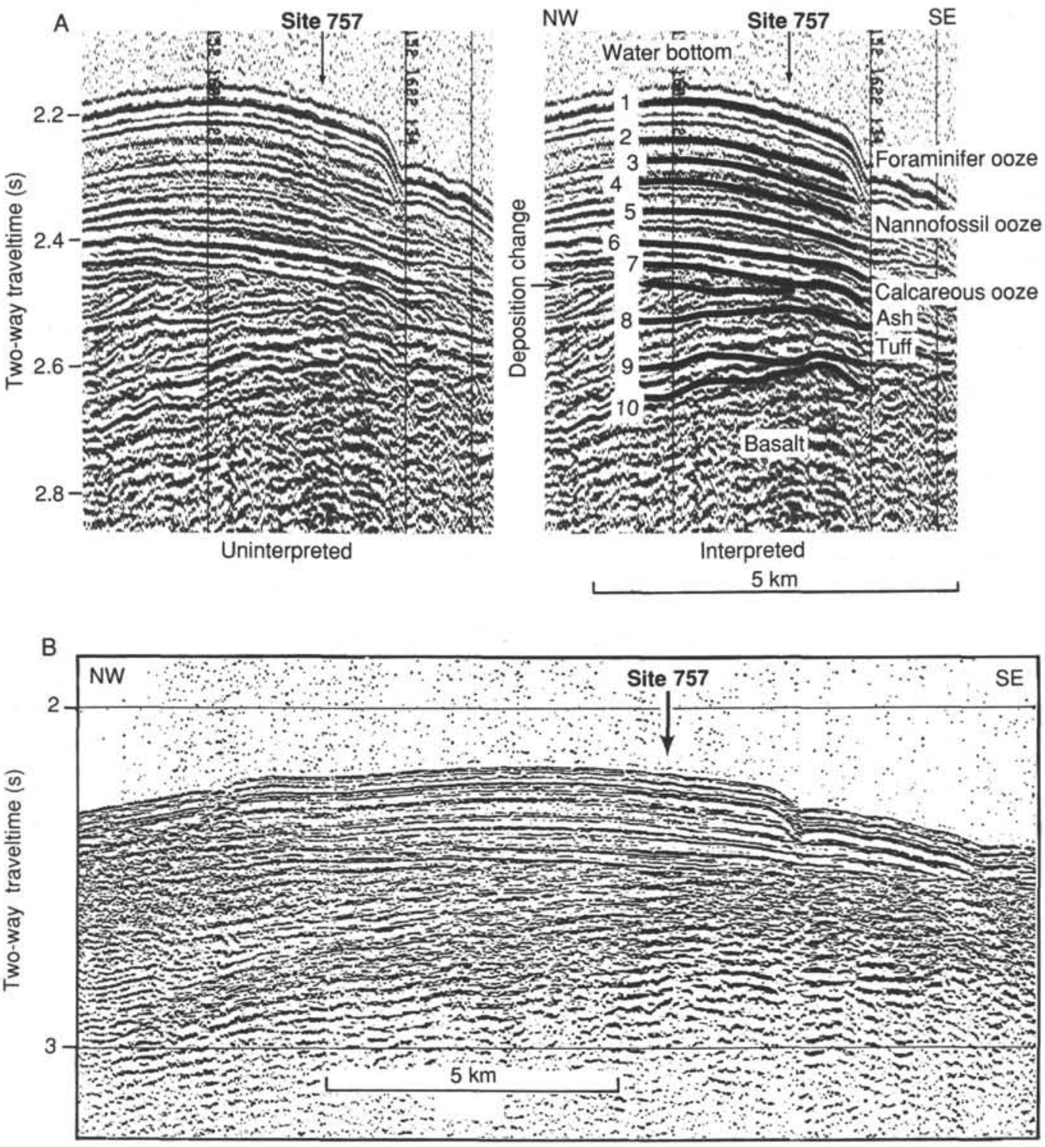

Figure 44. Seismic dip line across Site 757. **A.** Shipboard analog record, uninterpreted on the left and interpreted on the right. **B.** Same line reprocessed post-cruise with less vertical exaggeration. Figure 12 of the "Ninetyeast Ridge Underway Geophysics" chapter (this volume, backpocket) shows the reprocessed version of the entire survey.

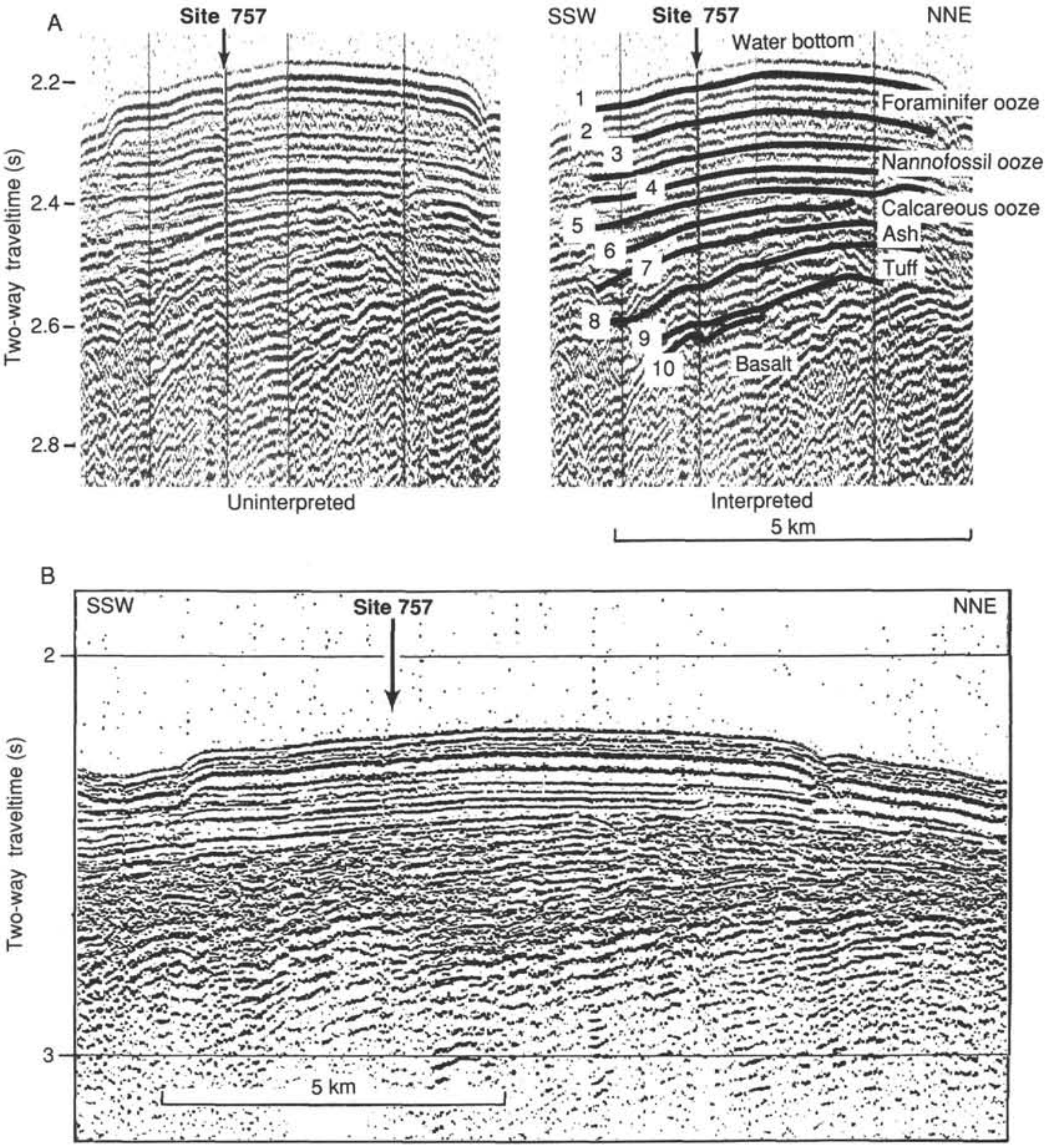

Figure 45. Seismic strike line across Site 757. **A.** Shipboard analog record, uninterpreted on the left and interpreted on the right. **B.** Same line reprocessed post-cruise with less vertical exaggeration.

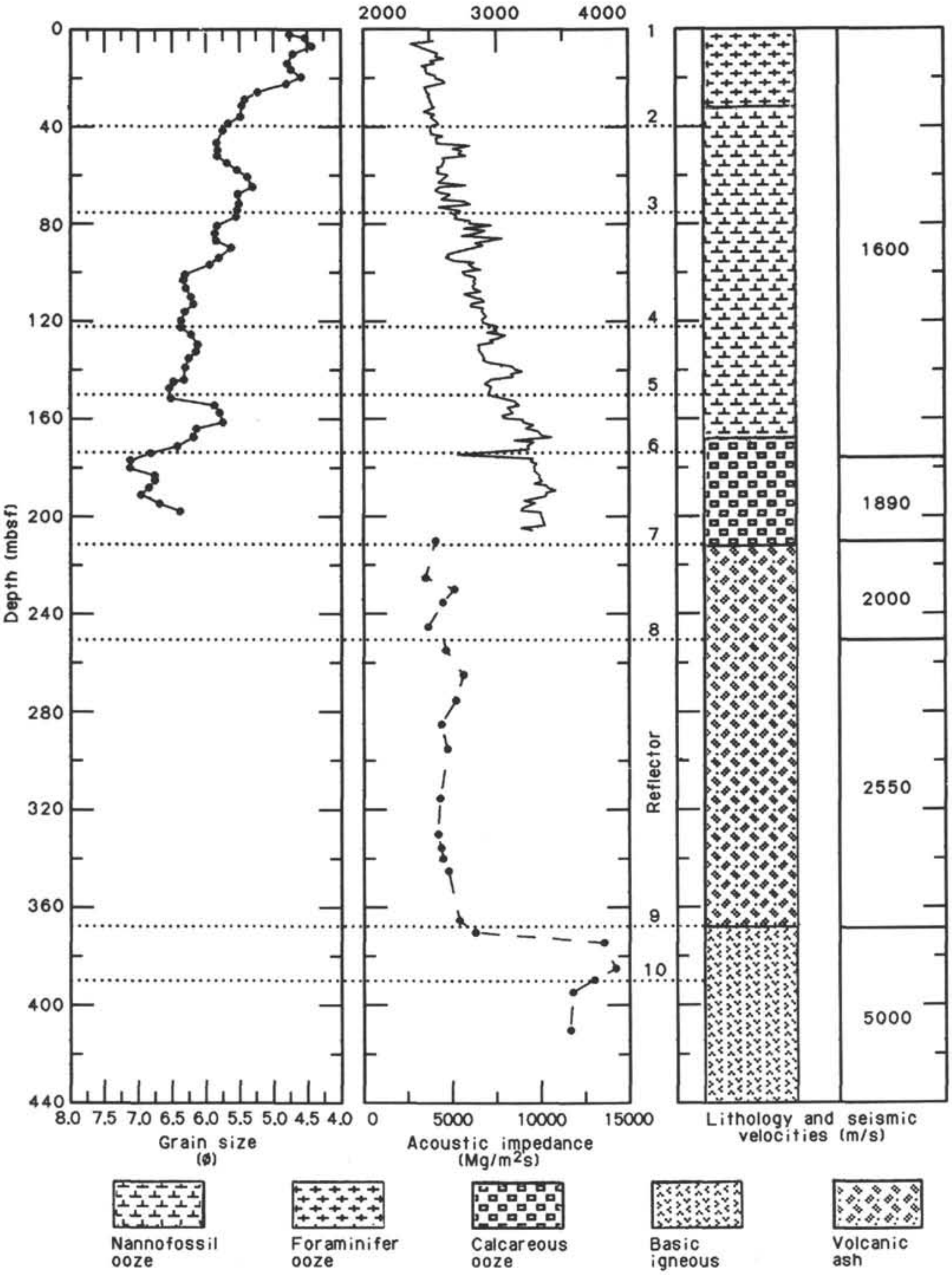

Figure 46. Correlation of 10 water gun seismic reflectors with grain size, acoustic impedance, and lithology at Site 757. The grain size is expressed in a three-value centered running average. The plot of acoustic impedance uses different scales above and below 210 mbsf, one for oozes and the other for ash, tuff, and basalt. Velocities to the right of the lithology column were used to calculate the depths of the reflectors.

Table 23. Dip and strike line reflector two-way traveltimes, Site 757.

Reflector	Dip line time (s/TWT)	Strike line time (s/TWT)	Remarks
1	2.201	2.202	Water bottom
2	2.248	2.255	
3	2.293	2.300	
4	2.350	2.357	
5	2.387	2.390	
6	2.420	2.420	
7	2.455	2.462	
8	2.498	2.501	
9	2.589	2.593	
10	2.595	2.605	Ringing reflection

Table 24. Velocity model for calculating reflector depths, Site 757.

Average time to reflector[a] (s TWT)	Depth to reflector (mbsf)	Velocity (m/s)
2.420	174	1600
2.459	211	1890
2.500	251	2000
2.591	367	2550
below	[b]420	5000

[a] Averaged times of dip and strike lines.
[b] Total depth, Hole 757C.